CRITERIA OF FAULT GEOMECHANICAL STABILITY DURING A PRESSURE BUILD-UP

Report: 2015/04

APRIL 2015

INTERNATIONAL ENERGY AGENCY

The International Energy Agency (IEA) was established in 1974 within the framework of the Organisation for Economic Co-operation and Development (OECD) to implement an international energy programme. The IEA fosters co-operation amongst its 28 member countries and the European Commission, and with the other countries, in order to increase energy security by improved efficiency of energy use, development of alternative energy sources and research, development and demonstration on matters of energy supply and use. This is achieved through a series of collaborative activities, organised under more than 40 Implementing Agreements. These agreements cover more than 200 individual items of research, development and demonstration. IEAGHG is one of these Implementing Agreements.

DISCLAIMER

COPYRIGHT

ACKNOWLEDGEMENTS AND CITATIONS

This report describes research sponsored by IEAGHG. This report was prepared by:

Norges Geotekniske Institutt

The principal researchers were:

- Bahman Bohloli
- Jung Chan Choi
- Elin Skurtveit
- Lars Grande
- Joonsang Park
- Maarten Vannest

To ensure the quality and technical integrity of the research undertaken by IEAGHG each study is managed by an appointed IEAGHG manager. The report is also reviewed by a panel of independent technical experts before its release.

The IEAGHG manager for this report was:

James Craig

The expert reviewers for this report were:

- Daniel Moos, Baker-Hughes
- Christopher Hawkes, University of Saskatchewan
- Dominique Copin, Total

The report should be cited in literature as follows:

'IEAGHG, "Criteria of Fault Geomechanical Stability during a Pressure Build-up, 2015/04, April, 2015'

Other information or copies of the report can be obtained by contacting IEAGHG at:

IEAGHG, Cheltenham Office Park, Pure Offices,
Hatherley Lane, Cheltenham,
GLOS., GL51 6SH, UK
Tel: +44(0) 1242 802911
E-mail: mail@ieaghg.org
Internet: www.ieaghg.org

CRITERIA OF FAULT GEOMECHANICAL STABILITY DURING PRESSURE BUILD-UP

Key Messages

- Faults typically consist of two sub-structures: a fault core; and a wider fault damage zone. Faults in low porosity rocks tend to have a fine-grained fault core whereas faults in coarse-grained, high porosity rocks, usually have low porosity deformation bands that can develop into high permeable slip surfaces.
- Fault zone permeability increases with increasing fluid pressure but permeability varies both across and along faults. Hydraulic properties also vary between the damage zone and the core where gouge material is concentrated. This concentration of fine grained minerals also reduces the mechanical strength of faults.
- Mechanical failure or reactivation occurs either when shear stress exceeds normal strength or when hydraulic fracturing is induced.
- Fault deformation can be either brittle or ductile. The former leads to the formation of cataclastite (fine grained granular) and shear fractures which dilate under low effective normal stress that can cause permeability enhancement. With increasing shear deformation, fracture asperities are sheared off leading to gouge production and a reduction in permeability. Thus, in brittle deformation permeability will generally increase under low effective stresses and small displacements but decreases with increasing effective stress and magnitude of displacement. Shear fractures created in ductile deformation contract during shearing and tend not to lead to an increase in permeability.
- Reactivation of faults can be assessed using both analytical and numerical approaches, but assessment is usually based on the Mohr-Coulomb failure criterion. This method can be used to determine the critical injection pressure.
- Numerical modelling can provide predictions of fault stability at different scales and incorporate different parameters such as the geometry of different faults. Numerical methods can be effective for identifying leakage potential and seal failure especially where dilatancy and stress dependent permeability changes occur.
- Experimental tests on minerals and rock samples exposed to CO_2 tentatively indicate that the coefficient of friction is not radically changed, however, this conclusion is based on limited exposure to CO_2.
- There is limited observational data on stress regimes and direct pore pressure measurements from core samples from cap rocks and fault zones. Acquisition of key data would enhance stress regime modelling and fault behavior.

Background to the study

The storage of CO_2 in geological reservoirs requires relatively permeable conditions bounded by very low permeable layers. Reservoirs can be bounded by faults that can act as seals if, for example, an impermeable formation is juxtaposed against it. The presence of faults in virtually all geological formations is a key consideration as their stability is crucial for the integrity of storage sites. Fault stability is affected by multiple factors including fault structure, material properties, geochemical reactions between CO_2 and fault gouges and pore pressure changes. Injection operation and pressurization of reservoirs usually changes the state of the in-situ stresses which may cause destabilization of previously stable faults. Instability occurs in the form of slip along pre-existing fault or fracture systems, which may be associated with seismicity. In addition, movement along fault planes, and the generation of factures, may create open conduits that breach the integrity of the storage site. Understanding how faults might respond to stress conditions caused by CO_2 injection is therefore fundamental.

Recent geomechanical studies for CO_2 geological storage have focused on initialising stresses in the overburden based on all available geological and well engineering data, modelling the impact of fluid/gas pressure build up on stresses in the storage formations, the caprock and the overburden in general. The challenge is to predict the acceptable overpressure before shear failure, or reactivation of a fault/natural fracture occurs. The prediction process begins by using a verified geomechanical model to calculate the effective normal stresses and shear stresses occurring along all the faults/fractures. These stresses are evaluated in the context of fault cohesion and sliding friction to predict the pre-injection state of stress on these features and to determine the critical fluid/gas pressure required to initiate shear failure on what may have previously been a stable fault/fracture. Stress and fault properties can vary in space and time.

Scope of work

This report highlights the key factors affecting fault stability and reviews the methodologies generally used to evaluate geomechanical stability of faults during CO_2 storage. It focuses on fault structure, hydro-mechanical properties of fault planes and the methodologies generally employed to assess fault stability. The objective of the report is to provide an overview of conditions that affect faults and highlight the essential components affecting mechanical stability of faults due to CO_2 injection and pressure build-up in reservoirs.

Findings of the Study

Faulting is the response of brittle material to a stress field that exceeds its strength threshold. Faults nucleate from micro-fractures or deformation bands in a critically stressed region and accumulate strain over time to grow. As faults extend, they can interact with neighbouring faults of various sizes and can form special features important in the context of CO_2 storage. A fault zone typically consists of two sub-structures: the fault core; and the fault damage zone. The fault core generally comprises gouge material, crushed particles/cataclasite or ultracataclasite (or combination of the two). The damage zone typically contains fractures at different scales. Faults in low porosity rocks have a fine-grained fault core surrounded by a fracture dominated damage zone. Faults in coarse-grained, high porosity rocks, usually have low porosity deformation bands that develop into high permeable slip surfaces (Figure 1).

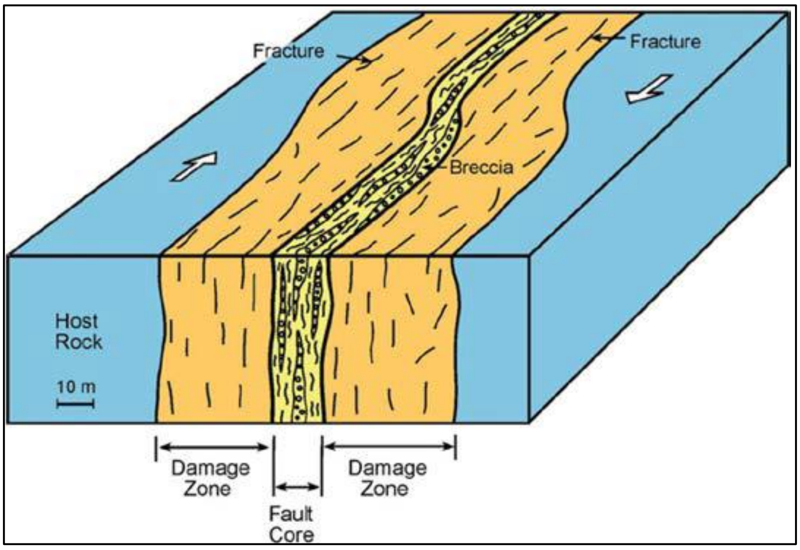

Figure 1 Schematic representation of a fault zone comprised of a fault core and damage zones in a strike-slip fault.

Leakage through faults is a function of the permeability of the fault zone. The fault zone permeability increases with increasing fluid pressure towards a critical threshold. However, fault permeability varies both across and along faults. The hydraulic properties of fault cores and damage zones can be quite different as exemplified in Figure 2. These differences are attributed mainly to the properties of fault gouge material. The gouges are either granular or clay-rich. The permeability of granular material depends on the grain size distribution and sorting of grains. The permeability of clay-rich gouges is a function of the type of clay, clay percentage, and its distribution. The deformation along the fault zone also reduces the strength of the fault core material due to the concentration of clay minerals and micro fractures in the fault core.

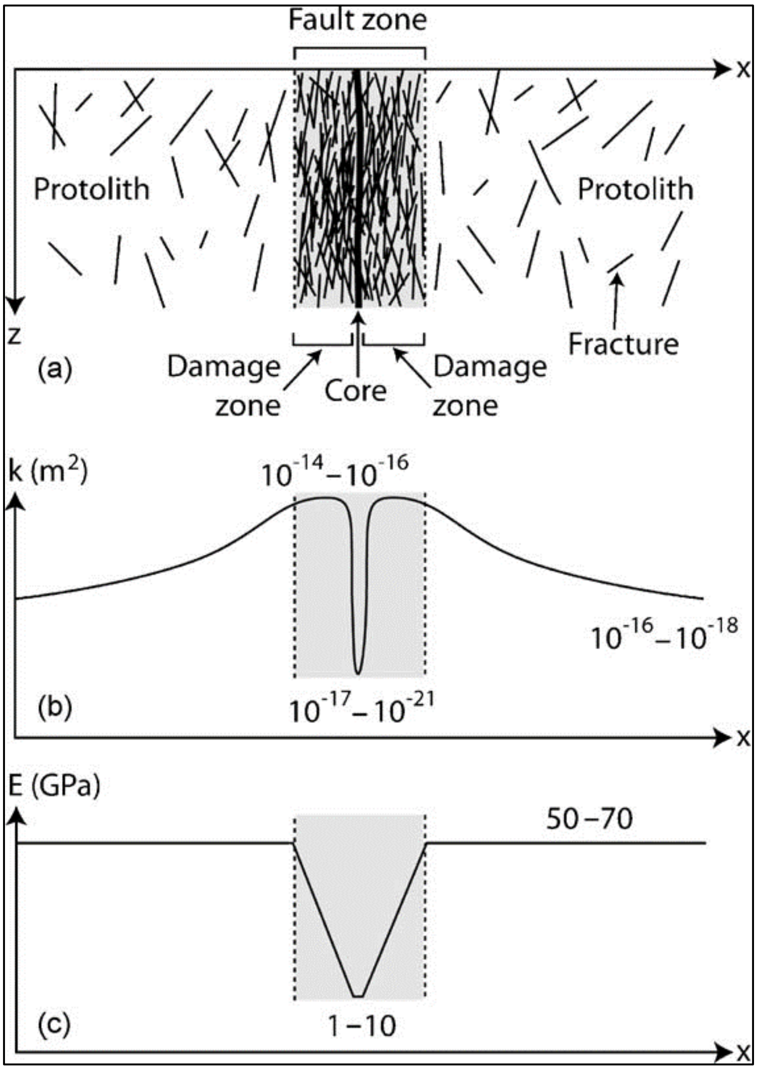

Figure 2 Permeability and mechanical properties of fault zone material.

Faults are usually the weak links in the rock mass and control hydraulic and mechanical behaviour of surrounding rock bodies. Mechanical failure or reactivation of faults may occur either: when shear stress exceeds shear strength of fault zone material; or when hydraulic fracturing (in case of cohesive faults) takes place. Under these conditions pore pressure exceeds the sum of the minimum in-situ stress and tensile strength of the fault. In the case of shearing, post failure deformation may be brittle or ductile, depending on the shear strength properties of the fault core and the level of the effective confining stress. In the brittle regime, deformation is associated with dilation which can contribute to the enhancement of permeability under low shear conditions, but as shear deformation increases, fracture asperities are sheared off leading to gouge production and a reduction in permeability. Ductile deformation may not significantly change permeability.

Reactivation of faults and fracture systems can be assessed using analytical and numerical approaches. The analytical approach considers static normal and shear stresses on a fault plane and relies on the Mohr-Coulomb failure criterion to evaluate stability of the fault. By applying this method the critical injection pressure can be calculated from the difference between the current stress state and the predicted failure envelope. The critical injection pressure, also called the maximum sustainable pressure, can be calculated for all possible fault orientations at given in-situ conditions.

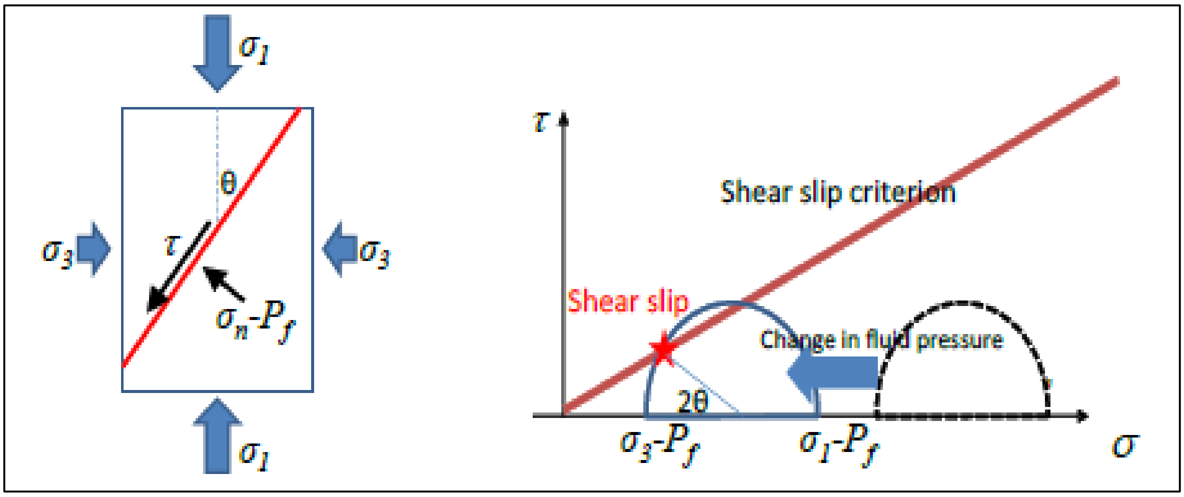

Figure 3 Schematic representation of stress fields on a fault plane and a representation of a change in effective stress due to injection (Mohr diagram) where τ = sheer stress, σ= normal stress, θ = dip angle of fault and P_f is the pore pressure

The critical pressure along faults within a reservoir can be calculated and then plotted on a polar stereographic projection to determine the predominant orientation of faults with susceptibility to shear (least stable).

An analytical approach is a simple and valuable tool for preliminary assessment of fault reactivation potential during injection or depletion. The analytical approach requires the following essential components:

- Magnitude and direction of in-situ stress
- Fault orientation (dip and strike)
- Shear strength, especially friction coefficient
- Initial pore pressure and pressure change

The limitation of this approach is that it is based on many assumptions and simplifications and may not necessarily capture complex physical processes that occur in the reservoir during injection. The stability of faults in the cap rock and overburden as well as reservoirs is crucial for storage reservoir integrity. Consequently fault stability analysis needs to apply to faults within the storage unit and the surrounding formations. The analysis should include the ability to predict the extent of reactivation into the caprock. This may require local modelling of faults in the interface region which could be difficult to capture with variable pore pressures and lithologies. Analytical approaches may be further limited by changes in the magnitude and direction of principal stress directions during repressurisation. These limitations may be overcome by using numerical tools.

Numerical analyses of fault stability can provide fault simulations at different scales and within different geological constraints. Faults can be presented in a global model as single discontinuities, e.g. as a zero-thickness element, in order to explore their general behaviour. If a fault is prone to instability, and the detailed behaviour of the fault zone is of interest, it may be modelled as a rock mass of continuum material. This may require a local model where detailed properties and geometry of the fault zone are assigned to the components of the model. Furthermore, post-failure behaviour of faults is important for determining the potential for fault leakage and seal failure which can be studied using numerical methods where dilatancy and stress dependent permeability are taken into account.

Following preliminary analysis a refined geomechanical model may be necessary. To progress to this more advanced stage a series of parameters will be required including:

- A geometrical description of the reservoir and surrounding rock formations
- Mechanical properties of reservoir and surrounding formations
- Spatial distribution of pore pressure stresses and temperature usually acquired from core and log data
- Loading conditions (time history of a pore pressure field during injection)

To build a more comprehensive model of fault behaviour and the potential for reactivation three main geomechanical components need to be determined:

- In-situ stresses (vertical (σ_v), maximum horizontal (σ_{Hmax}) and minimum horizontal (σ_{Hmin})),
- Fault zone strength
- Pore pressure profile

To determine in-situ stresses real data on formation geomechanical properties are required. Different techniques can be used to measure or infer the direction and magnitude of in-situ stresses. Horizontal in-situ stresses can be determined from borehole caliper logs, borehole image logs and televiewers. Vertical stress can be inferred from the depth of the overburden. Density measurements can be made from core samples and calculated from density and sonic logs. Determining horizontal stresses is more challenging by comparison. Leak-Off tests, formation integrity tests and minifrac tests can be used to assess the minimum in-situ stress. The maximum horizontal stress can be deduced from hydraulic fracture tests, however values recorded from deep cased wellbores can be very uncertain. If exact stress values are not available they can be estimated using the Stress polygon method which is based on the frictional strength of faults. The upper bound of horizontal stresses can be determined by plotting the limits of fault stability in the form of a stress polygon (Figure 4).

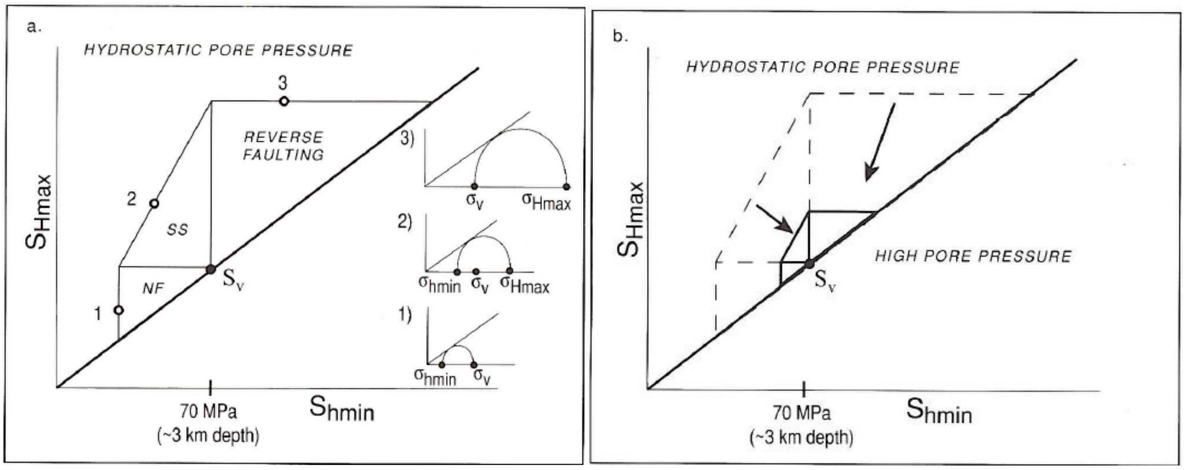

Figure 4 Stress polygon method used to define ranges of stress magnitudes at a specific depth.

A key component that needs to be included in any fault slip or reactivation scenario is the strength and friction coefficient of faults. The strength of faults (τ) can be calculated as a function of depth provided the correct value of friction coefficient (μ) and pore pressure (P) for the fault plane are known:

$$\tau = \mu(\sigma_n - P)$$

Data from laboratory tests and field observations show that friction coefficient of faults generally varies between 0.6 and 0.85, although values as low as 0.2 have also been reported in the literature for clay material. The strength of faults in a CO_2 storage reservoir may be affected by the presence of CO_2 but not substantially. A few studies tentatively indicate that the coefficient of friction of the fault-filling minerals does not change pre- and post-CO_2 treatment. This observation is, however, based on a few laboratory studies where the effects of CO_2 on rocks and minerals was only performed over short time spans.

Experimental work has shown that the presence of water decreases friction in cap rocks but not necessarily reservoir sandstones. An investigation into the effects of carbonic acid on carbonate reservoir rock indicated that there was a reduction in the frictional and tensile strength of the lithology which can be inferred from the Mohr circles and failure envelop for pre- and post-CO_2 treated carbonate illustrated in Figure 5. Another test using supercritical CO_2 on the frictional behaviour of simulated anhydrite fault gouge revealed that the friction coefficient of the material at 0.65 and 80°C can be reduced to 0.55 with an increase in temperature to 150°C.

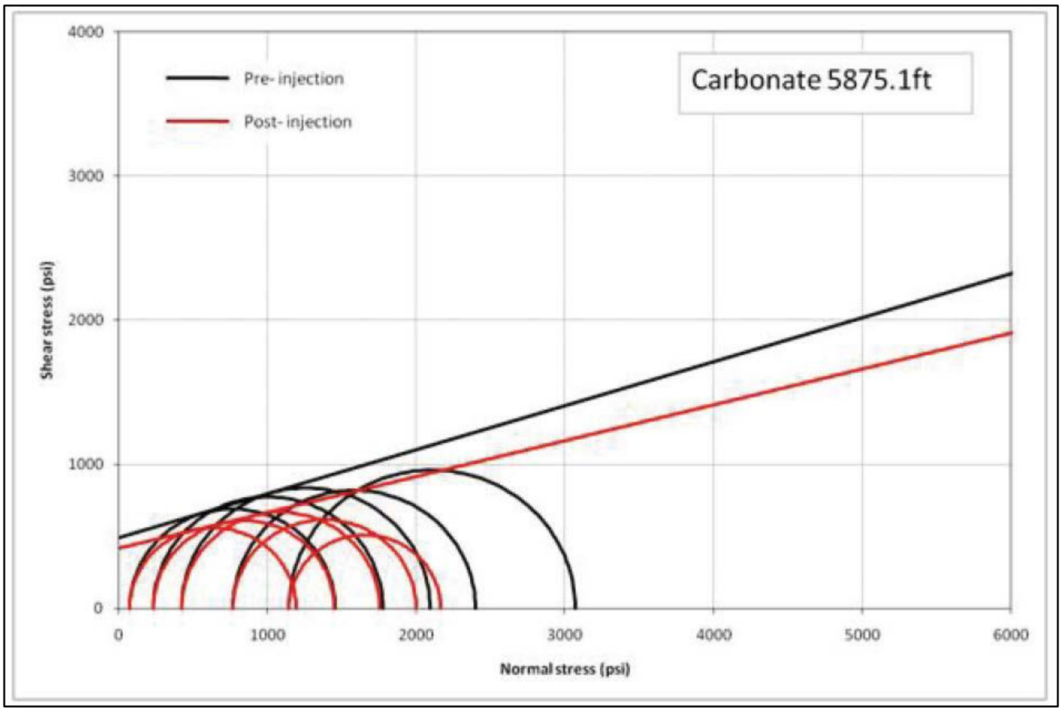

Figure 5 Failure envelop for pre- and post-CO_2 treated carbonate.

Expert Review Comments

There was a general consensus that the information compiled in the report provides a useful perspective on the subject. It is also complemented effectively by figures and tables. The report offers a comprehensive review of the subject and provides valuable information to companies or organisations who lack familiarity in fault development and associated analytical techniques. However, the study does not increase the level of knowledge for companies that have a strong geotechnical background.

One of the main criticisms of the report was the poor grammar and inaccurate use of references. The initial draft required substantial editing. Occasional clarification of technical terminology was also needed. The reviewers thought that the report contained useful references but these could have been more extensive and, for example, included more work published in SPE journals. Some figure captions also required modification and in some cases more detailed explanations.

One reviewer commented that the report was very detailed in some parts particularly the sections dealing with faulting and fault properties. However, it lacked detail on standard oil industry practice.

One concluding remark proposed that a more detailed follow-on study is now required to provide confidence for site operators and stakeholders. A future study needs to explain when faults remain stable and when reactivation might occur, and under what conditions.

Conclusions

- Fault zone permeability depends on the type of deformation (brittle or ductile) and lithology (mineral composition).
- Fault zone permeability increases with increasing fluid pressure. Hydraulic properties vary between the core and the damage zone.
- Mechanical failure or reactivation occurs either when shear stress exceeds normal shear strength or when hydraulic fracturing is induced.
- The Mohr-Coulomb failure criterion can be used to determine shear strength and critical injection pressure but its application is limited by the pattern of stress regimes near faults and changes during depletion / injection. As an analytical method it can only be applied to reservoir formations because of the contrast in cap rock lithology and pore pressure regime.
- Numerical methods can be effective for identifying leakage potential and seal failure especially where dilatancy and stress dependent permeability changes occur.
- Experimental tests on minerals and rock samples exposed to CO_2 tentatively indicate that the coefficient of friction is not radically changed, however, this conclusion is based on limited exposure to CO_2.
- There is limited observational data on stress regimes and direct pore pressure measurements from core samples from cap rocks and fault zones.

In summary, the Mohr-Coulomb failure criterion is the major technique employed to determine stress-strength relationships and stability analysis of faults. It can be applied to assess fault stability during and after injection of fluids such as CO_2, or depletion of hydrocarbons. Analytical methods combined with the numerical solutions provide the best approach for assessing geomechanical stability of faults. Modelling can be used to determine the relative stability of different faults in reservoirs subject to repressurisation and the pressure thresholds required to maintain fault stability.

Knowledge Gaps

The study has highlighted a number of knowledge gaps in the understanding of fault stability analysis:

- Faults within reservoirs are generally well characterised in terms of stress regime and orientation but there is less detail on fault properties that transect cap rocks and extend into the overburden. Changes to mechanical and hydraulic properties of faults that extent into cap rocks and the overburden, that become reactivated during and post CO_2 injection, are not fully understood.
- In-situ stresses on a fault in a sealing formation may be different from those within a reservoir because of pore pressure differences. Insitu tests, such as leak-off tests or laboratory measurements from core samples, would be ideal but are rarely obtained because historically sealing formations have been of limited interest.
- Geomechanical modelling of faults requires detailed data on fault properties however detailed core samples of fault material are usually limited and the geometry is not necessarily known. This can lead to uncertainties in modelling results. Better calibration is necessary to develop constitutive models to predict various failure modes caused during fault reactivation.
- Fault stability and movement is strongly dependent on pore pressure. The pattern of pore pressure change within fault zones is not usually known. The CO_2 entry pressure into a fault zone might differ compared with the overburden. More detailed knowledge of pore pressure

distribution between permeable and less-permeable formations, including fault zones, would improve modelling and reduce uncertainty.

- Relatively few studies have been completed on the influence of CO_2 on the frictional properties of different rock types. Longer exposure times, under experimental conditions, might provide more representative results.
- Observations from oil and gas reservoirs have revealed that the same stress path during depletion is not followed during repressurisation. This phenomenon is important for estimating reservoir compaction/expansion, surface movement and identification of minimum pore pressure required to cause fault reactivation.

Rapport / Report

Criteria of Fault Geomechanical Stability During a Pressure Build-up

Final Report

20130613-02-R
26 September 2014
Revision: 0

Project

Project title:	Criteria of Fault Geomechanical Stability During a Pressure Build-up
Document title:	Final report
Document No.:	20130613-02-R
Date:	26 September 2014
Revision/Rev. date:	0

Main office:
PO Box 3930 Ullevål Stadion
NO-0806 Oslo
Norway

Trondheim office:
PO Box 1230 Sluppen
NO-7462 Trondheim
Norway

T (+47) 22 02 30 00
F (+47) 22 23 04 48

BIC No. DNBANOKK
IBAN NO26 5096 0501 281
Company No.
958 254 318 MVA

ngi@ngi.no
www.ngi.no

Client

Client:	IEAGHG
Client's contact person:	James Craig
Contract reference:	IEA/CON/13/214

For NGI

Project manager:	Bahman Bohloli
Prepared by:	Bahman Bohloli, Jung Chan Choi, Elin Skurtveit, Lars Grande, Joonsang Park, Maarten Vanneste
Reviewed by:	Hans Petter Jostad, Nazmul Haque Mondol

Executive Summary

This report provides a thorough overview of faults and their geomechanical stability due to CO_2 injection and pore pressure changes in reservoirs. It focuses on fault structure, hydro-mechanical properties of fault planes and the methodologies generally employed to assess fault stability. The approach of the report is to offer a solid background on faults from a geomechanical point of view and highlight the essential components affecting the mechanical stability of faults due to CO_2 injection and pressure build-up in storage units.

Injection operation and pressurization of reservoirs usually changes the state of the in-situ stresses which may cause destabilization of previously stable faults. The instability occurs in the form of slip along pre-existing faults or fracture systems, which may be associated with seismicity. In addition, the movement of faults and the generation of fractures may create open conduits that breach the integrity of storage reservoirs and lead to the leakage of fluids to the surrounding overburden or even to the surface. Induced seismicity and the risk of leakage are two major concerns over the geological sequestration of CO_2.

Faulting is the response of brittle material to a stress field that exceeds its shear strength threshold. Faults nucleate from micro-fractures or deformation bands in a critically stressed region and accumulate strain over time to grow. As faults develop, they may interact with neighbouring faults of various sizes and form special features important in the context of CO_2 storage. A fault zone typically consists of two sub-structures; a fault core and a fault damage zone. Slip often occurs along a single plane but damage can accumulate in large faults. The fault core generally comprises gouge material, crushed particles/cataclasite or ultracataclasite (or a combination of the two). The damage zone typically contains fractures at different scales. Faults in low porosity rocks have a fine-grained fault core surrounded by a fracture dominated damage zone. On the other hand, faults in coarse-grained, high porosity rocks usually have low porosity deformation bands that develop into high permeability slip surfaces.

Leakage through faults is a function of the permeability of a fault zone. Fault zone (bulk) permeability increases with increasing fluid pressure towards a critical threshold. Permeability of the fault core depends mainly on the properties of fault gouge material. The gouges are either granular or clay-rich. Permeability of granular material depends on the grain size distribution and sorting of grains, and permeability of clay-rich gouges is a function of the type of clay, clay percentage, and its distribution. The extent of hydration and the adsorption and swelling properties of clay can also affect permeability.

Faults are usually the weakest components in the rock mass and control hydraulic and mechanical behavior of rock bodies. Mechanical failure/reactivation of faults may occur through:

i) shear failure when shear stress exceeds shear strength of fault zone material,
ii) hydraulic fracturing (in case of cohesive faults) when the pore pressure exceeds the sum of the minimum in-situ stress and the tensile strength of a fault,
iii) Ductile aseismic slips.

In the case of shearing, post failure deformation may be brittle or ductile, depending on the shear strength properties and the level of the effective confining stress. Temperature, hydration state and chemistry also influence deformation. In a brittle regime, deformation occurrences associated with dilation strongly contributes to the enhancement of permeability and increases the risk of leakage. In contrast, ductile deformation may have only a limited effect on the permeability and may in the long term decrease it.

Reactivation of faults and fracture systems can be assessed using analytical and numerical approaches. Typically the analytical approach considers static normal and shear stresses on the fault plane and relies on the Mohr-Coulomb failure criterion to evaluate fault stability. The critical injection pressure is assessed from the difference between the current stress state and the predicted failure envelope. The critical injection pressure, also called the maximum sustainable pressure, can be calculated for all possible fault orientations at given in-situ conditions. The critical pressure is then plotted in a variety of ways but often using a polar stereographic projection to present stable versus unstable faults with certain dip and strikes. The analytical approach is a simple and valuable tool for preliminary assessment of fault reactivation potential during injection or depletion in the above form. It, however, is based on many assumptions and simplifications that ignore the complex structural setting and cannot capture complex physical processes and fault interactions that could occur during injection operations. These limitations require the use of numerical tools that model the entire system.

Numerical analyses of fault stability can provide fault simulations at different scales and within different geological constraints. A fault can be presented in a global model as a single discontinuity, e.g. as a zero-thickness element, in order to explore its general behaviour. If the fault is prone to instability, and the detailed behaviour of the fault zone is of interest, it may be modelled as a rock mass of continuum material. This may require a local model where the detailed properties and the geometry of the fault zone are assigned to the components of the model. Furthermore, post-failure behaviour of faults is important for fault leakage and seal failure which can be studied using numerical methods where dilatancy and stress dependent permeability are taken into account.

The widely used criterion for stability analysis of faults is the Mohr-Coulomb failure criterion which requires knowledge of the in-situ and induced stresses as well as the strength of faults. The strength of a fault is usually expressed in terms of cohesion and friction angle/coefficient. Data from laboratory tests and field observations show that friction coefficients of faults generally vary between 0.6 and 0.85, although values as low as 0.2 have also been reported in the literature for clay material. The strength of faults in a CO_2 storage reservoir may be affected by the presence of CO_2 to a limited extent. Evidence from a few studies available in the literature show that the coefficient of friction of the fault-filling minerals does not change pre- and post –CO_2 treatment. This observation is, however, based on a few laboratory studies and only valid for short-term effects of CO_2 on rocks/minerals.

In brief, the Mohr-Coulomb failure criterion is the major stress-strength relationship employed for stability analysis of faults during injection of fluids such as CO_2, or depletion of hydrocarbons. Analytical methods combined with the numerical solutions provide the best approach for assessing geomechanical stability of faults.

Contents

1 Introduction 8
1.1 Background 8
1.2 Objective of the study 9
1.3 Fault reactivation and its consequences 10
1.4 Structure of the report 10

2 Faulting and fault zone properties 12
2.1 Formation of fractures and faults 13
2.2 Growth and interaction of faults 17
2.3 Fault zone structure 20
2.4 Permeability of fault zones 25
2.5 Fault seal vs fault leak 30

3 Assessment of CO_2 injection-induced fault reactivation 35
3.1 Analytical approach to evaluate fault reactivation 36
3.2 Limitations of the analytical approach 39
3.3 Numerical approach 46
3.4 Effect of fault reactivation on sealing integrity 55
3.5 Summary and recommendation 57

4 Input parameters for fault reactivation analysis 60
4.1 Determination of in-situ stresses 60
4.2 Strength and friction coefficient of faults 68

5 Conclusions and Knowledge Gaps 79
5.1 Conclusions 79
5.2 Knowledge Gaps in Understanding Fault Stability Analysis 80

6 References 83

Review and reference page

1 Introduction

1.1 Background

Geologic sequestration of CO_2 is one of the promising solutions to mitigate greenhouse gases and combat drastic climate change. In order for underground CO_2 storage to have a noticeable impact on the reduction of atmospheric greenhouse gases, it should be implemented at large scale, i.e. in the order of Giga tonnes per year. To accommodate such enormous quantities of CO_2, geological formations of sufficient capacity and injectivity are required. Experience from several CO_2 storage projects like Sleipner, Snøhvit, In Salah and Weyburn shows that geological sequestration of CO_2 is technically feasible despite some challenges, e.g. the geomechanical response of formations to injection-induced stress. In all these projects, the volume of injected CO_2 is in the range of hundreds of thousands of tonnes to a maximum of about one million tonnes per year. Already at this scale, some geomechanical instabilities of reservoir structures or surroundings have been observed due to the overpressure in some of these CO_2 storage reservoirs. Thus, for injecting larger amounts of CO_2, detailed investigation of storage sites, and design of appropriate injection strategies, will be crucial.

Storage capacity, maximum sustainable pressure and the risk of CO_2 leakage are all dependent upon the structural integrity of the storage complex. As shown diagrammatically in Figure 1.1, injection operations alter stress conditions not only in CO_2 storage reservoirs but also in the surrounding formations. Additional risks may be associated with engineering deficiencies. If these operations are not well controlled, they may lead to failure of rock masses along pre-existing faults or fractures (fault/fracture re-activation), which may increase the risk of fluid leakage to the surrounding overburden or to the surface (Rutqvist, 2012). In addition, fault reactivation may generate felt events and raise negative public perspectives (Ellsworth, 2013).

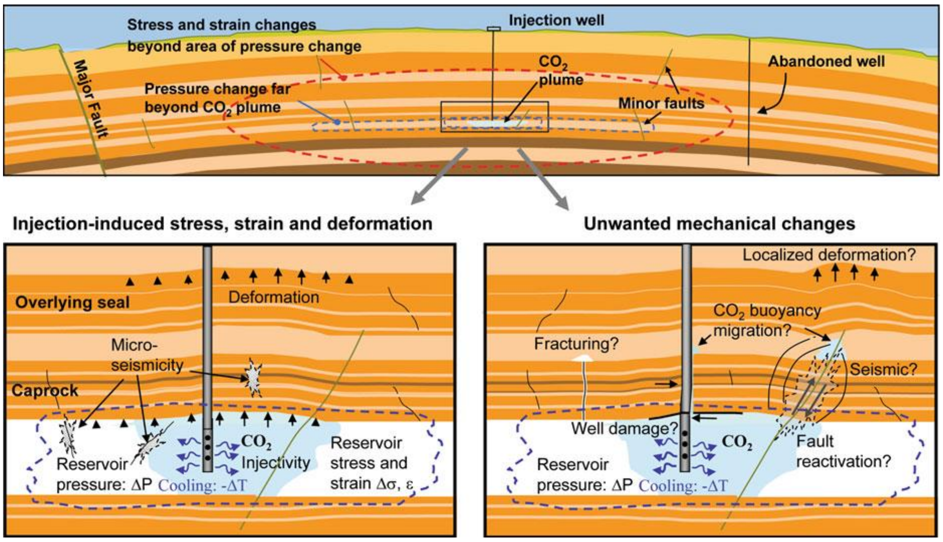

Figure 1.1 Geomechanical processes and key technical issues associated with CO_2 storage in deep sedimentary formations (after Rutqvist, 2012).

A fault is defined as a planar discontinuity in a geological formation, across which relative displacement has occurred. The risk of fault reactivation is one of the crucial elements in the assessment of a site for CO_2 storage. There is considerable evidence for fault reactivation during geological time. O'Brian et al. (1999), for instance, studied fault reactivation and consequent fluid migration in Timor Sea, Australia. They reported significant fluid migration through reactivation of faults and concluded that, the moderately reactivated faults leaked for a relatively extended time period of about 100,000 to 1,000,000 years while the strongly reactivated faults leaked for time periods of about 10,000 to 100,000 years. Therefore, fault stability should be considered carefully during pressurization of a geological system which likely contains faults that are visible on seismic sections, or below the resolution of seismic surveys. Fault reactivation and consequent trap breach is commonly accepted as the mechanism to explain dry traps that preserve evidence of widespread oil leakage (Dyt et al., 2012; Zoback and Zinke, 2002; O'Brian et al., 1996).

Depleted hydrocarbon reservoirs are attractive options for CO_2 sequestration sites as their seals have kept hydrocarbons in place over geological timescales providing efficient hydrocarbon traps. Their initial reservoir pressure is often assumed to provide a rough indication of the sustainable pressure in the reservoir. However, the stress state in such formations might have been altered by pore pressure reduction in the reservoir during production and the stress path may not necessarily be reversible. Therefore, the reservoir stress path during depletion and CO_2 injection should be considered carefully for such storage sites. Usually a threshold pressure is designed for each reservoir, and injection pressure is kept below that level to avoid breaching the seal. However, the threshold pressure for shear or hydraulic fracturing of intact formations is different from that for pre-existing faults (Sibson, 2003a). Thus, fault stability analysis is an important factor for the safety assessment of any CO_2 storage project (Hung and Wu, 2012) as is also the case for water or cutting slurry injection.

Assigning properties to fault zones is a difficult task and involves several uncertainties. To overcome this issue, a sensitivity study is usually carried out to investigate the impact of various material properties on fault reactivation. For example, Rutqvist et al. (2013) reported that the dilation angle did not have any significant impact on the estimated rupture length if it is between 0 and 20 degrees. However, the residual friction angle had a significant effect on the rupture length and the associated magnitude of induced or triggered events. A friction angle reduction from 20 to 11, (i.e. friction coefficient from 0.36 to 0.2) increased the seismic magnitude from 0.15 to 0.72, a five-fold increase.

1.2 Objective of the study

This study aims to provide a comprehensive literature review of assessments of fault geomechanical stability due to pressure build-up in CO_2 storage sites. It presents various approaches for fault reactivation analysis and comments on the methodologies and concepts.

1.3 Fault reactivation and its consequences

Faults are generally speaking weak zones within the rock volume. They may be the primary planes of slip or movement if any such displacement has to occur. Depending on the geological stress regime, rock bodies and thus faults, are under compression, shearing or extension. When the compressional or tensile stress on the fault plane increases, it may trigger fault failure and cause slip. This is called fault reactivation. Fault reactivation has a wide range of consequences. It may release the stored energy dynamically and induce seismicity, shear boreholes, and change formation permeability.

In the context of CO_2 storage, the key issues for reactivation of faults are leakage of the gas and induced seismicity. Fault reactivation may increase permeability of fault zones and thus provide conduits and leakage paths to surrounding formations. Leakage from the reservoir may be small or large depending on the response of the fault to pressure release. However, in some circumstances this may provide a benefit in terms of storage capacity or pressure reduction. If leakage occurs, reservoir pressure drops. When local pressure falls below the critical pressure, the reactivated fault may be closed off. This may lead to a limited leakage of gas from the storage reservoir. On the other hand, if fault displacement has resulted in conduits that are open, and do not heal after pressure decrease, the leaked volume of CO_2 may be large.

Displacements resulting from fault reactivation may happen quickly or slowly. In the first case, earthquakes will happen at the time of slip (called seismic fault slip). In the latter case, no earthquake may be observed due to the slow movement of rock bodies against each other (called aseismic fault slip). The magnitude of induced earthquakes is a function of fault rock properties, the size of the slip patch which is affected by the volume of fluid injected or extracted and the rate of injection/extraction. Induced earthquakes are generally small (less than M4.5) but on very rare cases may exceed M6 (IEAGHG, 2013). The largest magnitudes (mainly between M5 to M7) have been reported from the extraction of fluids and the medium to lowest ones (M1.1 to M4.8) from fluid injection and enhanced geothermal systems (for further details see Table 1 p 55 in IEAGHG, 2013).

1.4 Structure of the report

This report includes five chapters. Chapter 1 gives a background for fault stability analysis. It provides a technical background to the problem along with some very general aspects of fault reactivation; e.g. what fault reactivation is and what are the consequences of a fault failure and breach of seal integrity. Chapter 2 presents faults and properties of fault zone material. The focus is on the permeability of faults since it is a paramount factor contributing to potential leakage in the case of fault reactivation. Chapter 3 gives an overview of the various methods used to assess reactivation of faults. It also provides an evaluation of the methods employed and their limitations for capturing all aspects of a geological system during a pressure build-up and possible shear failure of faults. Chapter 4 reviews input parameters required for analysis of fault stability and the methodologies to determine such factors. Chapter 5 summarizes the results of the study and lists some of the knowledge gaps for geomechanical stability analysis of faults.

2 Faulting and fault zone properties

Faults are planes of discontinuity in geological formations across which relative displacement of adjacent layers has occurred. Faulting is the response of brittle material to a stress field that exceeds its strength threshold. They nucleate from micro-fractures or deformation bands in a critically stressed region and accumulate strain over time to grow (Fossen, 2010). Different types of faults may form depending on the stress field (Figure 2.1). Details of fault terminology, geometry and characteristics can be found in e.g. Price and Cosgrove (2005), Fossen (2010) and Burg (2013). Initiation of fractures, formation of faults and their properties are important components when considering fault stability analyses, fault reactivation potential and possible propagation of faults through the sealing units. These components are elaborated further in the following sections.

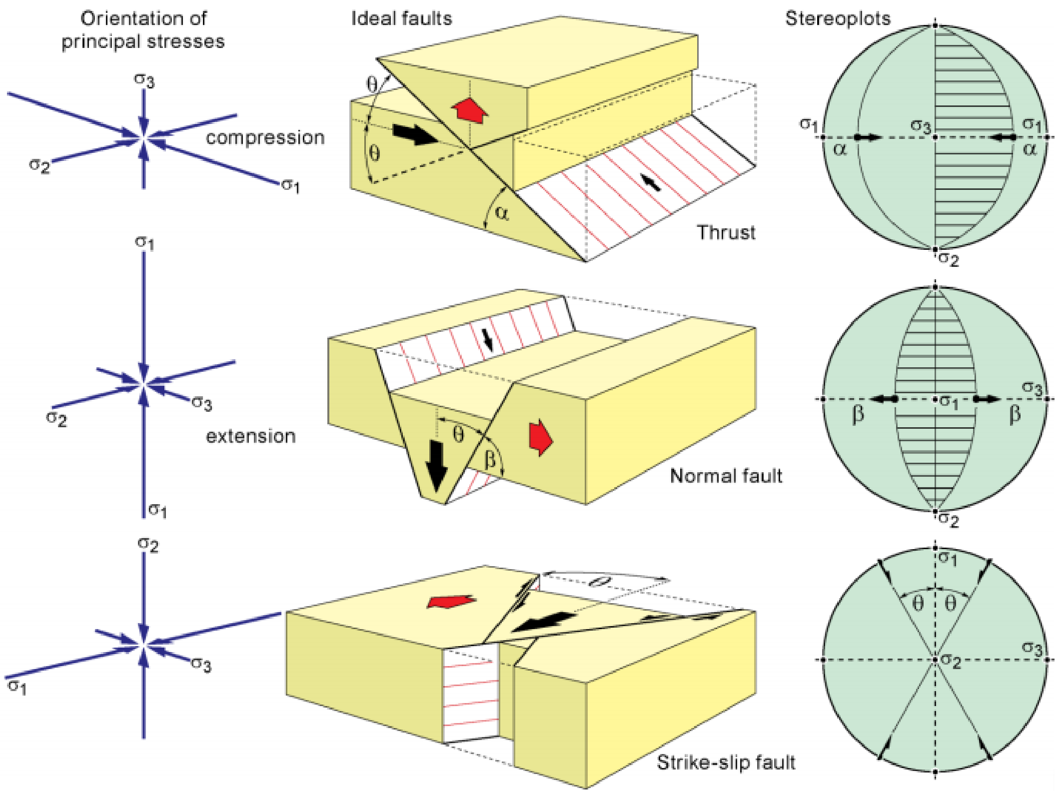

Figure 2.1 Orientation of principal stresses and associated fault types (After Burg, 2013). Stereoplots present the state of principal stresses along with the slip plane on the lower hemisphere.

2.1 Formation of fractures and faults

2.1.1 Fracture initiation mechanisms

There are several theories on fracture initiation in solid material among them the Griffith criterion of fracturing which is widely accepted as an explanation for the behaviour of rock material under critical loading conditions. Griffith (1921) based his analysis on the assumption that material contains numerous defects in form of microcracks, voids, grain boundaries and flaws of various sizes (Figure 2.2). He considered, for mathematical simplicity, that flaws have elliptical shapes. When material is loaded, stress concentration and magnification occurs at the extremities of the flaw leading to initiation of tensile cracks (Figure 2.2). The stress magnification is a factor of (2L+1)/l where L and *l* are the larger and smaller diameter of ellipse respectively (see Figure 2.2a). This means that elongated and flattened flaws will experience larger stresses and start cracking first.

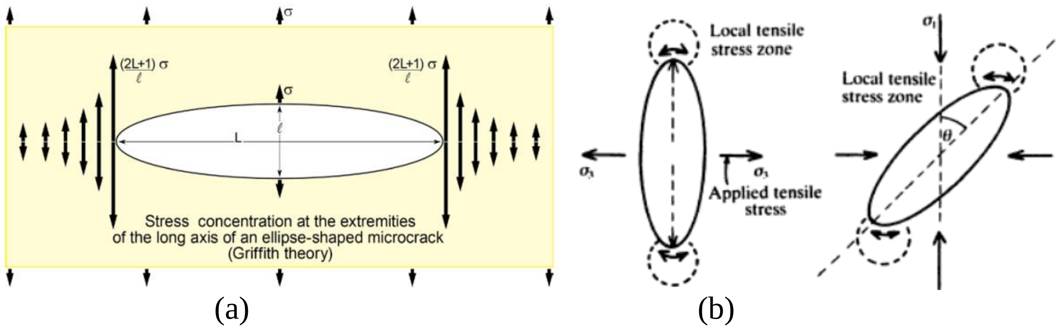

Figure 2.2 Stress concentration around elliptical spaces based on Griffith's theory of failure. Stresses around the extremity of flaws; (a) under uniaxial tension (after Burg, 2013) and (b) under biaxial compression (after Price and Cosgrove, 2005).

Under axial compression, larger cracks become activated first. Without lateral confinement, they continue to grow leading to axial splitting (Horii and Nemat-Nasser, 1986; Alves and de Lacerda, 2012). In the presence of lateral confinement, their growth is arrested and optimally oriented cracks will be activated. This builds a narrow zone containing many microcracks that develop to a macroscopic failure plane (Horii and Nemat Nasser, 1986; Moore and Lockner, 1995; Jung 2013) (see Figure 2.3).

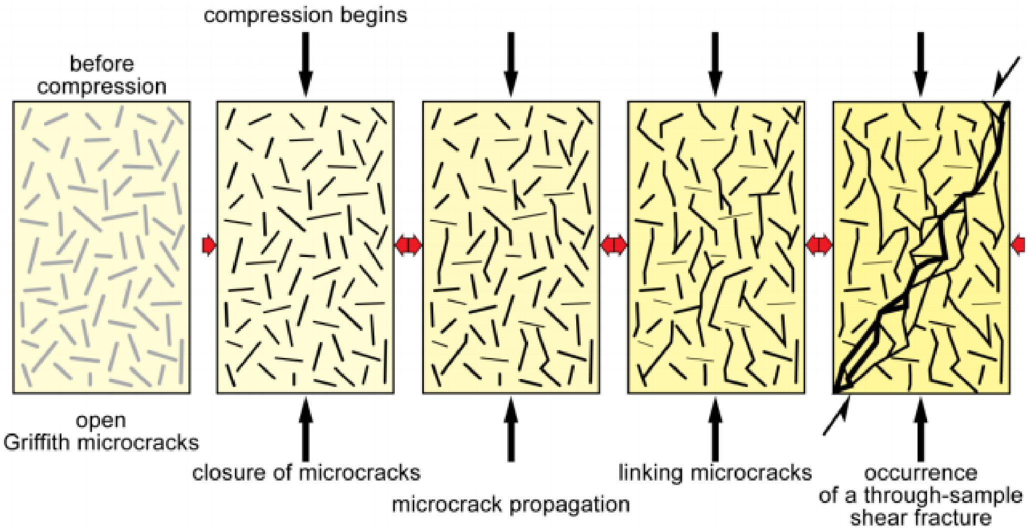

Figure 2.3 *Griffith's theory of fracture in brittle material. Optimally oriented flaws in a specimen subjected to compressional loading will start cracking in tension. Coalescence of these cracks creates a macroscopic shear failure plane (after Burg, 2013).*

Horii and Nemat-Nasser (1986) carried out an extensive experimental study on a 6 m thick Columbia resin, CR39, containing a straight slit. They observed nucleation and growth of tensile cracks from the tip of the pre-existing flaw leading to axial splitting, if there is no lateral stress, but observed a tilted failure plane in the presence of lateral confinement. Griffith's theory seems to provide a good explanation for the initiation of fractures in rocks (Hori and Nemat Naser, 1986; Ashby and Hallam, 1986; Ashby and Sammis, 1990; Moore and Lockner, 1995).

2.1.2 Fracture propagation at an interface

Development of fractures in a material is a function of the local stress field. Stress field in a rock mass may vary because of its inhomogenieties such as layering, faulting and discontinuities and thus control propagation of fractures within the rock mass or a fault zone. When a propagating fracture reaches a discontinuity, it may a) become arrested, b) penetrate through the interface or c) become deflected (Figure 2.4). Fracture deflection or arrest at a contact depends on several factors (Gudmundsson et al., 2010):

i. the induced tensile stress ahead of the propagating fracture tip,
ii. rotation of principal stresses at the interface, and
iii. material toughness of the discontinuity relative to that of the adjacent layers.

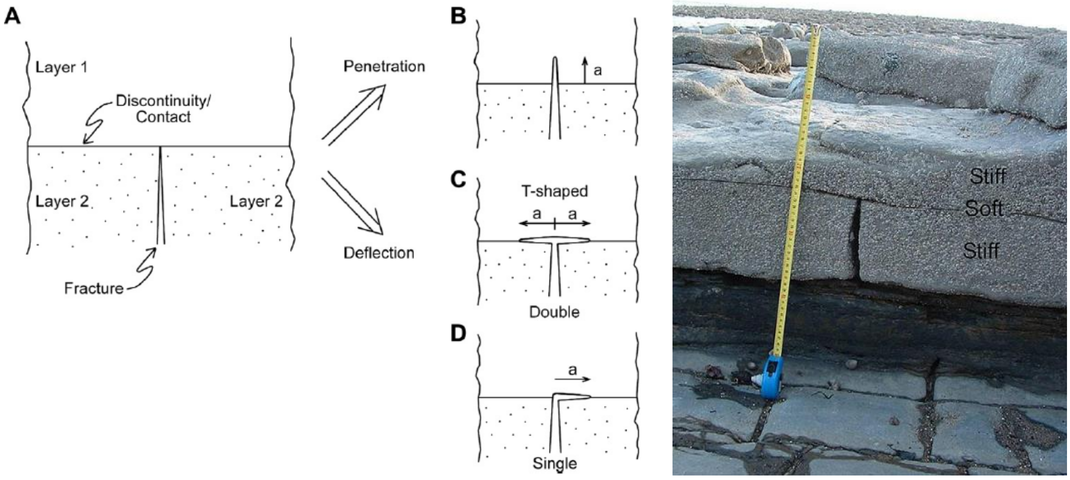

Figure 2.4 *Fracture propagation in a solid material. Left) Different scenarios for a propagating fracture that reaches an interface, and right) a picture showing a fracture arrested at the interface between two rock layers, (after Gudmundsson et al., 2010).*

An extension fracture will penetrate across a discontinuity, if layers on either side of the discontinuity have the same mechanical properties and if there is stress coupling. Under this condition the strain energy release rate (*Gp)* for penetration reaches the critical value for fracture extension, namely the material toughness of the layer into which the fracture is approaching:

$$G_p = \frac{(1-\nu^2)K_I^2}{\mathrm{E}} = \Gamma_L \tag{2.1}$$

where ν is the Poisson's ratio, K_I is the stress intensity factor, E is Young's modulus and Γ_L is the material toughness of layer.

By contrast, the fracture will deflect into the discontinuity if the strain energy release rate reaches the material toughness of the discontinuity itself (G_d). Fracture propagates in a mixed-mode (mode I (K^2_I) and II (K^2_{II})) along the discontinuity (Xu et al., 2003; Wang and Xu, 2006). Deflection into the discontinuity occurs if:

$$G_d = \frac{(1-\nu^2)}{\mathrm{E}}(K_I^2 + K_{II}^2) = \Gamma_D \tag{2.2}$$

where the stress-intensity factors K_I and K_{II} refer to the discontinuity. From Equations (2.1) and (2.2), the extension fracture penetrates the discontinuity if:

$$\frac{G_d}{G_p} < \frac{\Gamma_D}{\Gamma_L} \tag{2.3}$$

but becomes deflected if:

$$\frac{G_d}{G_p} \geq \frac{\Gamma_D}{\Gamma_L} \tag{2.4}$$

Equations (2.1-2.4) control, at least partly, whether a fracture penetrates or becomes deflected along a discontinuity in a fault zone. Fracture penetration, deflection and arrest has a big impact on how fault damage zones and cores grow and change hydro-mechanical properties with time (Gudmundsson et al., 2010).

Numerical modelling of fracture propagation at interfaces has been tried more recently by Garcia et al. (2013) (Figure 2.5) which shows a similar pattern to those presented in Figure 2.4.

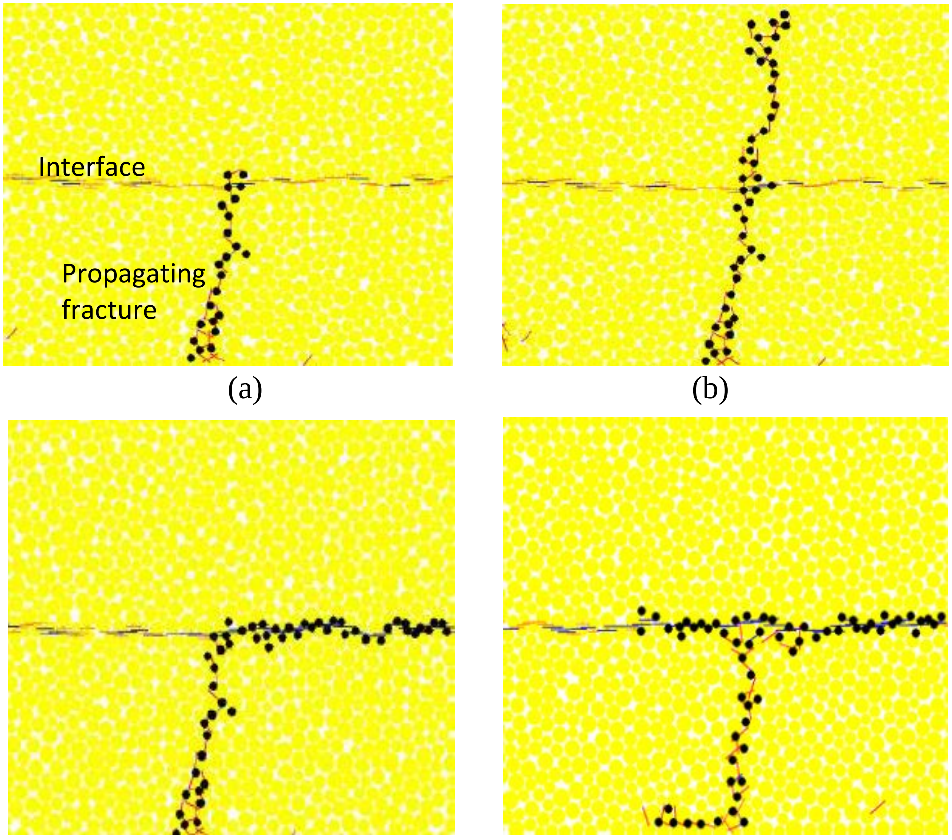

(a) (b)

(c) (d)

Figure 2.5 Fracture propagation at an interface (modified after Garcia et al., 2013). Fracture is either arrested at the contact (a), penetrated through the interface (b) or is deflected (c) and (d).

Propagation and development of fractures at a larger scale in homogeneous brittle material is illustrated in Figure 2.6 in which a material is subjected to shear deformation, concentrated over the zone A-B (Figure 2.6a). Extension cracks form in the direction of maximum principal stress. Rotational movement in later stages of the shearing process may cause propagation of the extension cracks such that they form characteristic S-shape fracture surfaces. The formation of shear fractures in "en échelon" arrangement with respect to the direction of shear deformation (Figure 2.6b) follows the extensional cracking. These fractures, commonly termed Riedel shears, can be distinguished into two different sets, named R1 and R2. R1 fractures are generated first, then alteration of the local stress field initiates R2 fractures. A third category, called P-shears or thrust shears can develop in the direction indicated in Figure 2.6d (Leijon, 1993). Progression of shearing often forms curved fractures that interconnect the already existing "en échelon" oriented shear cracks. The result is a zone with a pattern of interconnected, undulating structures containing elongated lenses of relatively undisturbed material. When total shear deformation increases, displacement accumulates over certain shear planes. Such planes accommodate further deformation and grow in length and width. They eventually develop into a distinct fault zone.

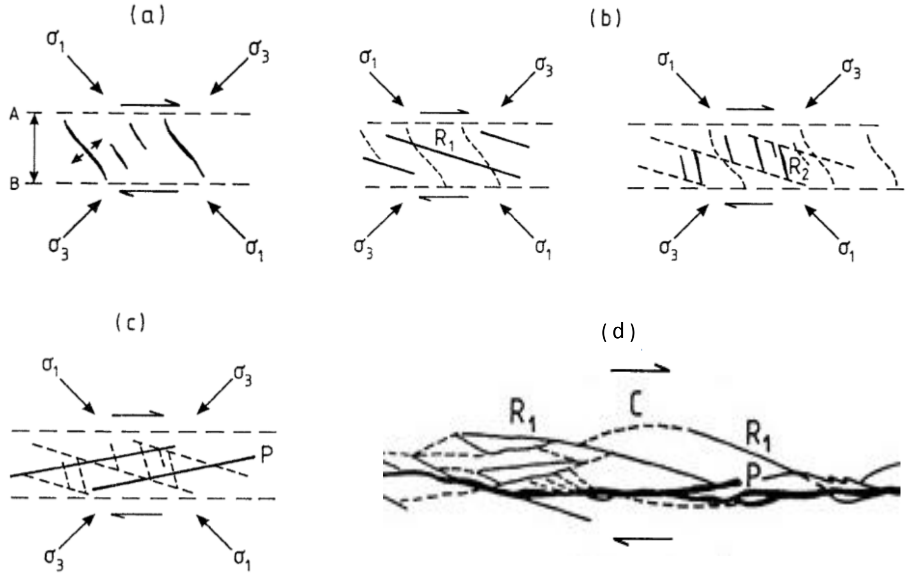

Figure 2.6 Schematic illustration of basic fracture types generated in homogenous, brittle material subjected to localized shear deformation. Extension cracks form parallel to the maximum principal stress within the section subjected to shear (a), development of Riedel shears, R1 and conjugate Riedel shear, R2 (b), and development of P shears (c). Interconnection of R- and P -shears by curved crack, through going shear planes and shear lenses (d) (modified after Leijon, 1993; Cuisiat and Høeg, 2002).

2.2 Growth and interaction of faults

As faults grow in length, they may interact with the neighbouring faults of various sizes and form special features important in the context of hydrocarbon production or fluid injection (Figure 2.7). The interaction zone between two faults may result in folding between them building structures called relay ramps (Fossen, 2010; see Figure 2.8). Relay ramps can play an important role in terms of hydraulic communication between faults that might otherwise have acted as seals (Di Bucci et al., 2005; Burg, 2013). Such structures may be below the resolution of seismic data.

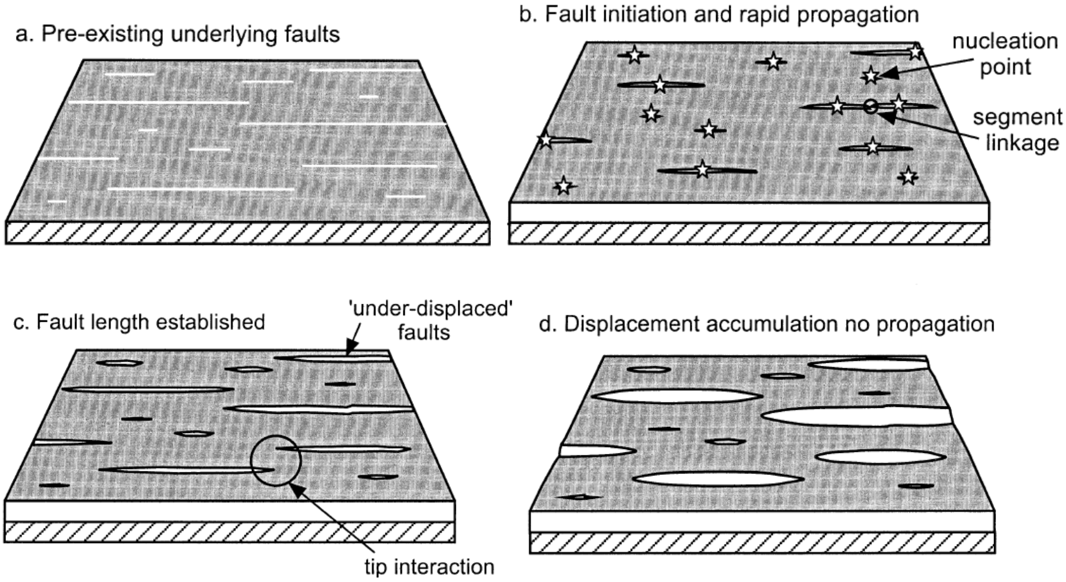

Figure 2.7 Schematic block diagram illustrating a model for growth of faults using sequential fault maps from the base of a syn-faulting sequence (after Walsh et al., 2002).

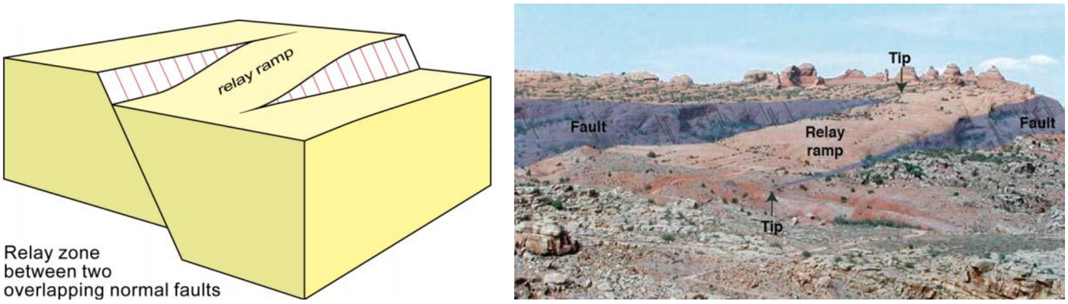

Figure 2.8 Linkage between two faults; (a) schematic illustration of two normal faults, building a relay ramp structure (after Burg, 2013) and (b) actual example of a relay ramp from Arches National Park, Utah (after Fossen, 2010).

When faults run sub-parallel and link together, the region between the faults will experience some deformation and thus may differ in hydromechanical properties than the surrounding rocks. This zone called a "linking damage zone" is illustrated in Figure 2.9. Such zones often have low strength properties, and dense fracture systems and thus might be prone to slip or leakage during pressurization of the formation (Cerveny et al., 2005).

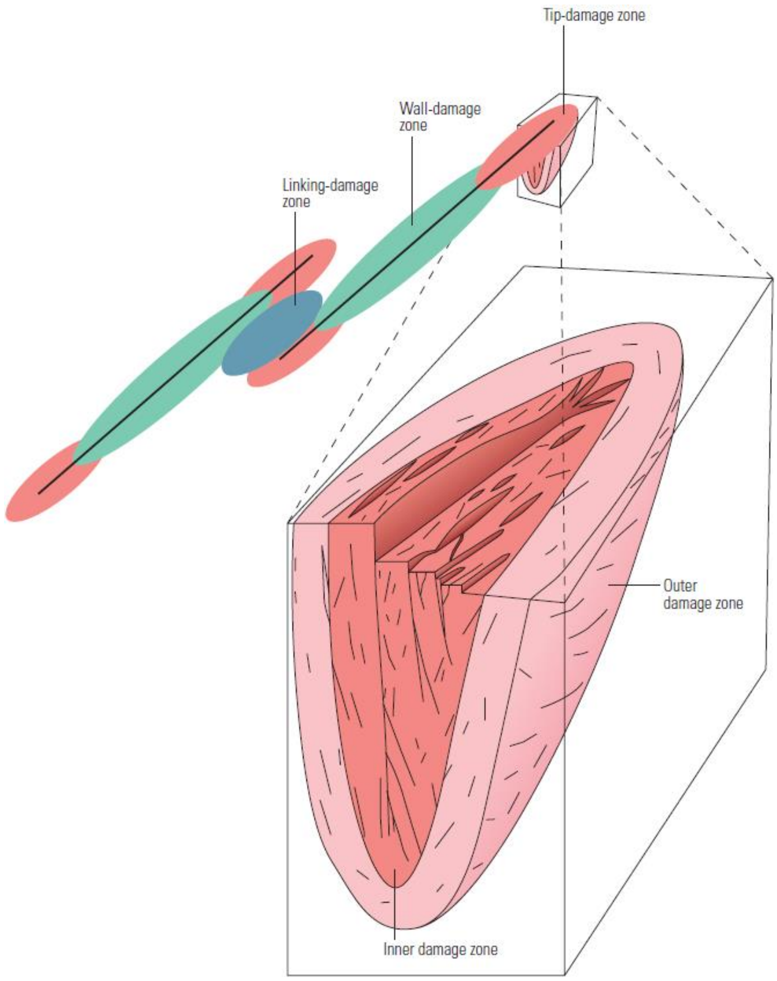

Figure 2.9 *A 3D conceptual model for illustration of different damage zones around faults (after Cerveny et al., 2005).*

Fault growth is a self-similar process over many orders of magnitude in which fault displacement (*D)* scales linearly with fault length (*L)* (Cowie and Scholz, 1992; Gillespie et al., 1992; Scholz et al., 1993; Schlische et al., 1996; Faulkner et al., 2010 and Fossen, 2010) (Figure 2.10):

$$D_{max}= \gamma L^n \tag{2.5}$$

where D_{max} is maximum fault displacement, L is the length of fault and γ and n are constants. Field measured fault data seems to fit well into a linear diagonal line of D_{max}-L plot in a logarithmic scale with slope γ (n=1). The maximum displacement (D_{max}) along a fault is a function of fault geometry and strength of rock. Particular trajectories on *D–L* diagrams can reveal physical controls on fracture growth, such as stratigraphic confinement or segment interaction and linkage (Schultz and Fossen, 2002).

The *D-L* relationship can be of interest in many applications. For instance, when displacement is known from underground exploration data sets such as seismic or well logs, the length of a fault can be estimated. Although this gives a rough estimation only, it may be useful for applications such as CO_2 storage and hydrocarbon exploration and production. Energy release is also related to the area multiplied by the displacement, i.e. estimate of moment (Aki & Richards, 1980).

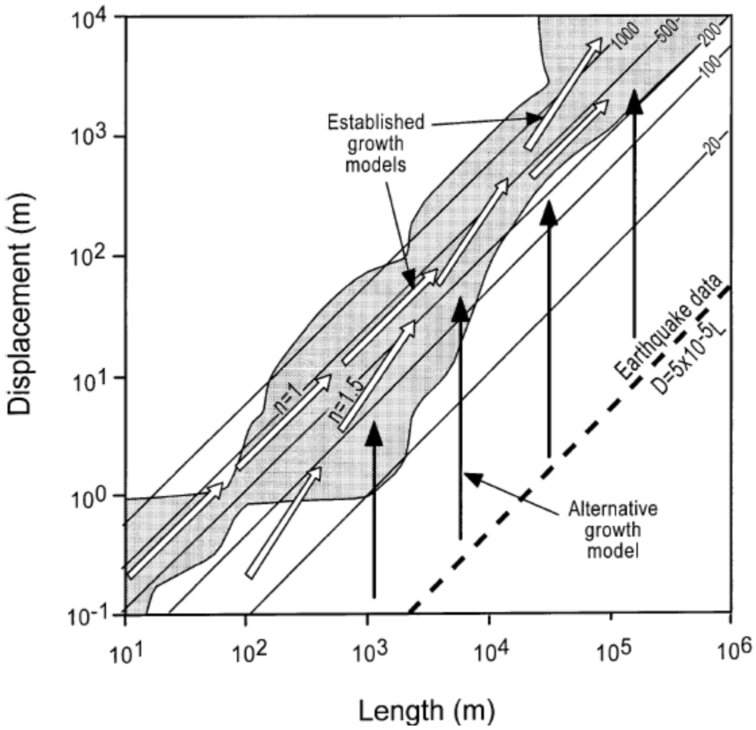

(a) (b)

Figure 2.10 Relationship between the maximum displacement and the length of faults (after Walsh et al., 2002).

2.3 Fault zone structure

Geometry, structures and characteristics of fault zones properties have been the focus of many studies over the past decades (e.g. Sylvester, 1988; Chester et al., 1993; Childs et al., 1996; Kim et al., 2001; Lyakhovsky et al., 2001; Chen et al., 2013; Luther et al., 2013). A fault zone typically consists of two sub-structures; the fault core and the fault damage zone (Figure 2.11). A fault core generally comprises gouge, cataclasite or ultracataclasite (or combinations of these materials). Damage zones typically contain fractures at different scales from micro- to macro-fractures that may accommodate small shear offsets and a small quantity of cataclasite (Faulkner et al., 2010). The concentration of deformation adjacent to larger faults forms the damage zone, which is important for the hydro-mechanical behaviour and the accumulation of strain (Chester and Logan, 1986; Koestler et al., 1992; Koestler and Milnes, 1992; Andresen et al., 1995). The fault damage zone evolves differently in three different stages of fault evolution:

a) the initial development of tip or process zone deformation,
b) the main slip accumulation stage, and

c) the late stage propagation (death zone features) which represents the last phases of fault activity.

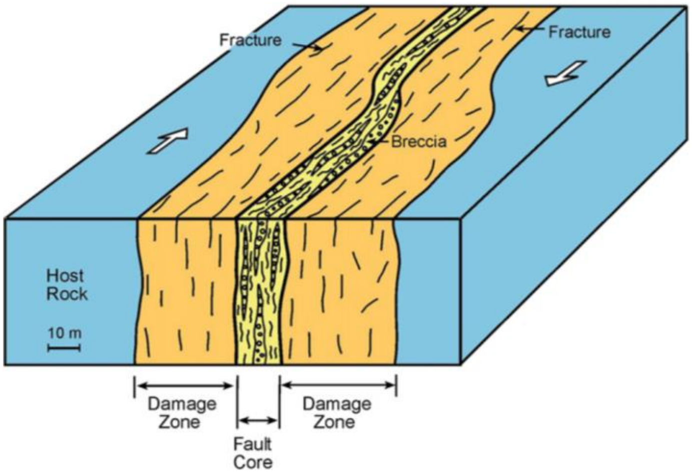

(a) (b)

Figure 2.11 (a) Illustration of fault core and damage zones in a strike-slip fault and (b) a photograph showing mineral-filled tensile fractures in a fault damage zone (after Gudmundsson et al., 2010).

In a study on small displacement faults, Vermilye and Scholz (1998) showed that the width of a fault damage zone scales with fault displacement. A similar observation was made by Mitchell and Faulkner (2009) (Figure 2.12). Thus, the width of the damage zone may be estimated from the length of faults, since the displacement of faults scales with their length.

Fracture density around faults is an important subject and has been investigated for many cases around the globe (Vermilye and Scholz, 1998; Hesthammer and Fossen, 2001; Wilson et al., 2003; Fossen et al., 2007; Mitchell and Faulkner, 2009; Faulkner et al., 2010). A maximum microfracture density is often observed immediately adjacent to the fault core and decreases with increasing distance from the core (Figure 2.13). Such plots of fracture frequency may also reveal the existence of unrecognized subsidiary faults. A damage zone is important for hydraulic conductivity because fracture intensity within such zones often lies above the percolation threshold (inter-connected fracture network), and thus allows fluids to migrate entirely through fractures (Koestler et al., 1992). This is also true for macrofractures detected on image logs (Paul and Zoback, 2008).

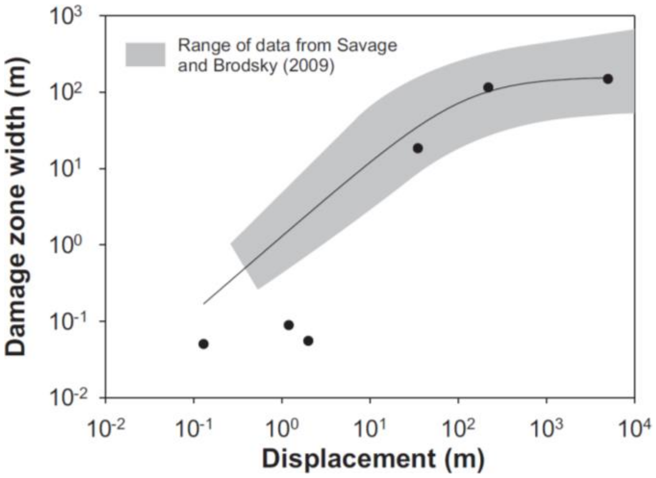

Figure 2.12 Width of damage zone versus fault displacement (after Faulkner et al., 2010). The black circles show microfracture data and the solid line shows the fitted line to the data from Mitchell and Faulkner (2009).

Studies from the North Sea (e.g. Koestler et al., 1992; Fossen et al., 2007) show that fracture frequency in sandstone reservoirs typically increases from a background frequency level of less than 50 fractures per 100 m, for the wells away (>200 m) from seismically mapped faults, to higher concentrations of 200-500 fractures per 100 m for wells closer to mapped faults. Even faults with throws of approximately 20 m can have structural frequencies above 100 fractures per 100 m.

In outcrops, damage zones can easily be recognized by significantly higher fracture frequency than in the adjacent blocks. The width and the total amount of fractures within a damage zone are highly dependent on burial depth during deformation, lithology of the faulted rocks and the faulting mechanism. Characteristics of fault zone sub-structures, e.g. widths of damage zones, types of fractures (i.e. shear or tensile), types of gouge materials, etc. have a significant impact on the fluid flow properties of fault zones.

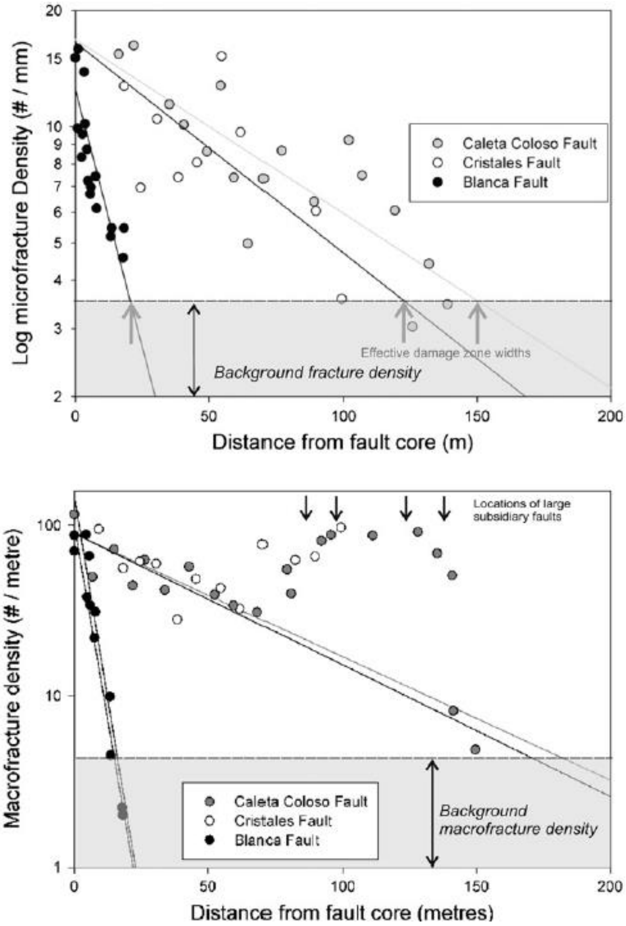

Figure 2.13 Density of microfractures and macrofractures around faults as a function of the distance from the fault core (Faulkner et al., 2010). Fracture density generally decreases with increasing distance from the fault. Data in the lower figure show the increase of macrofractures at the distance of about 70-100 m from fault core which is a signature of the subsidiary faults.

A fault may consist of a single core or multiple, sub-parallel cores (Figure 2.14). The structure of a fault zone depends on the properties of host rock, tectonic regime, depth of formation, magnitude of displacement, fluid flow, etc. For instance, faults in low porosity rocks have a fine-grained fault core surrounded by a fracture dominated damage zone (Faulkner et al., 2010; Balsamo et al., 2010). In contrast, faults in coarse-grained, high porosity rocks usually form low porosity deformation bands that often develop into high permeable slip surfaces (Fossen et al., 2007).

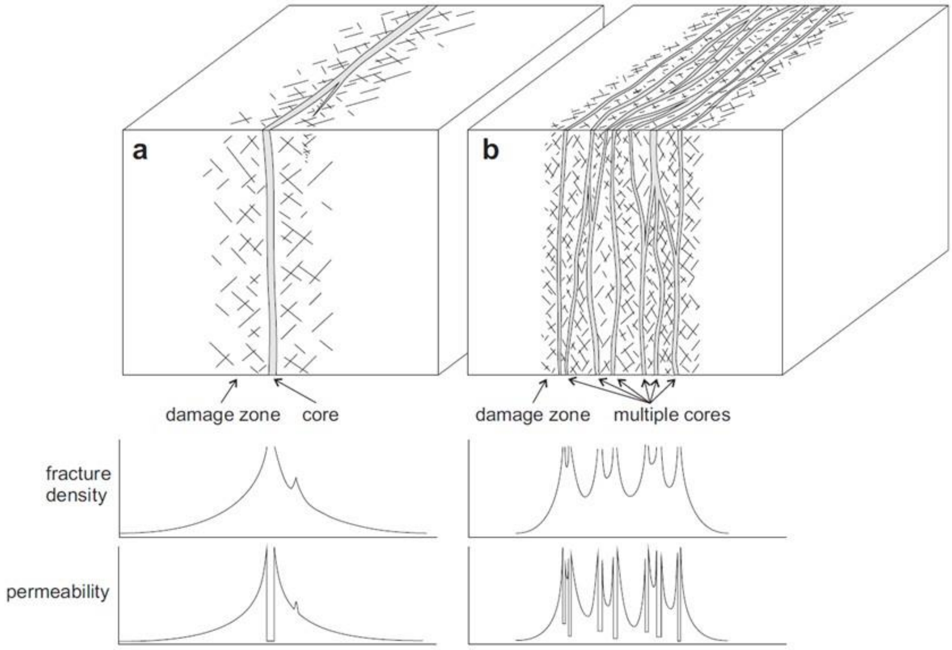

Figure 2.14 Diagram of the structures of single core and multiple core faults and their associated hydro-mechanical properties (after Faulkner et al., 2010).

Studies of the structure and properties of the San Andreas Fault (SAF) (Figure 2.15), explored during the SAFOD drilling program, revealed the presence of features around the fault similar to those discussed above (see e.g. Zoback and Hickman, 2005; Zoback et al., 2007; Zoback et al., 2010; Holdsworth et al., 2011; Hadizadeh et al., 2012). In addition, it showed a clear difference between active and inactive gouge zone materials (Figure 2.16). An active gouge zone contains numerous fractures at different scales while an inactive gouge zone material looks dense without clear fractures. These features affect hydraulic and strength properties of the damage zone material. The mechanically weakest material of the fault zone is found at the borders of and within the currently active shear zones, suggesting that the zones represent large-scale shear localization within the SAF core zone (Hadizadeh et al., 2012).

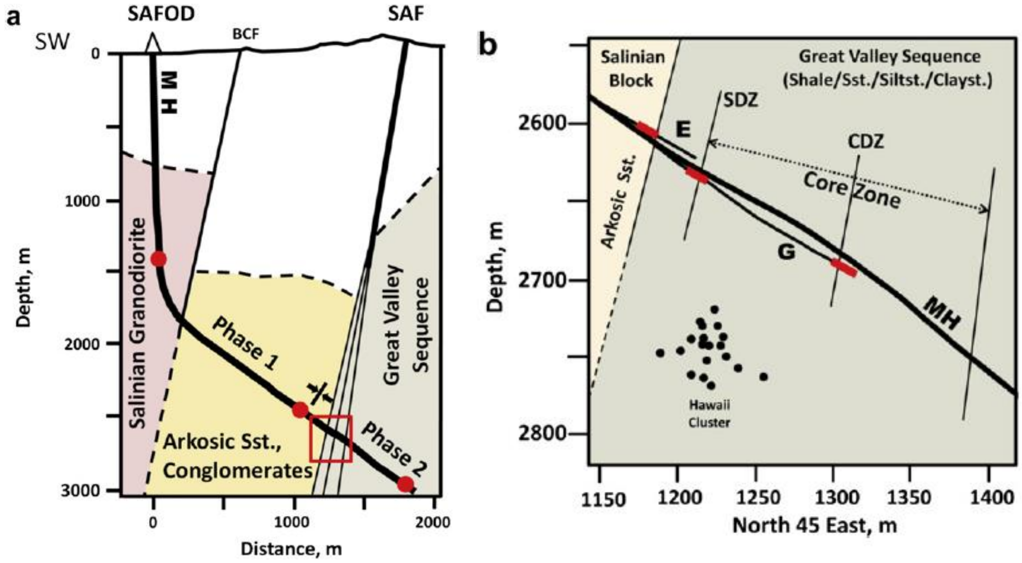

Figure 2.15 Structure of the San Andreas fault and the cored intervals (after Hadizadeh et al., 2012). The right figure shows the zoom-in of the red marked rectangle in the left panel within which the Phase II well penetrated a series of active slip zones.

a) b)

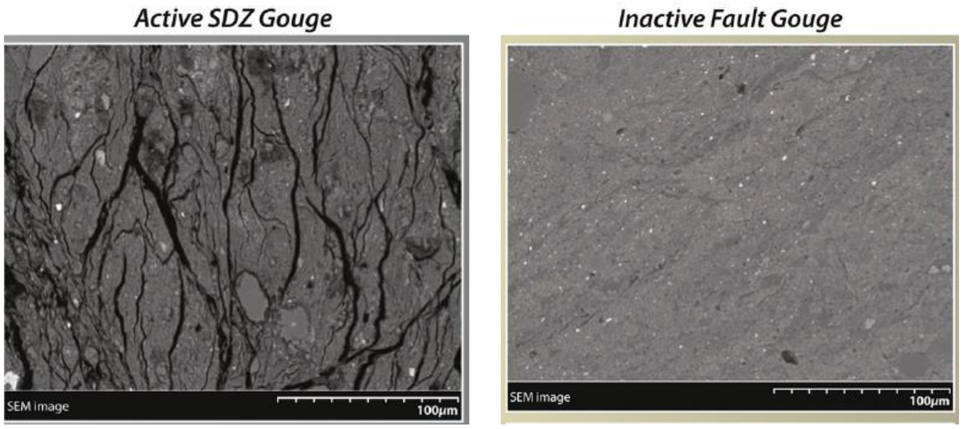

Figure 2.16 Structure of fault rocks from the damage zone of the San Andreas Fault. (a) An image of a rock sample from gouge of an active damage zone (South Damage Zone, SDZ) which shows significant fracture development, and (b) image from inactive fault gouge with almost no visible fractures (after Holdsworth et al., 2011).

2.4 Permeability of fault zones

Determining the permeability of faults is not an easy task. The conventional method for permeability measurement is to test a core specimen in the laboratory under specified stress conditions. This may not be applicable to faults as fault properties vary on multiple scales both across and along the fault (Mathias, 2012). In addition, the hydraulic properties of the fault core and of damage zone are quite different which makes the problem more complicated.

Permeability of fracture zones and faults has been studied by many researchers in the context of the structural integrity of hydrocarbon traps (Watts, 1987; Heggland, 1998; Talwani et al., 1999; Tadokoro et al., 2000; Faulkner and Rutter, 2000; Mildren et al., 2002; Bretan and Yielding, 2005; Dewhurst et al., 2005; Baghbanan and Jing, 2008; Faulkner et al., 2010 and Medeiros et al., 2010), as well as the injection of fluids into the subsurface (Rutqvist and Tsang, 2002; Li et al., 2006; Iding and Ringrose, 2010; Cappa and Rutqvist, 2011; Bissell et al., 2011). A number of conclusions can be drawn from their studies. For example:

- Macro- and micro –structures of fault zone material vary greatly for different rocks and under different stress conditions.
- Permeability of faults is a function of the stresses acting on the fault plane.
- Permeability is greatly enhanced as the stresses approach critical state (Faulkner et al., 2010; Mathias, 2012). For instance, fault permeability in the Pathfinder well on Eugene Island Gulf of Mexico, has increased from original value of 1 mD to about 1000 mD as fluid pressure increased towards the minimum in-situ stress (Losh and Haney, 2006; Mathias, 2012).

Bulk permeability of fault zones may be measured in-situ in a variety of ways (e.g. pressure interference tests, seismic method, etc.). In the pressure interference test, a section of the fault, intersected by the well, is isolated and a fluid is injected into the interval. The relationship between injection pressure and rate is employed for assessing permeability of the fault zone. Lecain (1998) reported such measurements from the Yucca mountain repository site, US, where a range of fault zone permeabilities from 1,100 to 41,000 mD were observed (Mathias, 2012).

Seismic method can be employed to estimate the permeability of fault plane. Assuming microseismic events are caused by pore-pressure induced shear-failure of faults, seismic event migration data can be translated to pore-pressure wave migration along the fault zone of concern (Mathias, 2012). This method was applied by Talwani et al. (2007) to estimate permeability along a fault plane at different sites across the world. They concluded that fault plane permeability generally ranges between 0.5 and 500 mD. However, Miller et al. (2004) reported along fault permeability of about 40,000 mD for a Northern-Apennine-carbonate sequence. Noir et al. (1997) also obtained a permeability value of 10^7 mD for a fault in the Gulf of Aden. These latter values of fault plane permeability, obtained from seismic events, are very large and may give conservative estimates if applied to CO_2 site evaluation. Another measure of fluid flow in a fault plane is to estimate its conductivity based on the permeability and width of the plane.

2.4.1 Permeability of fault core

Permeability of fault core depends mainly on the properties of fault gouge material. Permeability of granular material is a function of grain size and sorting, and permeability of clay-rich gouges depends on the type of clay, clay percentage, and its distribution.

Few studies are available on the permeability of granular gouge material (Sammis et al., 1987; Marone et al., 1990; Zhang and Tullis, 1998) and all suggest that permeability is a function of grain size. Crawford et al. (2008) and Main et al. (2000) found that the permeability of granular fault gouge decreases by a factor of two to three when deformation bands formed. This is in agreement with field observations that suggest there is a significant permeability drop across faults which are dominated by deformation bands with grain size reduction and compaction (Shipton et al., 2002).

2.4.2 Permeability of the damage zone

Permeability of fault damage zones is a combination of the permeabilities of the host rock, the fracture network, the compaction/deformation bands and of the geometry of the system i.e. along or across stacked elements. Microfractures improve permeability while deformation bands reduce permeability. In low porosity rocks, permeability of the damage zone is dominated by fractures. In high permeability rocks, permeability is a function of both low permeable shear/compaction bands and of high permeability slip planes (Faulkner, 2010; Jewell et al., 2012). Generally, damage zones have the highest permeability and fault cores have the lowest (Figure 2.17). Laboratory tests performed on core specimens from fault gouge and from the two damage zones (SDZ and CDZ) of the San Andreas Fault shows that permeability of the gouge material is 2-3 orders of magnitude lower than that of the damage zone samples (Morrow et al., 2013). They concluded from these results, and its known structure, that the San Andreas Fault is an effective barrier to cross-fault fluid flow.

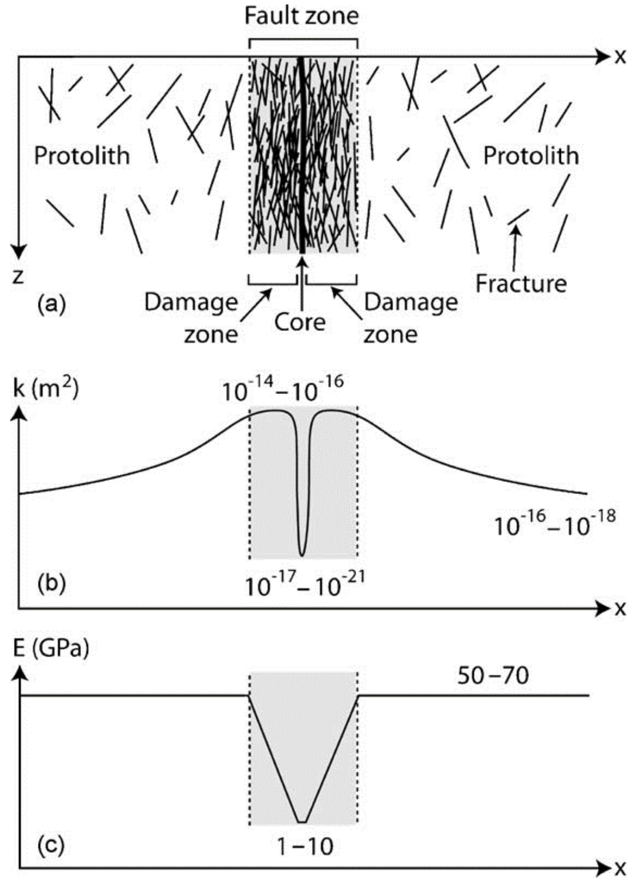

Figure 2.17 Permeability and Young's modulus of fault zone material (after Cappa and Rutqvist, 2011). Permeability (expressed in square meter (m^2) in the middle diagram, 1mD = 10^{-15} m^2) is very low for the fault core. Similarly, stiffness (Young's modulus) of core material (shown at the bottom panel) is also very low, which may result from the presence of low strength material such as clay minerals as well as the development of microfractures.

2.4.3 Permeability of the fault zone

Permeability values of bulk fault zone materials and the structure may be obtained from in-situ testing of wells which penetrate faults including well tests, wireline tests and packer tests. Such data are seldom available in the literature. An option, in the absence of direct fault permeability measurement, is to do a Slug test in a well close to the fault. This test is based on an induced pressure pulse inside a well adjacent to the fault followed by accurate monitoring of the pressure dissipation. Modelling of test results provides estimates of the permeability of the bulk fault zone. Such a study by Talwani et al. (1999) showed fault plane permeability of about 1 mD. Tadokoro et al. (2000) estimated the along-strike permeability of 1 mD for a shallow fault, based on induced seismicity, caused by injection experiments. In another case study, Noir et al. (1997) reported extremely high fault zone permeability of about 10,000 D in the Central Afar Rift.

Permeability of faults is pressure dependent and faults that are stable and sealing may leak upon pressurization or depletion. A direct industry measurement in a Pathfinder well in the Eugene Island, Gulf of Mexico in an overpressured silisiclastic setting has shown high up-fault permeability of about 1 mD which sharply increases to 1D as the fluid pressure is reached the minimum effective principal stress (Losh and Haney, 2006; Faulkner et al., 2010).

Generally, the types of fault rock developed and their petrophysical properties depend on the phyllosilicate content of their host rocks and the burial depth at the time of faulting (Fisher and Knipe, 1998; 2001). Different mechanisms such as cataclasis, drag or smear of some lithologies along the fault plane, mineralization and disaggregation can form fault rocks that fill the fault plane and control the permeability of fault. Cataclasis usually occurs at depths greater than 1000 meters where normal stresses are higher and shearing happen due to mechanical breaking or milling of the surrounding rocks. This leads to grain crushing and grain size reduction of material filling the fault plane and thus reducing fault permeability (Cuisiat and Høeg, 2002). Mineralization can occur during or after movement along a fault plane. Most common mineral fills are silicate or calcite. Both are transported in solution and deposed in the low pressure zone of the fault or fracture. Silicate or calcite precipitation results, in most cases, from pressure solution of the neighbouring rock volume, however, long distance transport is also documented (Gabrielsen and Koestler, 1987; Koestler et al., 1992). Smear (of clay or shale) can occur as a product of drag (friction) of plastic material along a fault if such a material is present within the faulted blocks. Thus, faults in different lithologies can show quite different behaviours.

Faults in clean sandstones (<15% clay) at shallow depth produce a disaggregation zone with only local grain rearrangement, no grain-fracturing and similar or even higher permeability than the host rock (Fisher and Knipe, 2001; Bense and van Balen, 2004). Faulting of the same sediments at greater depth results in grain-fracturing (cataclasis) with clogging of the pore space by smaller grain fragments. Experimental data show that the onset of grain-fracturing may start at depths as low as 500 m, or 5 MPa effective vertical stress (Chuhan et al., 2002). Post-faulting burial may lead to quartz cementation for temperatures greater than circa 90ºC or about 3 km in normally subsided basins. Quartz cementation occurs most intensively at burial depths between 3.5 and 5 km (120-170 ºC) (Bjørlykke and Høeg, 1997). In impure sands with a clay content of between 15 and 40% faulting leads to a fault gouge or phyllosilicate framework fault rock (Fisher and Knipe, 2001) with mixing of sand and clay often structured parallel to the shear plane (Rutter et al., 1986; Wibberley and Shimamoto, 2003; van der Zee and Urai, 2005).

The permeability of phyllosilicate framework fault rocks can be over six orders of magnitude lower than their hosts (Fisher and Knipe, 2001). Sediments containing more than 40% phyllosilicates deform to produce clay smear. Furthermore, faulting of very clay-rich sediments results in the injection of clay gouge into less clay-rich layers.

One of the best ways to investigate permeability and leakage rates of faults, is the analysis of faults that are currently leaking, e.g. in Tyrrhenian Central Italy (Zhang et al., 2010; Evans et al., 2002; Chiodini et al., 1999). These faults give incredible information on the conductivity of faults under actual in-situ stress conditions. Data on some natural CO_2 leakages have been summarized in Mathias (2012, see Table 2.1) showing CO_2 leakage rates through faults varying from less than 1 to about 40 tonnes/year per square meter of fault. Further information on natural leakage rates can be found in Lewicki et al. (2007), Streit and Watson (2004), Pearce et al. (2004) and Cardellini et al. (2000).

Table 2.1 Some natural CO_2 leakage sites, their leakage rate and leak pathways (after Mathias, 2012).

Site	Leakage pathway	CO_2 leakage rate (tonne/yr/m^2)	Reference
A1. Mammoth Mountain, CA USA	Faults and fractures	0.19	Lewicki et al. (2007)
A2. Solfatara, Italy	Faults and fractures	1.10	Lewicki et al. (2007)
A3. Albani Hills, Italy	Faults and fractures	0.44	Lewicki et al. (2007)
A12. Paradox Basin, UT, USA	Faults and fractures	0.04	Lewicki et al. (2007)
Otway (Penola)	Fault conduit	5.7×10^{-3}	Streit and Watson (2004)
Otway (Pine Lodge)	Fault conduit	$1,5 \times 10^{-2}$	Streit and Watson (2004)
Otway (Pine Lodge)	Permeable zone	3.7×10^{-3} to 7.5×10^{-3}	Streit and Watson (2004)
Mátraderecske, Hungary	Fault conduit	< 6.4	Pearce et al. (2004)
Latera, Tuscany	Permeable zone	39.4	Pearce et al. (2004)
Mesozoic carbonate	Permeable zone	1.76×10^{-5} to 3.96×10^{-4}	Chiodini et al. (1999)

2.5 Fault seal vs fault leak

Faults may form preferential pathways to fluid flow or may make impermeable barriers to the migration of fluids (Bretan et al., 2011; Mathias, 2012). There is ample evidence that faults act as conduits; e.g. leakage of contaminated ground water, preferential oil migration, geothermal anomalies and elimination of overpressure fluids (Bense and Person, 2006). On the other hand, hydrocarbon reservoirs beneath or beside faults have proven that they can act as efficient seals over geological time scales. There are primarily two ways in which faults are thought to seal and compartmentalize reservoirs. The first where a juxtaposition seal is formed where a reservoir formation is placed against a low permeable layer such as shale, mudstone or salt. The second, is the smearing where low permeable rocks are smeared across the fault boundary to form a sealing layer (Mathias, 2012; van der Zee and Urai, 2005; Gluyas and Swarbrick, 2004).

Fault seal assessment includes two aspects; i) membrane seal evaluation and ii) dynamic seal analysis. Membrane seal or static fault seal evaluation involves the geometrical aspect and composition of fault rocks. The geometrical aspect of fault sealing can be assessed using the juxtaposition technique or buoyancy pressure profile. The composition of fault rocks can be assessed through the evaluation of the shale-gouge ratio. Allan's juxtaposition technique (Allan, 1989) is a standard method for evaluating static fault sealing in mixed low and high permeable layers (shale-sand). The reservoir and non-reservoir layers are mapped on a three dimensional fault surface and thus, predict the likely fault rock composition where the reservoir is in contact with other formations (Figure 2.18). If the throw of a fault is greater than the thickness of the reservoir layer, it might be placed against another layer of different lithology, mechanical characteristics and hydraulic properties. If the permeability of that layer is lower than the reservoir permeability, cross-fault flow may not be an issue and a juxtaposition seal may form. If the new layer has a high permeability, fluid flow and leakage may occur across the fault. The second method for estimating static seal potential is the buoyancy pressure profile (Figure 2.19 and Figure 2.20) which relies on empirical relationships between fault rock permeability, capillary entry pressure and clay content determined from laboratory tests on fault gouge material (e.g. Gibson, 1994; Fischer and Knipe, 2001; Sperrevik et al., 2002).

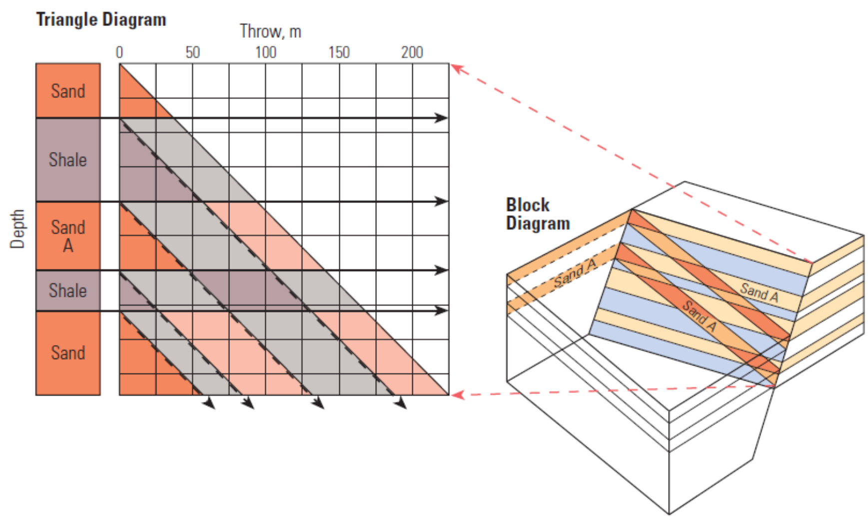

Figure 2.18 Analysis of sealing potential of faults using the juxtaposition method. If, for instance, a permeable formation is juxtaposed against an impermeable shale, a seal will form (after Cerveny et al., 2005).

The capacity of membrane fault seals is usually assessed using the shale-gouge ratio (SGR) that can predict failure of fault membrane seals as well as the maximum column height for a trapped fluid before a fault starts to leak (Langhi et al., 2010). The maximum capillary pressure that a fault can sustain systematically increases as the shale-gouge ratio (SGR) increases (Bretan and Yielding, 2005). Another method is the clay smear potential (Dewhurst et al., 2005; Lindsay et al., 1993) which will be elaborated on in the next section.

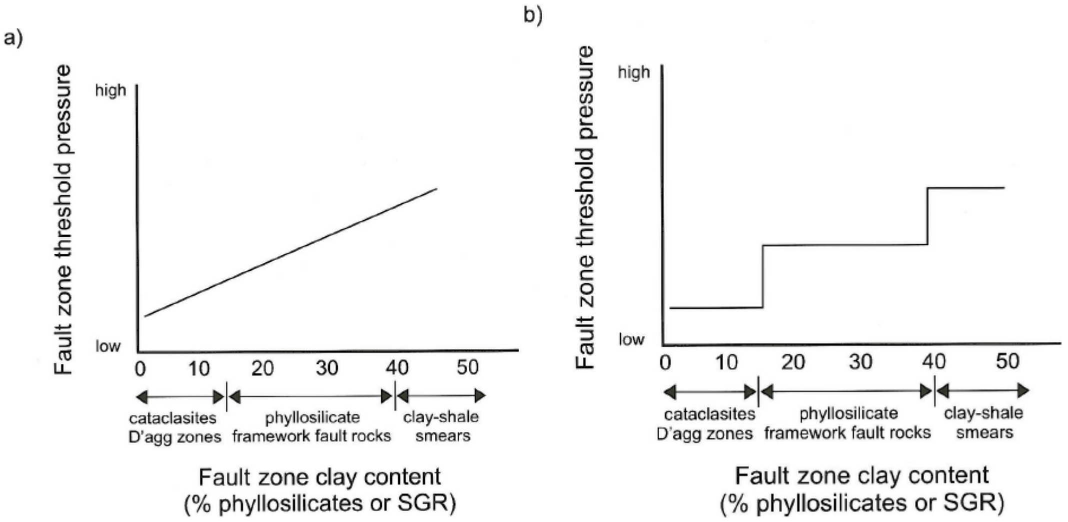

Figure 2.19 Typical relationship between fault zone capillary entry pressure for seal failure and fault rock classification based on clay content in the fault zone (after Bretan and Yielding, 2005).

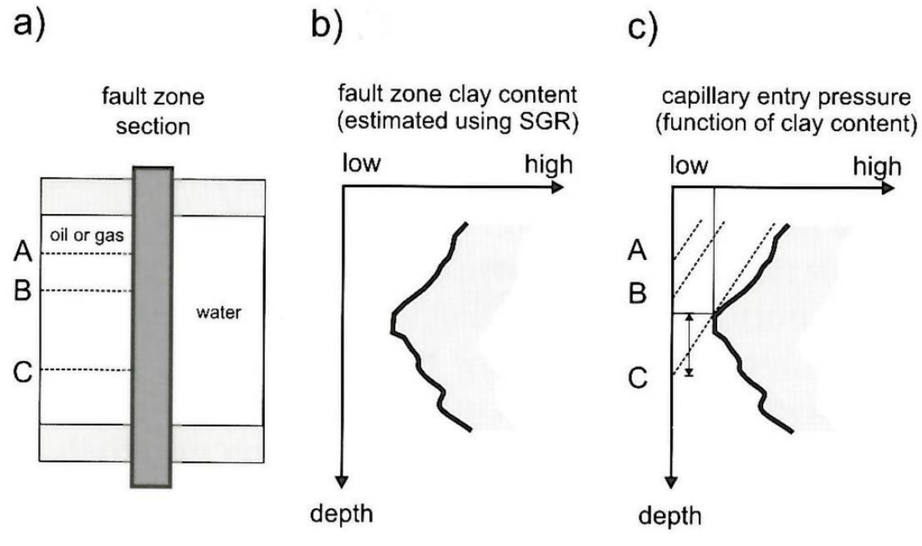

Figure 2.20 A schematic figure showing a) a fault zone section, b) fault zone material composition and c) the predicted capillary entry pressure and buoyancy pressure trend lines versus depth. Leakage occurs when the buoyancy pressure trend line intersects the minimum fault zone capillary entry pressure (after Bretan and Yielding, 2005).

2.5.1 Clay smear in faults and its impact on fluid flow

In clay-rich sequences (clay content >40%), faulting is commonly associated with clay smear that can significantly reduce fault permeability (Antonellini et al., 1994;

Caine et al.. 1996; Sibson 2000; Clausen et al., 2003; Cuisiat et al., 2010a). Therefore, determination of the volume of clay or shale that may be smeared along a fault trace is important for estimating fluid connectivity in subsurface systems (Egholm et al., 2008). Smearing of low permeability clay has been presented as one of the most efficient mechanisms for fault sealing. Several processes have been suggested to explain the occurrence of clay smear based on field observations (e.g. Lindsay et al., 1993; Lehner and Pilaar, 1997; van der Zee and Urai, 2001; Clausen et al., 2003), laboratory experiments, or numerical modelling (Sperrevik et al., 2000; Egholm et al., 2008). Some of the mechanisms include clay abrasion, lateral clay injection from source-layers (Mandl, 2000; van der Zee and Urai, 2001; van der Zee, 2002) shearing/smearing within faults, and material instabilities. Clausen and Gabrielsen (2002) for instance, based on a study at Bornholm Island, Denmark, suggested three models for clay smear along faults: i) development of clay smear by shearing; ii) intrusion of plastic or even liquefied clay into the fault core; and iii) a combination of shear and intrusion. Smearing of clay is analysed through clay smear potential. The abrasional mixing of different materials is analysed using the shale-gouge ratio (Figure 2.21).

Generally, there is non-linear dependence of fault zone permeability on clay content under hydrostatic conditions. At lower clay contents (25-40 volume %), permeability is strongly controlled by clay content (Takahashi et al., 2007; Crawford et al., 2008) while at higher clay content (>40%) permeability is less sensitive to clay content (Faulkner et al., 2010). The permeability of fault gouge is also dependent on stress history (Bolton et al., 1998; Zhang et al., 1999) and the temperature domain it has been subjected to (Olsen et al., 1998; Tenthorey et al., 2003; Yasuhara et al., 2005; Giger et al., 2007). Despite presentation of different conceptual models, no real mechanics-based predictive model for fault seals is yet available in the literature.

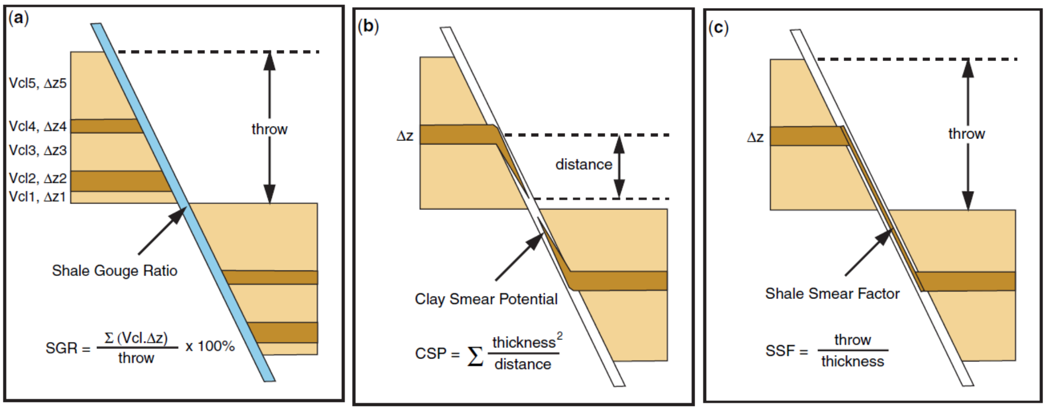

Figure 2.21 Clay smear in faults and the related terminology (after Jolley et al., 2007).

The laboratory shear tests (Cuisiat et al., 2010a; Sperrevik, 2010; Giger et al., 2013) or sand box models (Schmatz et al., 2010) are usually used to simulate clay smear processes. A few experimental studies dedicated to clay smear and shear band formation were carried out at the Norwegian Geotechnical Institute (NGI) in a classical geotechnical ring shear apparatus which allowed for large deformations, but was limited to low stress conditions (Sperrevik et al., 2000; Clausen and Gabrielsen, 2002; Kvaale, 2002). More recently, an advanced ring shear apparatus (Figure 2.22) was used to investigate shear band formation and clay smear in unconsolidated sediments at greater burial depths (Torabi et al., 2007; Cuisiat et al., 2007; Cuisiat et al., 2010a). The experiments consist of shearing a ring of sand with embedded clay segments, thereby simulating faulting through a layered sand–clay sequence. They observed deformation processes such as grain reorientation, clay smear and cataclasis. The complexity of the shear zone was observed to increase with greater burial depth at time of faulting. They concluded that at shallow burial depth, in clay-rich sediments, clay smear is the most efficient mechanism for permeability reduction. At shallow depth, sand–sand juxtaposition shear is dominated by grain rolling causing only minor permeability reduction. At greater burial depths, permeability reduction is dominated by grain crushing. They also reported that the thickness of clay smear was more sensitive to the thickness of the sheared clay layers rather than other parameters tested.

Shearing of multiple clay layers (3 layers) produced a composite clay smear 2–3 times thicker than for a single clay layer, whereas when reducing the thickness of clay layer to one half of the reference layer, a thin and discontinuous clay smear was produced. The permeability across the clay smear was found to increase as the thickness of the clay source decreased for single clay layer, but the permeability for composite smear was more complex and a clear trend was not observed from the two tests they performed. They suggested further work on the mechanics of deformation bands in multiple clay layers and also the effect of composite smear on fault permeability, formation of phyllosilicate framework in unclean sand with varying clay content, clay mineralogy, burial depth, and fault throw.

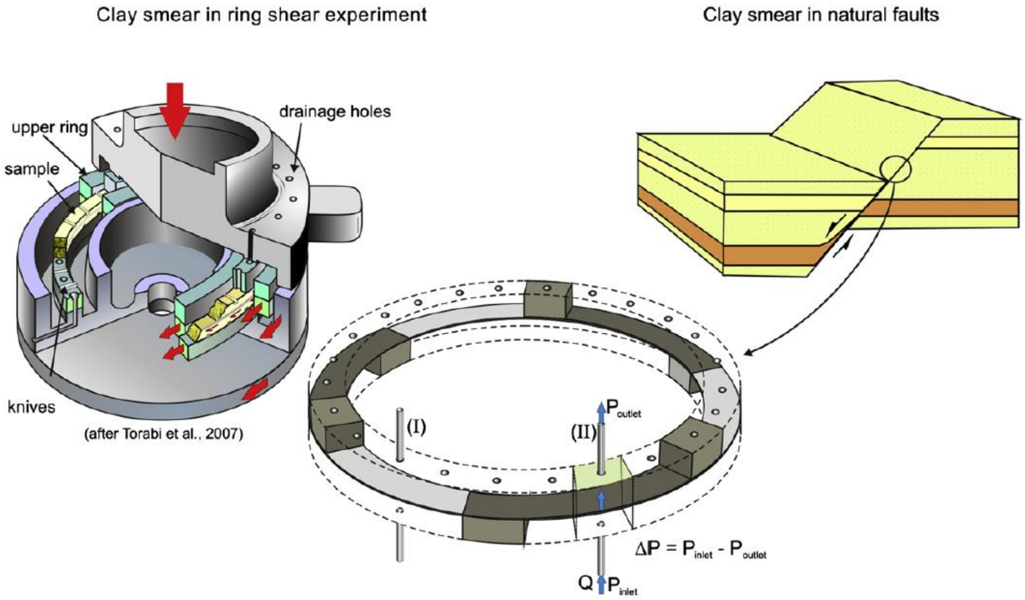

Figure 2.22 Clay smear analysis in laboratory using ring shear test (Cuisiat et al., 2010a).

3 Assessment of CO_2 injection-induced fault reactivation

As previously stated faults are present in almost all geological formations. In general, faults may be sealing or non-sealing (Chanpura, 2001). Sealing boundary faults may become non-sealing during the process of CO_2 storage and reservoir pressurization. Sealing integrity may be damaged through capillary leakage or mechanical fracturing. Capillary leakage is beyond the scope of this study but mechanical failure is the subject of this work and will be discussed further in the following sections.

Mechanical failure of faults may occur through i) shear failure when the shear stress exceeds the shear strength of fault zone material, and ii) hydraulic fracturing (in case of cohesive faults) when the pore pressure exceeds the sum of the minimum in-situ stress and tensile strength of rock. There are two classifications for modes of failure in brittle regime fracture mechanics:

- Tensile fracturing occurs under extensional regimes, i.e. fracture opening (see Figure 3.1a).
- Shear failure occurs when differential stress is large enough to generate shear stresses in excess of the shear strength of the rock mass (Figure 3.1b). Tensile fracturing tends to increase the permeability dramatically whilst shear failure does not have a large impact on the permeability of the sheared zone.

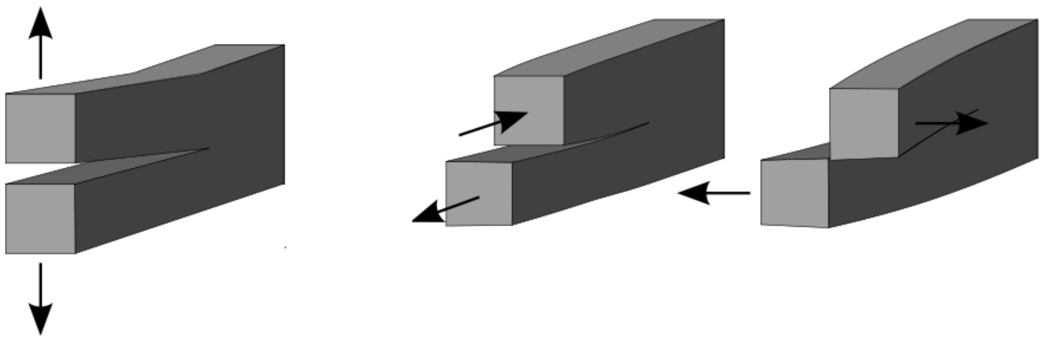

a) Tensile fracture (Mode I) b) Shear fracture (Mode II and III)

Figure 3.1 Different modes of failure.

In the case of shearing, post failure deformation may be brittle or ductile, depending on the shear strength properties and the level of the effective confining stress. In a brittle regime, deformation associated with dilation occurs until sudden failure at peak shear strength, followed by strain softening down to residual shear strength. Ductile deformation, on the other hand, produces contraction of the sample and more diffuse deformation. In brittle deformation, shear fractures dilate under low effective normal stress and cause permeability enhancement with increased shearing. With increasing shear deformation, fracture asperities are sheared off leading to gouge production and reduction of permeability (Gutierrez et al., 2000). Thus, in brittle deformation permeability will generally increase under low effective stresses and small displacements but decreases with increasing effective stress and magnitude of displacement. Shear fractures created in ductile deformation contract during shearing and do not lead to an increase in permeability.

Experience from petroleum fields show that fault reactivation is more likely to occur following depletion of soft reservoirs compared with rigid ones (Chanpura, 2001). This is because of larger poro-elastic reservoir strains. Soft reservoir refers to an unconsolidated, low strength formation while rigid reservoir refers to a consolidated/cemented, high strength rock. Deformation of soft reservoirs is more likely to be ductile rather than brittle. Following the discussion in the previous paragraph, ductile deformation in soft reservoirs may not necessarily increase the permeability of sheared zones. This is positive for the integrity of reservoirs.

As mentioned in the introduction, reactivation of faults (and fracture systems) during injection or depletion can be assessed using different methods and approaches. Two commonly used methods for evaluating potential reactivation of faults include the analytical and numerical solutions (Mildren et al., 2002; GeoScience, 2004; Lucier et al., 2006; Moeck et al., 2009; Cuisiat et al., 2010b; Verdon 2010; Vidal-Gilbert et al., 2010; Cappa and Rutqvist, 2011; Morris et al., 2011; Preisig and Prévost, 2011; Fang et al., 2012; Hung and Wu, 2012; Jeanne et al., 2013; Kano et al., 2013; Rutqvist et al., 2013; Tenthorey et al., 2013). This chapter describes these two methodologies as follows:

- Firstly, the methodology (the analytical Mohr-Coulomb failure criterion) is elaborated on as a preliminary tool for fault reactivation analysis. Its assumptions and its associated limitations are addressed;
- Secondly, numerical approaches are outlined which address some of the limitations of the analytical method and;
- Thirdly, the impact of fault reactivation on fault leakage is discussed using brittle and ductile failure classifications.

3.1 Analytical approach to evaluate fault reactivation

Injection of a fluid into a reservoir increases the pore pressure and changes the effective stresses in the reservoir and surrounding formations. When differential stresses increase, and shear stress acting on a fault plane exceeds its shear strength, the fault may be reactivated and slip occurs (Figure 3.2). The shear slip condition can be expressed using the linear Mohr-Coulomb criterion:

$$\tau_{crit} = C + \mu\left(\sigma_n - P_f\right) \tag{3.1}$$

where τ_{crit} is the critical shear stress, C is the cohesion, μ is the friction coefficient, σ_n is the normal stress and P_f is the pore pressure. The shear and effective normal stresses acting on a fault plane can be expressed in terms of the angle of the fault to the principal stresses (Figure 3.2 a) and their magnitudes as (Figure 3.2b):

$$\tau = \frac{\sigma_1 - \sigma_3}{2} \sin 2\theta \tag{3.2}$$

$$\sigma'_n = \frac{\sigma'_1 + \sigma'_3}{2} - \frac{\sigma'_1 - \sigma'_3}{2}\cos 2\theta \qquad (3.3)$$

where σ'_1 and σ'_3 are the maximum and minimum principal effective stresses acting on the fault plane; and θ is the angle between the normal vector to the fault plane and the direction of maximum principal stress, σ_1, acting on the fault. σ denotes the total stress. Byerlee (1978) showed that for most rocks, the friction coefficient, μ, in Equation 3.1 ranges between 0.6 and 0.85. However, this parameter is affected by many factors and conditions. More details on the estimation of friction coefficient of faults and discussion on factors affecting rock friction are addressed in Section 4.2.

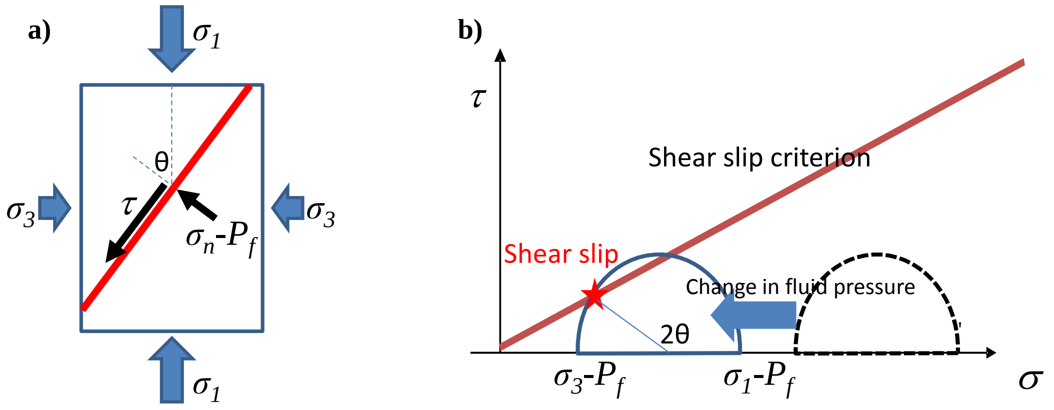

Figure 3.2 *Schematic presentation of stresses on a fault plane (a) and illustration of the change in effective stresses due to injection on Mohr diagram (b).*

In most cases, the strike of a fault plane is not parallel with the intermediate in-situ stress. The shear and effective normal stresses acting on a fault in a 3D space can also be plotted on Mohr-Coulomb diagram using all three components of principal stress and relevant angles to the directions of each principal stresses as shown in Figure 3.3. The critical injection pressure can be calculated from the horizontal distance between the current stress state and the failure envelope (Wiprut and Zoback, 2002).

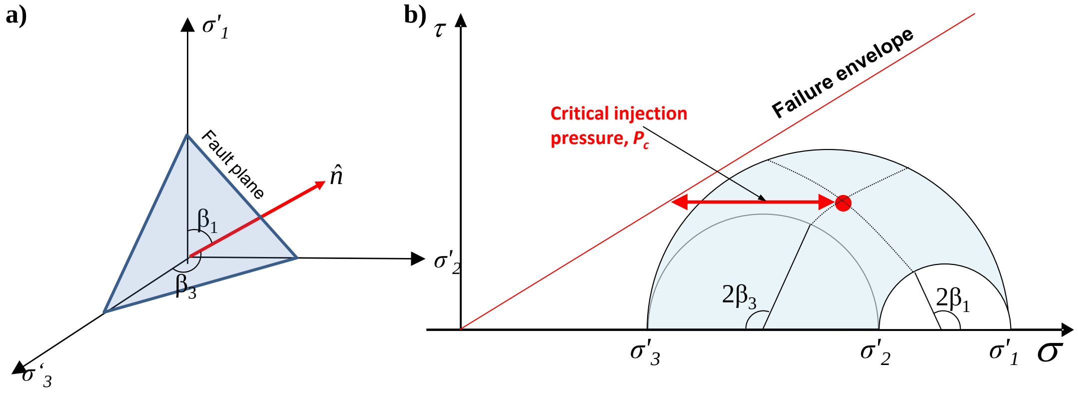

Figure 3.3 a) orientation of a fault plane in a 3D stress field. b) Mohr circle representation of stress state and critical injection pressure.

For rocks in which cohesion is zero the potential fault slip can be expressed as the ratio of shear stress to effective normal stress acting at the location of the fault plane. This ratio is known as the fault slip tendency (Morris et al., 1996). For cohesionless rocks (i.e. C = 0), there will be a fault slip when the calculated slip tendency (i.e. τ/σ'_n) exceeds the friction coefficient, μ. The potential for fault reactivation can also be expressed in terms of the maximum sustainable fluid pressure or the critical injection pressure (P_c) as (Rutqvist et al., 2007; Streit and Hillis, 2004):

$$P_c = \sigma_n - \frac{\tau}{\mu} \tag{3.4}$$

The critical injection pressure, also referred to as the maximum sustainable pressure, can be calculated for all possible fault orientations at a given depth using the 3D equivalents of Equation 3.1 as illustrated in Figure 3.3. The critical injection pressure is then plotted in a lower hemisphere stereographic projection of poles to planes to evaluate the critically oriented faults. Figure 3.4 shows an example of the fault reactivation modelling of CO_2 injection risk for the Naylor Field, Otway Basin, Australia where the fault regime is strike-slip (Vidal-Gilbert et al., 2010). The stereographic projection of poles to planes in Figure 3.4a shows that sub-vertical faults striking 120° to 165° (i.e. 90° from the pole locations plotted in Figure 3.4) are the most critical ones for reactivation (i.e. hot colours in Figure 3.4a). Then, if the fault strength is known the fault reactivation potential, represented by the critical injection pressure for the known faults, can be quantified as shown in Figure 3.4b.

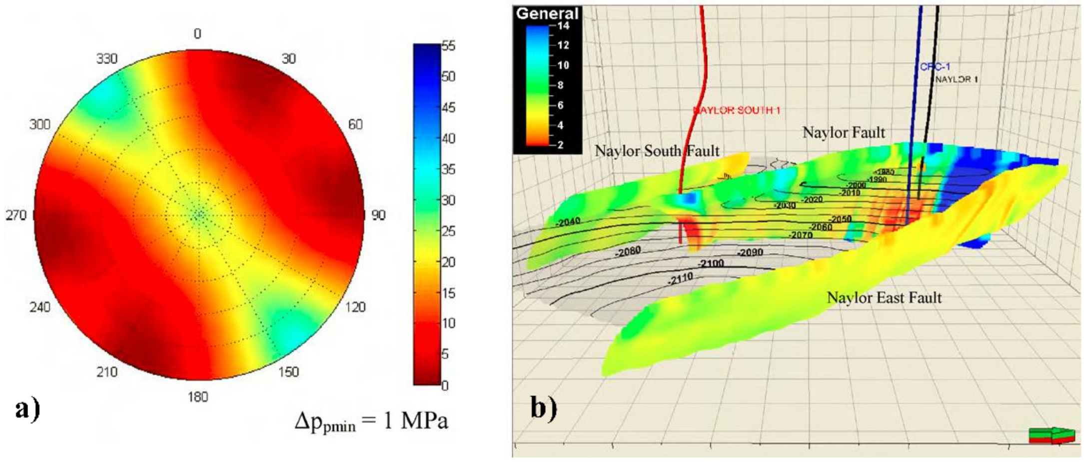

Figure 3.4 Calculated critical injection pressure using the analytical approach for the Naylor Field, Otway Basin, Australia. The scale shows how much the reservoir can be pressurized before shearing. a) lower hemisphere stereographic projection of poles to planes showing the critical pore fluid pressure on faults and potential for reactivation, and b) critical pore pressure for all faults in the reservoir (Vidal-Gilbert et al., 2010).

3.2 Limitations of the analytical approach

The aforementioned analytical approach is a useful tool for a preliminary or first-order assessment of fault reactivation potential. It has been widely used not only for CO_2 storage projects but also for geothermal reservoirs and waste disposal sites (Holloway, 1997; Moeck et al., 2009; Langhi et al., 2010). The analytical approach relies on many assumptions and simplifications and thus has limitations for applicability to complex in-situ conditions. This section presents some of these limitations.

3.2.1 Alteration of in-situ stress field during injection

In the analytical approach, it is assumed that the total stress is constant (i.e. equal to the initial in-situ stress) during injection. However, the knowledge from depleted hydrocarbon reservoirs states that change in the reservoir pressure alters the stresses (Hettema et al., 2000; Teufel et al., 1991). Examples from geomechanical modelling of CO_2 sequestration sites also indicate the alteration of in-situ stress fields during injection (Rutqvist et al., 2007). This alteration may be governed by several factors; e.g. geometry of reservoirs, contrast between the stiffness of reservoirs and their surroundings.

Injection and depletion operations not only change the magnitude of in-situ stresses but also their orientation. The change may be local but may affect fracture propagation direction and conditions (Day-Lewis, 2008).

Poro-elastic stressing (injection induced in-situ horizontal stress change)

For laterally infinitely extended thin reservoirs, injection-induced change of vertical stress can be assumed negligible due to the free movement of ground surface. But in the horizontal direction, change of in-situ stresses might be significant due to confinement by surrounding rock bodies. This stress alteration is known as poro-elastic stressing (Rutqvist et al., 2007; Streit and Hillis, 2004). Assuming uniaxial condition (i.e. no change in total vertical stress), the change of in-situ horizontal stress can be calculated by (Fjær et al., 2008):

$$\Delta\sigma_h = \alpha \frac{(1-2\nu)}{(1-\nu)} \Delta P \tag{3.5}$$

where α is the Biot's coefficient, and ν is the drained Poisson's ratio. When α is assumed as 1.0 and the range of Poisson's ratio is assumed from 0.2 to 0.3, the change of horizontal stress can be approximated by a value between 0.5 and 0.6 of the pore pressure change. From Equation 3.5, the change of effective vertical and horizontal stresses for a laterally extended thin reservoir can be expressed as:

$$\Delta\sigma'_v = 0 - \alpha\Delta P = -\alpha\Delta P \tag{3.6}$$

$$\Delta\sigma'_h = \Delta\sigma_h - \alpha\Delta P = \frac{\nu}{1-\nu}\alpha\Delta P \tag{3.7}$$

The effect of poro-elastic stress on the critical injection pressure depends on the fault stress regime. As shown in Figure 3.5a, the change of in-situ horizontal stress is less critical for fault stability in the normal faulting regime (i.e. $S_v > S_h$). It means that there is more margin to the critical injection pressure than assuming constant in-situ stress condition. However, for a thrust fault regime (i.e. $S_v < S_h$) (Figure 3.5b), change in the in-situ horizontal stress moves the Mohr circle towards the critical injection pressure indicating failure which would have otherwise been assumed to be a stable stress condition.

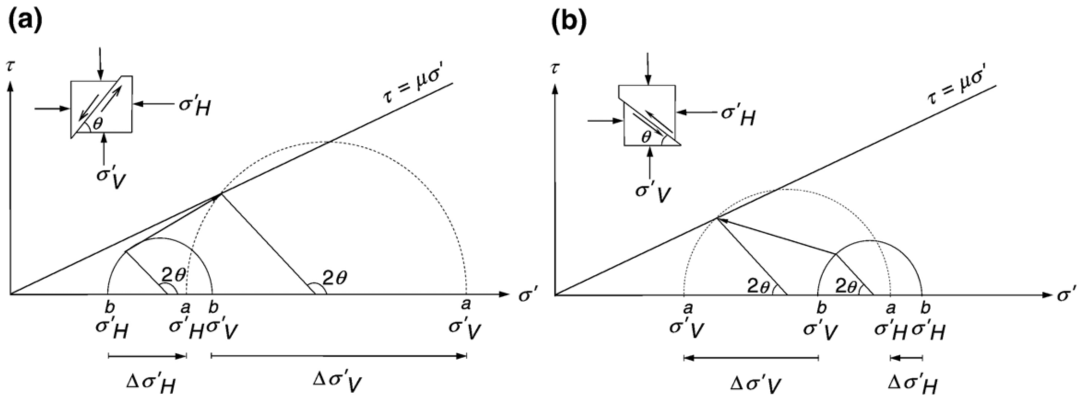

Figure 3.5 Mohr-circle representation of stress changes resulting in fault reactivation for (a) a normal fault within a reservoir during depletion, and (b) a thrust fault within a reservoir during injection. Index a denotes "after change in pore pressure" and index b denotes "before change in pore pressure" (Soltanzadeh and Hawkes, 2008).

Stress arching effect (injection induced vertical stress change)

In reality, reservoir formations do not behave like the uniaxial conditions discussed previously. According to Segall and Fitzgerald (1998), an assumption of a uniaxial condition of a reservoir can be only valid for laterally extended thin reservoirs that have a ratio of a lateral width to the thickness of more than 10:1. In many cases, there are changes in the magnitude of the vertical total stress due to injection/depletion, which is known as stress arching. Change of vertical and horizontal stresses during injection or depletion can be defined by the stress path coefficient as follows (Hettema et al., 2000):

$$\gamma_v = \frac{\Delta \sigma_v}{\Delta P} \tag{3.8}$$

$$\gamma_H = \frac{\Delta \sigma_H}{\Delta P} \tag{3.9}$$

The coefficient γ_v is also called the arching coefficient where $\gamma_v = 0$ means the constant vertical in-situ stress during the injection or depletion.

If the shape of a reservoir becomes more like a sphere, there is more change in vertical stress (arching effect). When the shape of a reservoir is ellipsoidal, the effect of the reservoir shape on the production-induced stress change can be estimated by Rudnicki's model (1999). When the depth of a reservoir is greater than the lateral extension of the reservoir, and the elastic contrast between the reservoir and its surroundings is assumed to be the same, the stress path coefficient can be calculated as (Fjær et al., 2008):

$$\gamma_v = \alpha \frac{1-2\nu}{1-\nu} \frac{e}{\sqrt{\left(1-e^2\right)^3}} \left(\arccos e - e\sqrt{1-e^2}\right) \tag{3.10}$$

$$\gamma_h = \alpha \frac{1-2\nu}{1-\nu} \left[1 - \frac{e}{2\sqrt{\left(1-e^2\right)^3}} \left(\arccos e - e\sqrt{1-e^2}\right)\right] \tag{3.11}$$

where *e* is the aspect ratio that can be defined as ratio of the thickness to the diameter of the ellipsoidal reservoir.

The normalized stress path as a function of the aspect ratio *e* is plotted in Figure 3.6. When *e* is zero (i.e. flat reservoir), the reservoir behaviour is like a uniaxial condition. However, when *e* is unity (i.e. spherical reservoir), the change of vertical in-situ stress becomes the same as that in the horizontal direction.

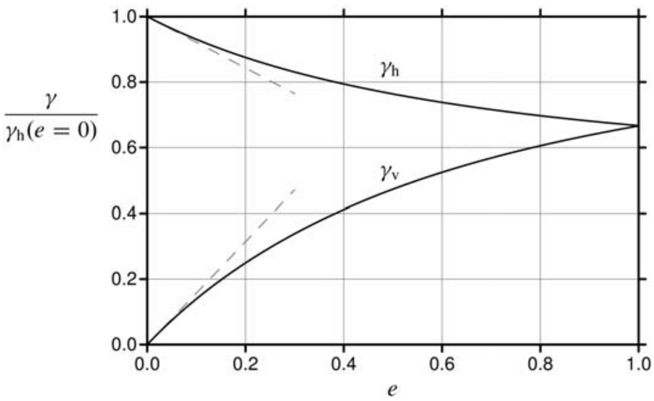

Figure 3.6 Normalized stress path coefficients versus the aspect ratio of the depleting reservoir zone, calculated from Rudnicki's model for the case of no elastic contrast. The stress path coefficients have been normalized by dividing with γ_h for uniaxial strain conditions (Fjær et al., 2008).

The elastic contrast between the reservoir and the surroundings also affect the stress path (stress arching) of the reservoir. Usually, it is known that there is more vertical stress change (i.e. more stress arching) when the stiffness of the reservoir is much lower than the surroundings (Fjær et al., 2008). Vidal-Gilbert et al. (2010) also investigated the effect of stiffness contrast on the horizontal stress path using Rudnicki's model (1999) for the geomechanical study of Otway basin, Australia. As shown in Figure 3.7, the coefficient of the horizontal stress path decreases with increasing the ratio of bulk modulus of host rock to reservoir, and this reduction of the horizontal stress path tends to increase with Poisson's ratio. A decrease in the horizontal stress path can enhance the stress arching as a counteracting behavior. In a normal stress regime, stress arching during injection can result in a reduced maximum sustainable injection pressure (i.e. more slip potential).

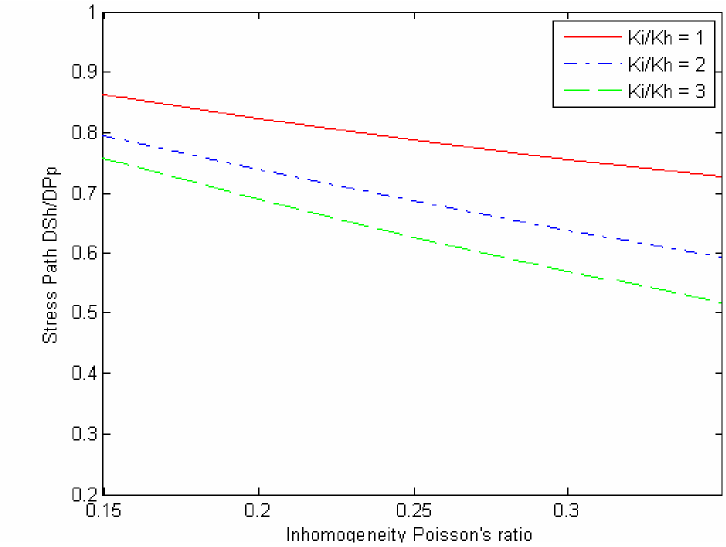

Figure 3.7 Horizontal stress path inside a reservoir against the Poisson's ratio for different ratios of bulk moduli (Vidal-Gilbert et al., 2010).

However, the aforementioned examples in this section are only for reservoirs that have a well-defined simple geometry. In reality, reservoir geometry is quite complex, and a change of pore pressure in a reservoir is not homogeneous. Therefore, valuation of reservoir stress paths should be calculated using geomechanical simulation for arbitrary reservoir geometry, and in associated with properly estimated in-homogeneous pore pressure distribution in the reservoir.

3.2.2 Undrained behaviour of the boundary faults

The aforementioned analytical method assumes the same amount of pore pressure change in a fault plane as that for a reservoir during injection/depletion. If faults are highly permeable and the drainage path is short (i.e. low thickness of the fault zone), pressure inside the fault may reach the reservoir pressure quickly. However, faults usually have very low permeability of 10^{-2} to 10^{-6} mD ($1x10^{-17}$ to $1x10^{-21}$ m^2) (Faulkner and Rutter, 1998; Wibberley and Shimamoto, 2003). Therefore, pressure equilibrium between the reservoir and fault may take a couple of months to years (depending on permeability), which is significant compared to the operational time frame. This problem is known as the effect of undrained behaviour and slow propagation of pore pressure in the boundary faults (Rice and Rudnicki, 1979; Rudnicki, 2001).

The change of pore pressure in a fault plane can be slower than that in a reservoir due to low permeability within the fault zone. At the edge of the reservoir, where the bounding faults exist, the change of effective stress inside the fault may be the same as the change in the total stress (i.e. undrained geomechancial behaviour). Then, the stress state changes from undrained to drained conditions as a function of time. The time for a fault zone to reach a drained condition can be roughly calculated using a consolidation coefficient and the thickness of the fault as follows (Cuisiat et al., 2010b):

$$t = L^2 / c \tag{3.12}$$

where L is the thickness of the fault core, and c is the consolidation coefficient given by:

$$c = \frac{k\left(K_u - K\right)\left(K + 4/3G\right)}{\mu_f \alpha^2 \left(K_u + 4/3G\right)} \tag{3.13}$$

where k is the intrinsic fault core permeability, K_u is the undrained bulk modulus, K is the drained bulk modulus, G is the shear modulus, μ_f is the dynamic viscosity and α is the Biot's coefficient.

3.2.3 Effect of irreversible stress path on geomechanics of depleted reservoirs: impact of stress history

Storage of CO_2 in depleted hydrocarbon reservoirs may be more feasible than in saline aquifers because they have proven seal integrity over a geological time scale. Depleted reservoirs will have experienced changes in the state of stress during the production phase (Orlic, 2009; Rutqvist, 2012). If a fault has been activated, or subjected to plastic behaviour during depletion, the stress path during injection may be partly irreversible.

Figure 3.8 shows a numerical example applied to determine the feasibility of injection into a depleted gas field in the Netherlands (Orlic, 2009). The right figure shows the stress path of a fault for each scenario. The dotted line indicates the reversible stress path (elastic response); and the solid red line indicates the irreversible stress path due to plastic behaviour during depletion. We can observe that an irreversible reservoir stress path during reservoir re-pressurization can cause a condition that leads to fault reactivation earlier than if a reversible stress path had occurred. In the case of an irreversible reservoir stress path, the stress path will only partly recover during reservoir re-pressurization and therefore converge faster towards the Mohr-Coulomb failure envelope. This type of stress development is less favourable as the conditions for fault reactivation will be reached earlier than the case for a reversible stress path. Orlic et al. (2013) recommended that the reservoir stress path during re-pressurization is monitored by conducting repeated minifrac and extended leak-off tests in order to decrease the uncertainty in the estimation of fault reactivation during CO_2 injection.

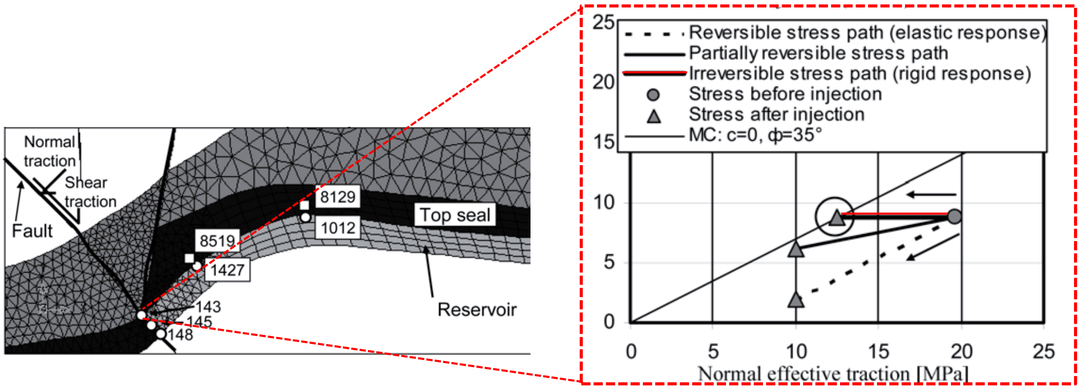

Figure 3.8 *Stress path on the boundary fault during injection into a depleted gas reservoir: dotted line represents the reversible path under elastic behaviour and the red solid line indicates the irreversible path due to fault reactivation during depletion (Orlic, 2009).*

3.2.4 Potential of fault reactivation in the cap rock

The stability of faults not only within a reservoir but also in cap rocks is crucial for storage reservoir integrity. A comprehensive criterion for fault stability analysis should be the ability to capture behaviour of faults both within the storage and in the surrounding formations. It should answer whether reactivation of a fault in a reservoir will propagate into the cap rock or not. Fracture propagation in a rock mass in microscopic scale has been explained by several researchers using the Inclusion theory, which is based on Griffith criterion (1921) (Horii and Nemat-Nasser, 1985). However, fracture propagation in faults in the interface region is difficult to capture using the pure analytical approach. The analytical method, which is briefly introduced in Section 3.1, is applicable to faults within the reservoir only (or to -reservoir-bounding faults).

The key question is how pressure change in the reservoir affects pore pressure inside the cap rock. Pore pressure distribution in the cap rock can be obtained using numerical methods. The pressure data can then be used in an analytical or numerical solution for assessing fault reactivation inside the cap rock. As illustrated schematically in Figure 3.9, the effective stress change in the top seal is relatively small compared to the effective stress change in the reservoir during injection or depletion. The difference between top seal and reservoir is typically one to two orders of magnitude (Fjær et al., 2008; Orlic, 2009). The minor stress change in the cap rock may be too small to cause mechanical failure or reactivation of faults in the cap rock. The small effective stress change on the boundary faults in the cap rock may not mechanically alter fault stability during production or injection even though failure may occur in the reservoir-bounding fault.

To examine the applicability of the conventional/analytical method on evaluation of fault reactivation in the cap rock, further investigation on i) variation of pore pressure in the fault zone due to pressure change in the reservoir, and ii) pattern of progressive failure from reservoir to the cap rock is required. This can be approached using numerical methods.

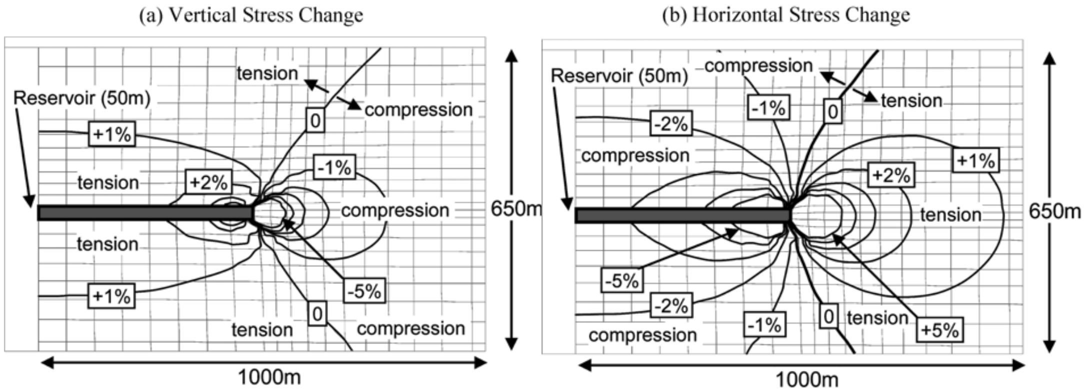

Figure 3.9 *Stress changes of reservoir surroundings during depletion. The change of vertical and horizontal stresses are only a couple of percentage values of pore pressure change in the reservoir (Orlic, 2009).*

3.2.5 Concluding remarks on the analytical method

Analytical approaches based on Mohr-Coulomb type failure criteria are simple and good tools for the first-order assessment of fault reactivation potential during injection or depletion. Recently, many approaches have been introduced to overcome the limitations of the analytical method. However, as discussed, analytical approaches still have some limitations for explaining real behaviour of faults during injection. Some approaches can consider changes in the in-situ stress magnitude. But injection or depletion changes not only the magnitude of principal stresses but also their direction. This is another factor that may introduce uncertainties to the estimated fault reactivation potential.

As discussed in Section 3.2.4, the analytical approach can only be applied to the reservoir-bounding or reservoir-crossing faults. Thus, the calculated fault reactivation from an analytical approach may have a limitation in its application to faults in the cap rock, and thus, may provide limited information on the slip tendency of faults in the sealing formations. The latter could be more important for integrity of the storage reservoir. In order to carry out a thorough assessment of fault stability, the first-order estimation by the analytical method should be combined with models that are able to explain geomechanical behaviour of cap rock (e.g. analytical approach based on fracture propagation using the inclusion theory; Griffith (1921) or a coupled numerical modelling).

3.3 Numerical approach

Reactivation of faults due to injection or production is a complex problem that requires comprehensive analyses of initial and induced stresses versus the strength properties of fault zone material. Some of these aspects can be captured by numerical modelling. Geomechanical simulation can provide a critical insight on the response of subsurface geological systems during injection or depletion. For hydrocarbon applications, geomechanical modelling has been widely used to estimate reservoir compaction, surface subsidence, wellbore stability, etc. Recently, this methodology has been extended to CO_2 geologic storage to evaluate cap rock integrity or fault reactivation during CO_2 injection and storage (Orlic et al., 2011; Rutqvist, 2012; Vidal-Gilbert et al., 2009).

Generally, geomechancial simulation includes several steps as listed in Figure 3.10. It requires the following input data:

- geometrical and geological description of the reservoir and surrounding formations,
- material model and properties of rocks, e.g. deformation properties, strength and permeability parameters for the reservoir and surrounding formations,
- hydraulic and strength properties of faults,
- initial conditions; spatial distribution of pore pressure, stresses and temperature, initial saturation data on the formations outside reservoir,
- boundary condition,
- loading conditions according to the project design, i.e. time histories of the spatial distribution of pore pressure and temperature field within the reservoir during depletion/injection.

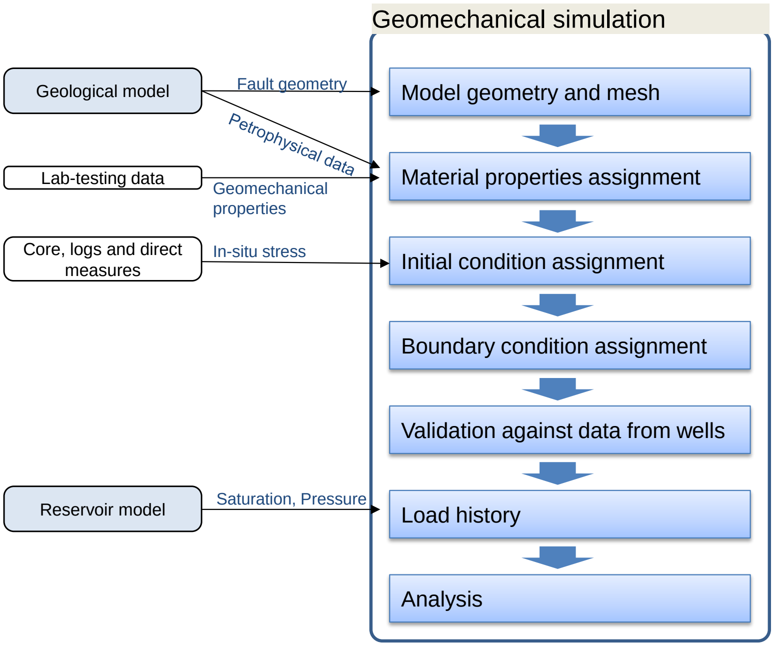

Figure 3.10 A general procedure for geomechanical analysis of fault reactivation.

For geomechanical simulation of fault reactivation analyses, we need to implement fault geometry and hydro-mechanical properties into the model. The thickness of faults, compared to the host formations, is very small. Properties of fault zone material may also be quite different from the surroundings. This discrepancy between faults and surrounding materials requires special considerations for implementing real fault characteristics to a geomechancial model.

In this section, the following elements are addressed to model fault reactivation using geomechanical simulation:

- including a fault in a geomechanical model,
- modelling a fault as a discontinuity in a global model,
- modelling a fault as an equivalent rock mass in a local model.

3.3.1 Fault modelling: problem of scale

Faults or fracture zones may be considered in conceptually different ways depending on the relations between the scale of the feature and the problem of concern. Figure 3.11 illustrates a fracture zone or fault as observed at different scales. It is important to realise that even if the feature at some scale appears as a single discontinuity, closer examination may reveal that it comprises smaller structural elements.

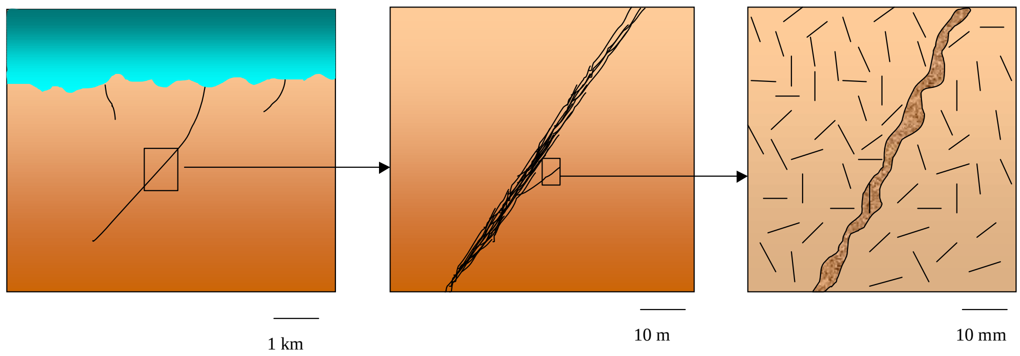

Figure 3.11 The problem of scale: fault viewed at different scales emphasises different components (after Cuisiat and Høeg, 2002).

Faults may be conceptualised in different ways in geomechanics, the choice being governed by two factors (Leijon, 1993):

- the scale of the problem to be considered in relation to the scale of the fracture zone,
- the possibilities to determine the required properties of the associated model.

In a global analysis, the major faults can be represented as single features, and their global strength properties are of concern. At a smaller scale, for instance considering the stability of a wellbore, the features of concern are the local fractures and their properties, degree of rock alteration, and pore pressure development.

The concept of fault properties at different scales can be modelled as shown in Figure 3.12. To do so, mechanical properties should be known for the following components:

- intact rock

- fault/fracture
- filling material, such as clay or fault gouge.

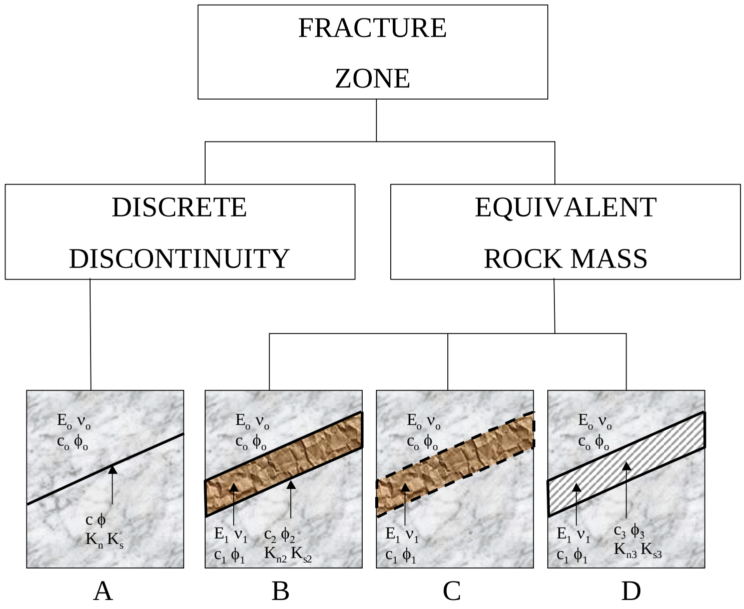

Figure 3.12 Representation of faults or fracture zones in geomechanical models, and associated key properties (after Leijon, 1993). A) Discrete discontinuity, B) Equivalent rock mass, discontinuities at boundaries, C) Equivalent rock mass, all continuum, D) Discrete representation of internal fracturing within fault zone.

Methodology for numerical modelling of faults is presented in the following sections.

3.3.2 Modelling fault as a single discontinuity

Modelling faulting discontinuity in continuum models

Numerical methods based on continuum mechanics, such as the finite element method (FEM) and the finite differences method (FDM), have widely been used for reservoir geomechancis because of their advantages in calculating the continuous strain and stress field in a global scale. However, in the continuum model, the displacement field is always continuous. Thus, the failure surface can only be defined by a concentration of plastic strain and can be mesh-dependent. For a global geomechanical model at km scale, it may be difficult to model discontinuous slip displacement in the fault by continuum mechanics unless the fault zone is modelled by a fine mesh size to represent discontinuous slip as a smooth continuous displacement. However, modelling a fault with a thickness in the order of a centimetre to a meter, with a fine mesh global model that has a scale of more than an order of a kilometre, may be practically challenging.

To model the thin discontinuities using the continuum geomechanical model, the "zero thickness interface element" is one of the widely used approaches in geotechnical and geoscience engineering (Carol and Alonso, 1983; Day and Potts, 1994). The interface element assigns a special connection of a node pair between shared nodes to allow differential movement of the rock across the fault as shown in Figure 3.13.

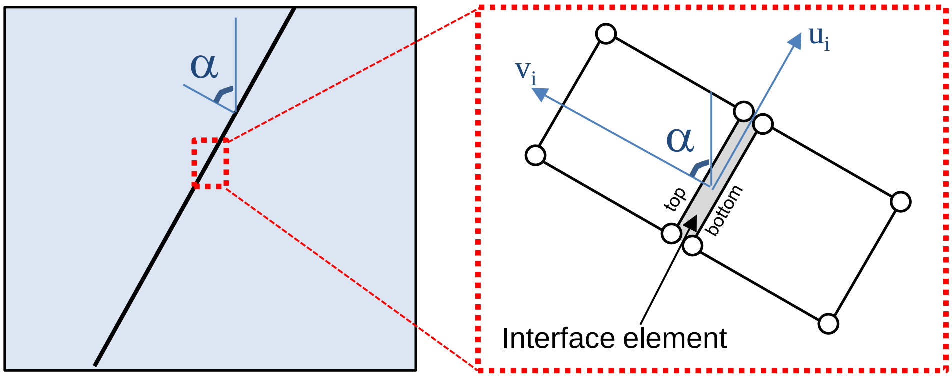

Figure 3.13 Schematic of modelling fault as an interface element.

Stresses acting on a fault plane can be analyzed into normal and shear components. The normal stress, σ_n, and the shear stress, τ, can be expressed as a normal and a tangential relative displacement between the top and the bottom of a block (see Figure 3.13), Δu_v and Δu_u , using the following constitutive equations:

$$\begin{Bmatrix} \Delta\tau \\ \Delta\sigma_n \end{Bmatrix} = [D]\begin{Bmatrix} \Delta u_u \\ \Delta u_v \end{Bmatrix} = [D]\begin{Bmatrix} u_u^{top} - u_u^{bottom} \\ u_v^{top} - u_v^{bottom} \end{Bmatrix} \quad (3.14)$$

When a fault is assumed as an isotropic linear elastic material, the matrix [D] can be expressed as:

$$[D] = \begin{bmatrix} K_s & 0 \\ 0 & K_n \end{bmatrix} \quad (3.15)$$

where, K_n and K_s are the elastic normal stiffness and shear stiffness respectively.

In the context of CO_2 geologic storage, numerical modeling of faults using the zero-interface elements have recently been introduced (Vidal-Gilbert et al., 2009; Cappa and Rutqvist, 2011; Orlic et al., 2011). Cappa and Rutqvist (2011) examined various hydromechanical models of faults to investigate fault behavior. They used different mechanical modeling approaches, including slip interface and finite-thickness elements with isotropic or anisotropic elasto-plastic constitutive models. The results of the investigation showed that hydromechanical behavior of faults can be appropriately represented with zero thickness interface element as well as a solid element as shown in Figure 3.14. In the field of hydrocarbon production, interface element concept has been employed by many researchers (Bostrøm and Skomedal 2004; Cuisiat et al., 2010b).

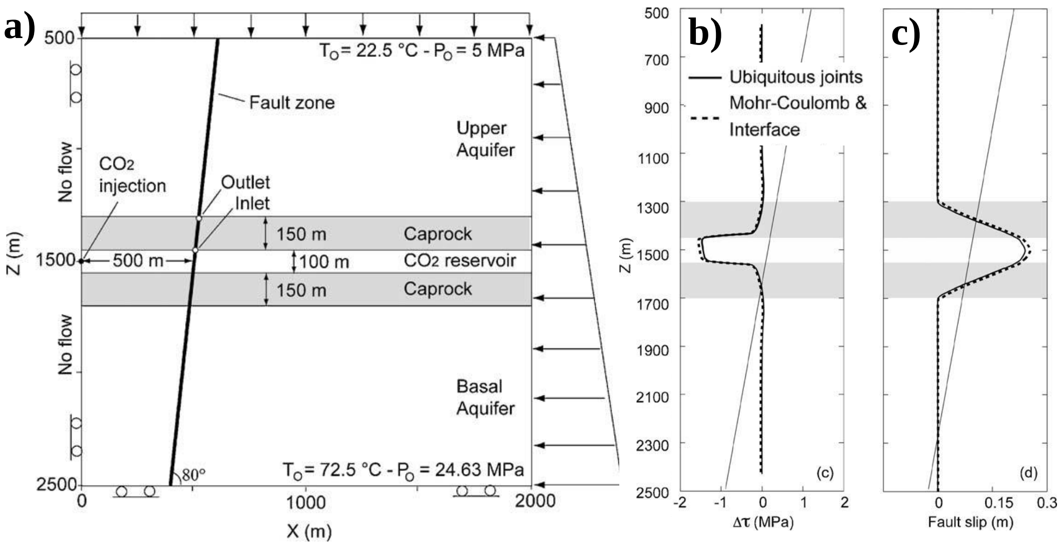

Figure 3.14 Comparison of modelling faults as interface element (dotted line) and solid elements (solid line) for geomechanical analysis of CO_2 geologic storage: a) model geometry, b) change in shear stress, and c) shear slip (Cappa and Rutqvist, 2011).

However, when implementing the zero-thickness interface element in the continuum model, it creates numerical instability, especially when the interface stiffnesses (i.e. K_n and K_s in Equation 3.15) are very different from the stiffness of surrounding continuum elements (Day and Potts, 1994). Thus, careful selection of the interface stiffnesses would be necessary for realistic analysis. Alternatively, contact formulations can be useful to model the discontinuity in global model (ABAQUS, 2001; Bostrøm and Skomedal, 2004).

Modelling fault discontinuity in discontinuum models

Discontinuum methods were originally developed for modelling relative displacement in large blocky bodies, which could be proper for modelling fault reactivation. Distinct element method (DEM) is a widely used dicontinuum method in rock mechanics to model behaviour of fractured rock (Bobet et al., 2009; Cundall and Hart, 1992). The DEM assumed that the fractured medium is divided into discrete bodies that are connected by a constitutive relationship as illustrated in Figure 3.15. Thus, the modelling of relative displacement at predefined fractures (e.g. faults) could be more straightforward in the DEM than the continuum methods.

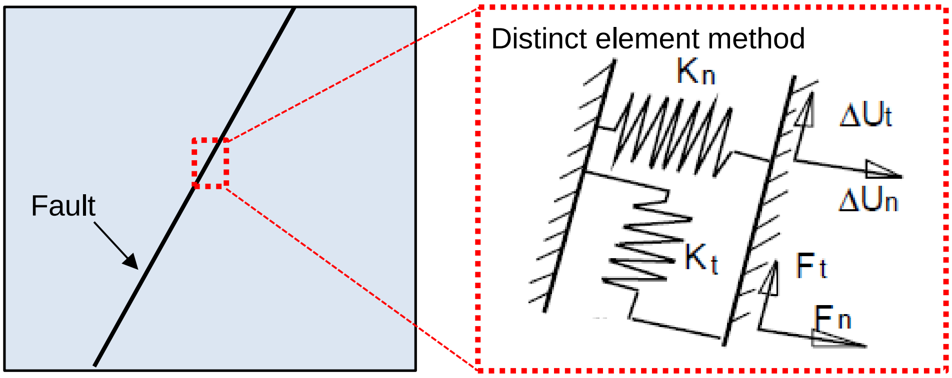

Figure 3.15 Schematic of modelling fault using distinct element method.

The DEM has been used to model fault reactivation or fracture opening for hydrocarbon reservoirs. Gutierrez and Makurat (1997) modelled the effect of cold water injection in fractured hydrocarbon reservoirs using DEM coupling with hydro-thermal behaviour. To model the non-linear plastic behaviour of rock fractures, they used the Barton-Bandis model (Barton et al., 1985). From their study, they showed the feasibility of the DEM on the injection related reservoir geomechanics. Recently, the applicability of the DEM to CO_2 related fault reactivation has also been reported. Morris et al. (2011) applied the DEM method (LDEC) to model an injection-induced mechanical deformation at In Salah CO_2 storage project as shown in Figure 3.16. They have simulated the mm-scale uplift of the overburden associated with the CO_2 injection and compared the results with the observed ground surface deformation measured by InSAR. The study estimated a surface deformation that has fairly good agreement with InSAR monitoring. They could get a more realistic morphology of the surface deformation when the pressurization of the reservoir and faults were combined rather than considering either in isolation.

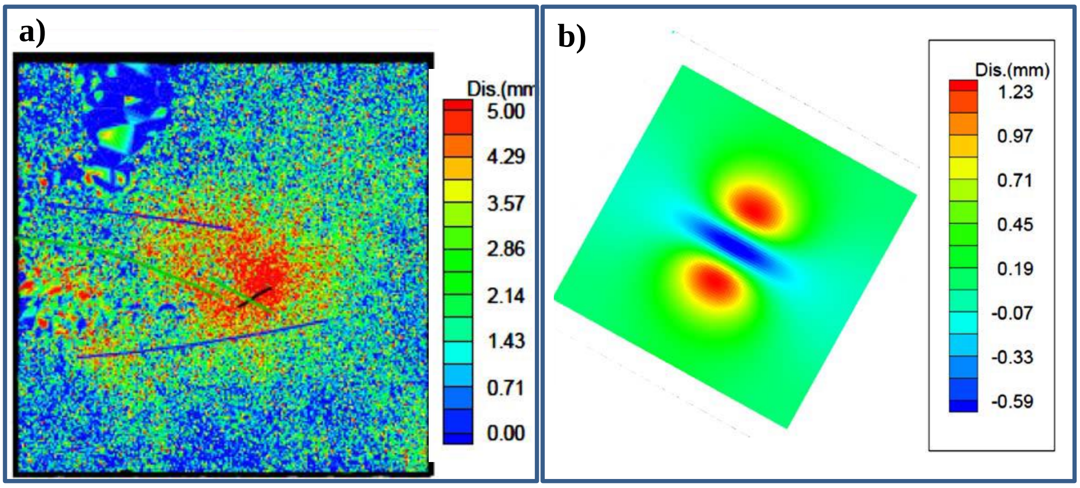

Figure 3.16 Comparison of the surface uplift monitored by InSAR data (a) with the predicted uplift using DEM method (b) the injector KB-502, In Salah CO_2 storage site (Morris et al., 2011).

There is no standard guideline for when to use a continuum (e.g. FEM or FDM) or a discontinuum model (e.g. DEM), either for petroleum/CO_2 related geomechanics or for the conventional rock mechanics problems. However, the choice of method may mainly depend on the scale of the discontinuity and its geometry. Figure 3.17 illustrates the effect of the scale of discontinuities based on the selection of a numerical method. If the medium is mainly composed of intact rock (Figure 3.17a) or heavily fractured rock (Figure 3.17d), continuum models can be used. When the rock is moderately fractured with definable spacing, a discontinuum method would be appropriate. When only a small number of discontinuities are present in the domain, as depicted in Figure 3.17b, both continuum and discontinuum approaches could be applicable (Bobet et al., 2009; Jing, 2003). It should be noted that the prediction of any of these methods must be validated using direct observations (e.g. deformation or seismic monitoring).

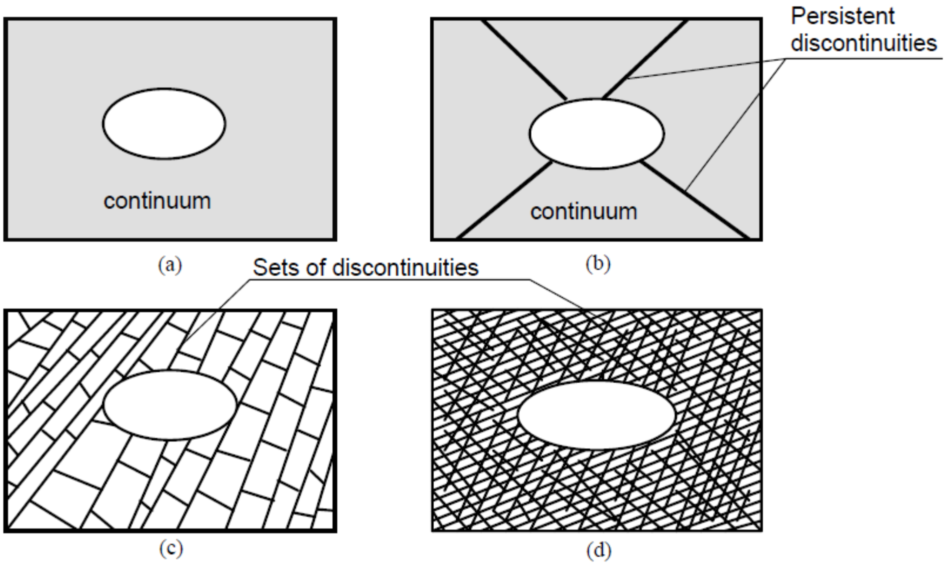

Figure 3.17 Effect of scale of discontinuities on the selection of numerical method: a) continuum method, b) either continuum with interface element or discrete (discontinuum) method, c) discrete (discontinuum) method, d) continuum method with equivalent properties (pseudo-continuum method) (after Jing, 2003).

Estimation of the normal and shear stiffness of fault zones

When we model a fault zone as a single discontinuity, we need the stiffness of the fault to estimate elastic deformation induced by pressure change. Generally, a fault zone is composed of both continuum material (e.g. intact rock/ damaged zone) and discontinuities (e.g. joints). The fault zone can be assumed to be layered material made of fractures and intact material defined by:

- mean fracture spacing s in the fault zone,
- normal and shear stiffness of the fractures k_n and k_s,
- Young's modulus E and shear modulus G of the intact material.

The shear and normal stiffness of faults can be estimated using equivalent value considering stiffness of both intact rock and fracture. The equivalent stiffness can be expressed as follows (Priest, 1993):

$$K_s = \frac{G_{fault}}{t_{fault}} = \frac{G}{1 + \frac{G}{sk_s}} \frac{1}{t_{fault}} \qquad (3.16)$$

$$K_n = \frac{E_{oed\_fault}}{t_{fault}} = \frac{E_{oed}}{1 + \frac{E_{oed}}{sk_n}} \frac{1}{t_{fault}} \qquad (3.17)$$

3.3.3 Modeling fault as rock mass of continuum material

As previously explained, although a model assumes a fault is a single discontinuity it can explain the fault behaviour at global scale (i.e. reservoir of km-scale). The model's limitation may be its ability to explain detailed behaviour of fault zones, which consist of a fault core and a damage zone. Modelling faults as a rock mass of continuum material, or fracture material, could be a suitable approach to investigate fault behaviour at a local scale.

Generally, Young's modulus and shear strength of the fault core are weaker than those for the damage zone (Gudmundsson, 2004). The fault zone in a rock body is more prone to shear slip with strain softening than the surrounding rock mass, as shown in Figure 3.18. To model the shear band using a continuum approach, the Mohr-Coulomb model with strain softening strength is usually used for the fault reactivation analysis (Cuisiat et al., 2010b; Rinaldi et al., 2014).

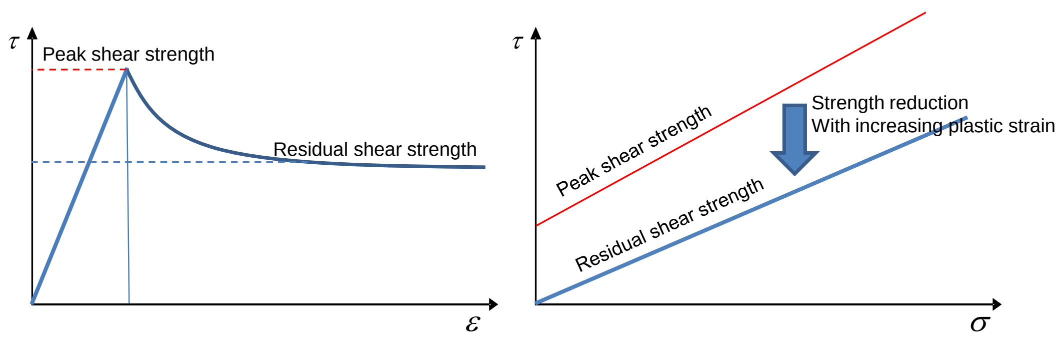

Figure 3.18 Material softening behaviour presented in a) shear stress versus strain and b) shear stress versus stress field.

It should be noted that fault modelling with strain softening using a continuum approach is sensitive to the mesh size (Tejchman and Bauer, 1996; Thakur, 2011). Some field observations indicate that the scale of fault slip could be in the order of 1 to 5 mm, which is much thinner than the thickness of even a fault core (Sibson, 2003b). To overcome the tendency in the continuum modelling that shear bands follow the pattern of mesh discretisation rather than real shear bands, new techniques such as non-local continuum or Cosserat continuum theory have been introduced and include the internal length (Brinkgreve, 1994; Sulem and Vardoulakis, 2004). These advanced continuum methods can model shear band thickness using a scaled internal length, which represents an area within which the average non-local strain is obtained. Consequently, the problem of the discrepancy between real shear bands and mesh-dependent modelled shear bands can be solved. However, these methods are not well implemented into commercial FE software yet. They also require the element size to be smaller than the internal length.

3.4 Effect of fault reactivation on sealing integrity

In previous sections, we reviewed the methodologies to evaluate fault reactivation analytically and numerically. Although the aforementioned methods can estimate the location and time for shear failures, shearing does not always imply leakage along reactivated faults. Sometimes, failure in reactivated faults can induce pore collapse and cause porosity reduction. Consequently, low porosity may lead to fracture healing and tightening of the seal. The permeability change during fault reactivation seems to be related to the ductile or brittle behavior of the material (Barton et al., 1985; Bjørlykke et al., 2005; Ingram and Urai, 1999).

The post failure deformation may be brittle or ductile, depending on the shear strength properties and the level of the effective confining stress, as shown in Figure 3.19. In the brittle regime, deformation occurs with associated dilation until sudden failure at peak shear strength, followed by strain softening down to residual shear strength. Ductile deformation, on the other hand, produces contraction of the sample and more diffuse deformation. Shear fractures in brittle deformation dilate under low effective normal stress and cause an increase in permeability with increased shearing. As shear deformation increases, fracture asperities are broken off leading to lower porosity and a reduction in permeability. Shear fractures created in ductile deformation contract during shearing which also leads to a decrease in permeability (Ingram and Urai, 1999).

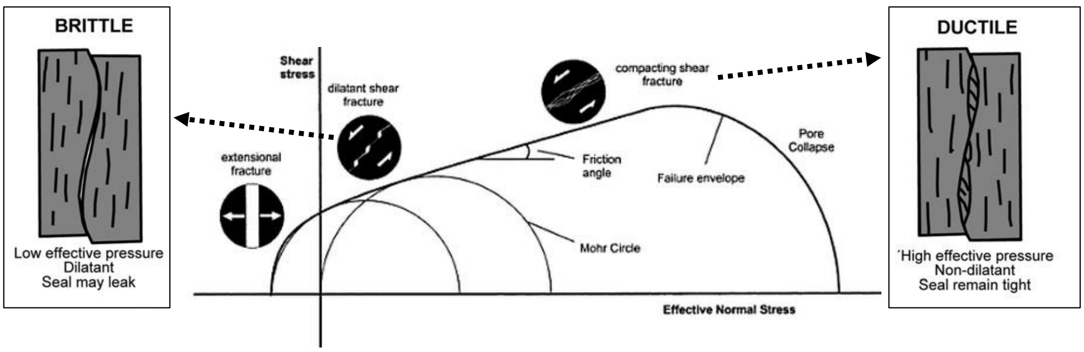

Figure 3.19 Effect of strength properties and confining stress on the brittle/ductile deformation (Ingram and Urai, 1999).

As previously discussed, brittle behaviour in the post failure regime is responsible for the enhancement of fault permeability. Thus, many empirical relations on the stress dependent permeability can be expressed as a function of the change of porosity, which is a consequence of brittle/ductile behaviour (Millington and Quirk, 1961; Chin et al., 2000; Cappa and Rutqvist, 2011). In soil and rock mechanics, the change of porosity can be simply regarded as change of volumetric strain.

When elasto-plastic behaviour of faults is considered in a numerical approach, an incremental vector of plastic strain can be plotted as shown in Figure 3.20. The negative direction of plastic strain on the x-axis indicates a dilation with shearing (i.e. increase of volumetric strain during shearing). The ratio between plastic volumetric strain and plastic shear strain can be defined by the angle between the normal to plastic potential and the vertical line, known as dilatancy angle, φ.

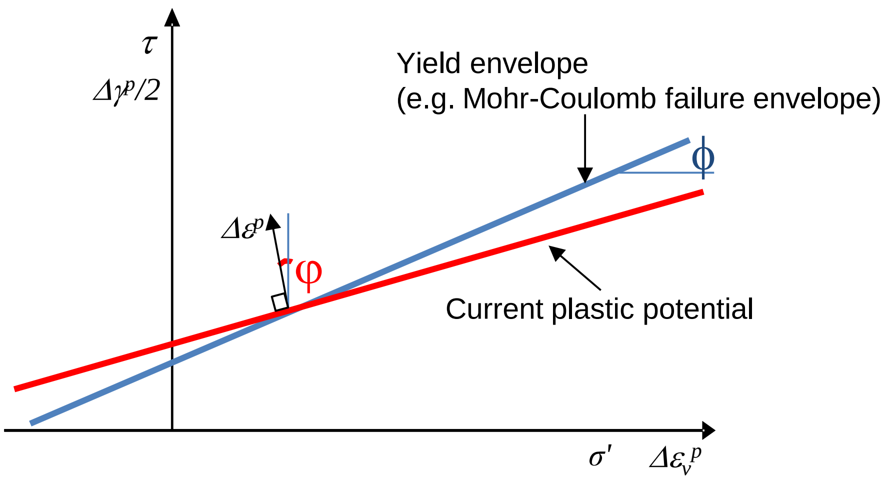

Figure 3.20 Incremental vector of plastic strain plotted along with the Mohr-Coulomb failure envelope for non-associative plasticity.

If we assume the same value of friction angle as the dilatancy angle (i.e. $\varphi = \phi$), the plastic potential becomes the same as the yield envelope – which is known as the associated flow rule. The associated flow rule for the Mohr-Coulomb model has an advantage because the direction of plastic strain is relatively easy to determine. However, the assumptions applied in this model have the following pitfalls and can result in unrealistic volumetric strain determination (Potts and Zdravković, 1999):

- The magnitude of the dilation using the associated flow rules (i.e. the extensional plastic volumetric strain) can be larger than rock/soil behaviour. Usually, $\varphi < \phi$ is common for real rock/soil behaviour.
- Once the dilation starts, it occurs permanently. In soil/rocks, the magnitude of dilation reduces with increasing strain. Finally, the increase of volumetric strain due to the dilation becomes zero at large strain, which is called a critical state in soil mechanics.

When fault behaviour is modelled using a Mohr-Coulomb type plastic model, over-estimation of dilatancy and consequent unrealistic permeability change in the fault needs to be avoided. This can be achieved if a realistic range for the dilatancy angle, which is less than the friction angle, is considered. When plastic strain increases, even though the dilatancy angle is less than a friction angle, it could still over-estimate the volumetric strain during large strains. Thus, implementation of dilatancy that varies with plastic strain, could result in a more realistic estimation of the change of permeability in a fault during reactivation especially if deviatory plastic strain occurs.

3.5 Summary and recommendation

In this chapter, the methodologies to evaluate fault reactivation potential and its relationship to fault leakage was addressed. Analytical approaches based on the Mohr-Coulomb type failure criteria are simple and provide useful tools for the first-order assessment of fault reactivation potential during injection/depletion. Essential components of the analytical method of fault reactivation potential are:

- Magnitude and direction of in-situ stresses,
- Fault dip and strike,
- Shear strength, especially friction coefficient,
- Initial pore pressure and pressure change.

The analytical approach has some limitations to explain real fault behaviour during injection/depletion. Some of the limitation are:

- Analytical approaches cannot consider a change of stress around faults. Some approaches can consider the change in total stress magnitude. But injection/depletion changes not only the magnitude but also the direction of principal stresses. This is another factor that may introduce uncertainties to the estimated fault reactivation potential.
- The slip tendency estimated by analytical approach and the change in reservoir pressure can only be applied to the reservoir-bounding or reservoir-crossing faults. Thus, the calculated fault reactivation derived from an analytical approach may provide limited information on the slip tendency of faults in the sealing formations. If we can estimate the change of effective stresses in a cap rock, then we can apply the analytical approach and predict the slip tendency. However, such an approach may need more validation. Sometimes, propagation of fault reactivation may act positively on the sealing integrity of a fault by activating a self-healing mechanism. Fault reactivation that affects the sealing integrity is a consequence of complex coupled stress changes.

Numerical modelling can provide information to overcome the limitation of the analytical approaches. Generally, the modelling approach on fault reactivation analysis is dependent upon the scale of interest. A fault can be implemented into numerical models as follows:

- In a global analysis, major faults can be represented as single discontinuities. In continuum models (e.g. FEM or FDM), a single discontinuity can be modelled as a zero thickness element or as contact formulations. In discontinuum models (e.g. DEM), faults can be modelled as a fractured medium that is divided by discrete bodies that are connected by a constitutive relationship. Both approaches have limitations because numerical instability can occur when the interface stiffness is quite different from the surrounding continuum material. Thus, careful selection of the interface stiffness is necessary to achieve a realistic analysis.
- If detailed behaviour of a fault zone is of interest, or localized substantial strain occurs around the fault, modelling the fault as a rock mass of continuum material can be a suitable approach. It should be noted that, if the model considers strain softening, or the resistance at the shear zone becomes too large, modelling faults using a continuum approach is quite sensitive to the mesh size to capture the thin shear localization.

Brittle behaviour of rocks in a post failure regime contributes to the enhancement of permeability. Proper implementation of strain/stress-dependent permeability changes within a model requires the following considerations:

- A realistic range for the dilatancy angle, which is less than the friction angle, should be used in the model to avoid an over-estimation of dilatancy and an unrealistic permeability change in a fault.
- Implementation of dilatancy that varies with plastic strain, especially deviatory plastic strain, could result in a more realistic estimation of the change of permeability in a fault.

Although various methodologies to evaluate fault reactivation potential have been reviewed in this report, understanding fault behaviour is complicated by the fact that:

- core samples with fault material are usually limited,
- various faulting episodes may have occurred throughout the geological formation of a field, resulting in different fault patterns and characteristics (geometry, extent, filling, etc.),
- most geomechanical fault models oversimplify fault architecture, e.g. simplifying the complex fault structure into a single plane of weakness.

For reasonable simulation of the composite behaviour of a complex fault zone in a global model using a single discontinuity, the equivalent discontinuity modelling needs to be validated. As a tool for the validation, calibration by a local numerical model of the fault zone, which also needs to include various components of the fault structure, could be a useful tool.

If all the factors affecting fault reactivation during an injection operation are taken into consideration in a modelling study it may practically be impossible to model. However, a numerical approach combined with analytical methods may provide efficient and useful information on the fault reactivation potential under certain circumstances. For a stream-lined fault reactivation analysis, following a stepwise procedure (illustrated in Figure 3.21), is recommended:

- The risk of fault reactivation can firstly be assessed using a Mohr-Coulomb type analytical solution,

- If preliminary analysis shows the risk of fault slip, refined geomechancial modelling can be considered. The following input parameters are required for a geomechanical model:
    - A geometrical and geological description of the reservoir and surrounding rock formations, usually from a geological/geophysical model,
    - The mechanical properties of the reservoir and surrounding rocks, usually from geomechanical laboratory testing,
    - The initial conditions in terms of the spatial distribution of pore pressure, stresses and temperature, usually from core and log data,
    - The loading conditions (i.e. time histories of pore pressure field during injection), usually from a reservoir model.

- Determination of a fault model: i.e. the approach required to integrate a fault into a numerical model will depend on the scale of interest.

- Evaluation of leakage potential using calculated fault dilatancy: If the simulation result shows a significant increase in plastic volumetric strain in the fault material, leakage through the fault during a pressure-build up can be suspected. In this case, more detailed flow simulation for faults using updated stress/strain dependent permeability (e.g. coupled flow-geomechnical analysis focusing on fault behaviour) can be helpful for understanding fault leakage during pressure build-up.

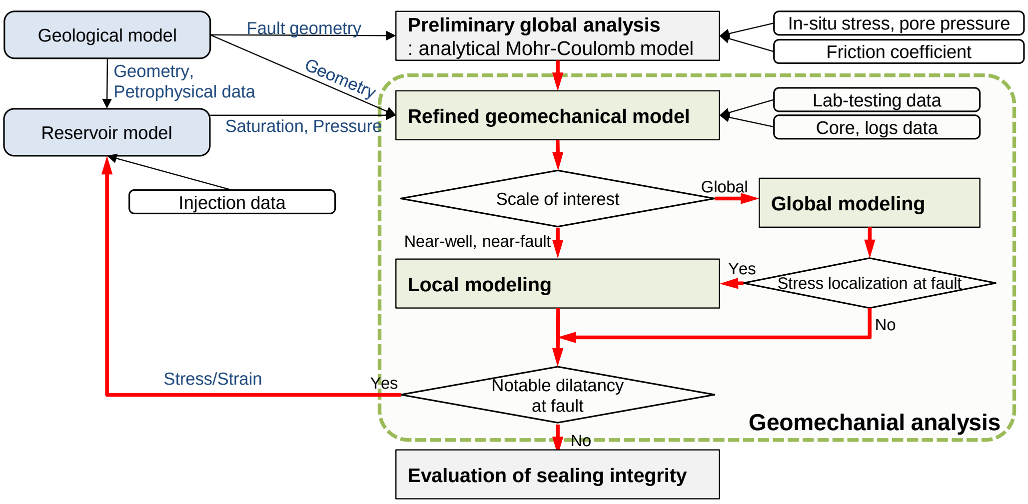

Figure 3.21 Recommended stream line procedure for analysis of fault-reactivation upon fluid injection into a reservoir and subsequent pressure build-up.

4 Input parameters for fault reactivation analysis

Evaluation of stress-induced fault reactivation requires knowledge of three main geomechanical components; namely the in-situ stresses, fault zone strength and pore pressure profile. Pore pressure measurement techniques, prediction or modeling is not covered in this report. A comprehensive review of pore pressure in sedimentary basins is given in Zoback (2007). The principal in-situ stresses include the overburden or vertical stress, σ_v, the maximum horizontal stress, σ_H, and the minimum horizontal stress, σ_h. Both the magnitude and orientation of in-situ stresses relative to the fault orientation are important for fault reactivation analysis and geomechanical modelling (Zoback, 2007).

4.1 Determination of in-situ stresses

A general relationship between the in-situ stresses can be assessed using the Anderson's theory of faulting. For a normal faulting regime, the maximum principal stress is the overburden stress, while for strike-slip and reverse regimes it is the horizontal stress; for normal fault regimes: $\sigma_v > \sigma_H > \sigma_h$, for strike-slip: $\sigma_H > \sigma_v > \sigma_h$ and for reverse regimes: $\sigma_H > \sigma_h > \sigma_v$. Thus, the relative magnitude of in-situ stresses can be constrained if the faulting mechanism of present day active faults is known for a region. However, for engineering operations such as injection and production, accurate orientation and the stress values are required. In this chapter, we will review various methods to estimate the three principal in-situ stresses; i.e. vertical stress, maximum horizontal stress, and minimum horizontal stress.

4.1.1 Stress orientation

The overburden stress is assumed to be vertical, along the axis of vertical wellbores. It is worth noting that in highly orientated wells vertical stress will not coincide with the wellbore axis. Different techniques and methods are used to measure, interpret or calculate the direction and magnitude of in-situ stresses. The widely used method for determining the direction of horizontal in-situ stresses inside wellbores, based on wellbore breakouts, uses data from the borehole caliper log, borehole image logs and borehole televiewer.

An example of determining the direction of horizontal stresses from caliper logs is presented in Figure 4.1 where the direction of two principal stresses normal to the borehole axis is easily recognized. Figure 4.2 shows a borehole image log where borehole breakouts and tensile fractures are visible on the walls of a vertical well. The breakouts imply that the direction of maximum horizontal stress is NE-SW and that of the minimum horizontal stress is NW-SE. In the case of directional wells however, determining stress orientation may be challenging. Further information can be found in Peska and Zoback (1998).

Borehole breakouts interpreted from the four-arms caliper tool are quite reliable and so is the direction of principal stresses (Zoback, 2007). This approach has provided stress orientation data consistent with those from focal mechanisms in many parts of the world (Zoback and Pollard, 1978; Hickman and Zoback, 1983). There are other methods which can be used for the determination of the in-situ stress directions, e.g. earthquake focal mechanism, fault slip data and geological indicators such as igneous dikes. These are generally used for the determination of stress orientations in a basin and at a regional scale and are not the subject of this study. More information on these methods can be found in Nakamura, (1977), Fowler (1990) and Zoback (2007).

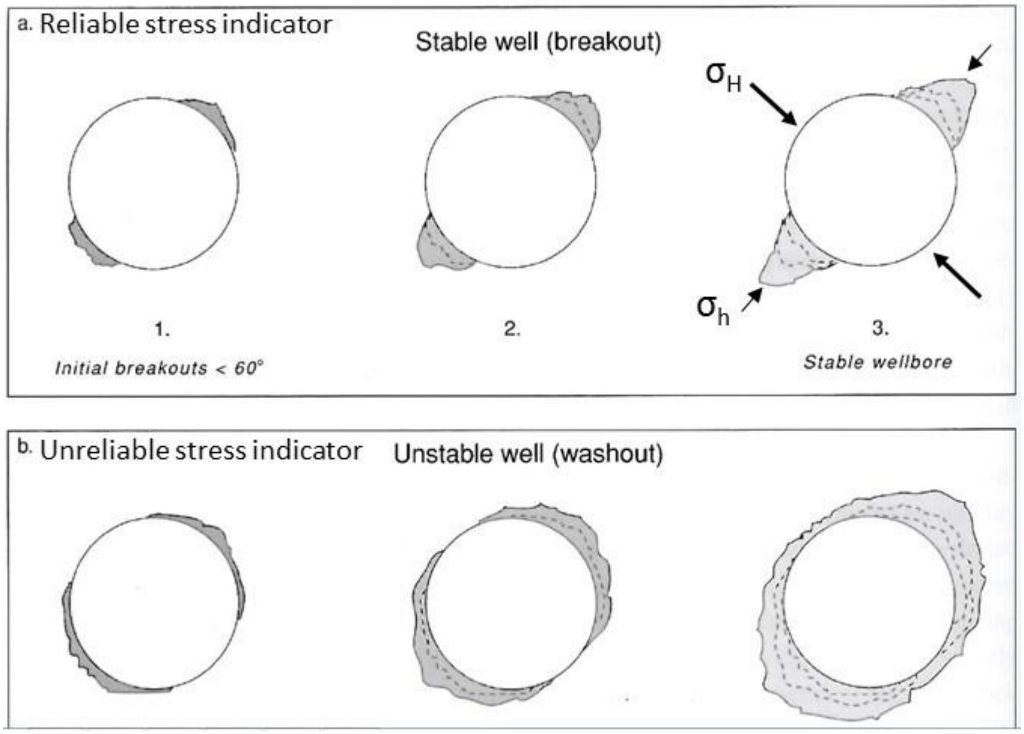

Figure 4.1 *Development of borehole breakouts when local stresses exceed rock strength at the wall of a vertical borehole (modified after Zoback, 2007). a) borehole breakouts with an almost stable width and b) washouts where the shape of bore hole and the width of the failed wall changes progressively.* σ_H *is the maximum in-situ stress and* σ_h *is the minimum horizontal stress.*

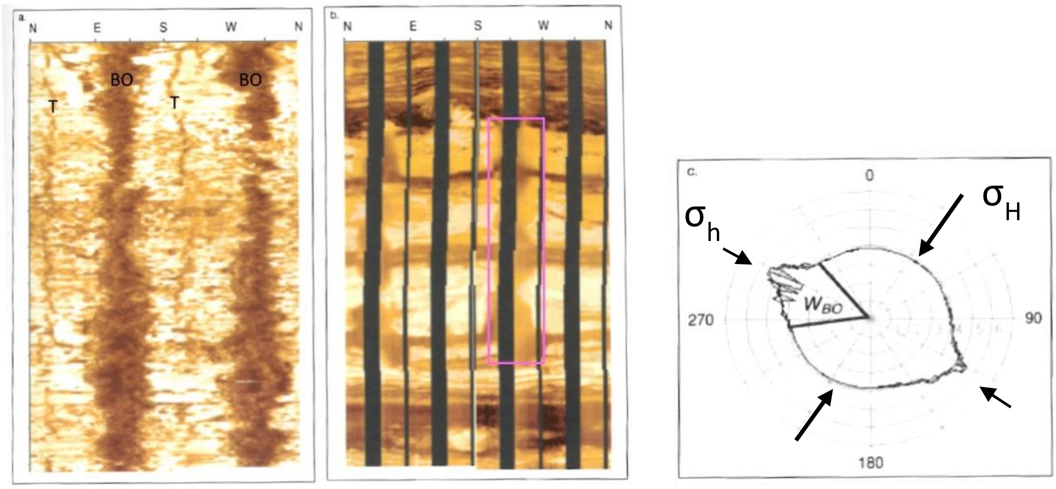

Figure 4.2 Borehole breakouts and tensile fractures in image logs and the interpreted direction of maximum and minimum horizontal stress (modified after Zoback, 2007). Borehole breakouts appear in an ultrasonic televiewer image as dark bands on either side of a well because of the low-amplitude ultrasonic reflections off the wellbore wall (BO in the left image). They also appear as out-of-focus areas in electrical image data because of the poor contact between the tool and the wellbore wall (purple-marked rectangle in the middle image). Tensile fractures are also observed on either side of the wellbore wall as dark lines (T in the left image). The maximum horizontal stress (σ_H) has NE-SW direction and the minimum horizontal stress (σ_h) (the elongated well axis) has NW-SE direction (see the right image).

4.1.2 Vertical stress

Magnitude of the vertical or overburden stress (σ_v) at a certain point can be calculated, to first orders, using Equation (4.1):

$$\sigma_v = \int_0^z \rho(z) g dz \tag{4.1}$$

where $\rho(z)$ is density of the overburden layers at depth z and g is the gravitational acceleration.

The density of rock formations can be either measured from core samples or estimated from density logs. Where cores are available, density is one of the simple and cheap parameters to measure. However, cores are seldom available for the overburden layers in petroleum fields, as the focus is on the reservoir section. Density and sonic logs are available but not for the entire well path. The density of rocks can be calculated from such logs using empirical equations if they are available. Integrating laboratory data with log data and using empirical relationships (e.g. Ludwig et al., 1970) may provide us with a profile of the density but not necessarily throughout the overburden. Density is the main input parameter for plotting vertical stress profiles versus depth as shown for instance in Figure 4.3 for the Bight basin, Australia.

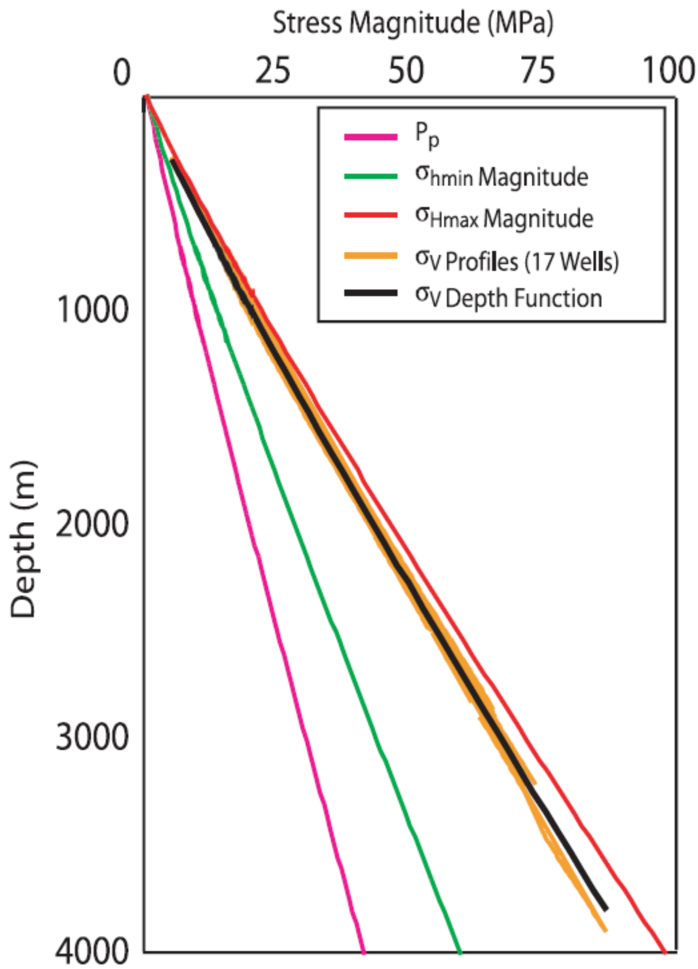

Figure 4.3 Effective vertical stress for the Bight Basin, southern Australia (after Mildren et al., 2002). The black line shows vertical stress determined from the density log. The yellowish lines show vertical stress profile for 17 wells from various assessment methods.

4.1.3 Magnitude of the minimum horizontal stress, σ_h

Determining the magnitude of horizontal stresses is more challenging than that of the overburden stress. There are both analytical models and well test methods for estimating the magnitude of minimum horizontal stress. A simple equation was presented by Eaton (1969) based on the theory of elasticity and bilateral constraint to determine the magnitude of minimum horizontal stress, σ_h:

$$\sigma_h = \frac{\nu}{1-\nu}\left(\sigma_v - P_p\right) + P \qquad (4.2)$$

where ν is Poisson's ratio, σ_v is overburden stress, and P is pore fluid pressure. Note that Equation (4.2) is valid for tectonically passive sedimentary basins under a normal faulting regime. It provides a primary estimation of the minimum horizontal stress but the actual stress should be measured on-site using techniques such as well pressure tests.

Different pressure integrity tests such as the Leak-Off Test (LOT), the Extended Leak-Off Test (XLOT), the Formation Integrity Test (FIT) and minifrac tests are used for the assessment of minimum in-situ stress. One of the most reliable methods for the determination of the minimum horizontal stress in boreholes is the extended leak-off test (Figure 4.4). If a leak-off test is performed with water or another less viscous fluid, the values of the Leak-Off Pressure (LOP), Fracture Propagation Pressure (FPP), Instantaneous Shut-In Pressure (ISIP) and Fracture Closure Pressure (FCP) present the range of the minimum horizontal stress value. If this test is run with a viscous fluid, the FCP will represent the value of the least in-situ stress (White et al., 2002; Lucier et al., 2006; Raaen et al., 2006; Zoback, 2007; Lin et al., 2008; Lorwongngam, 2008).

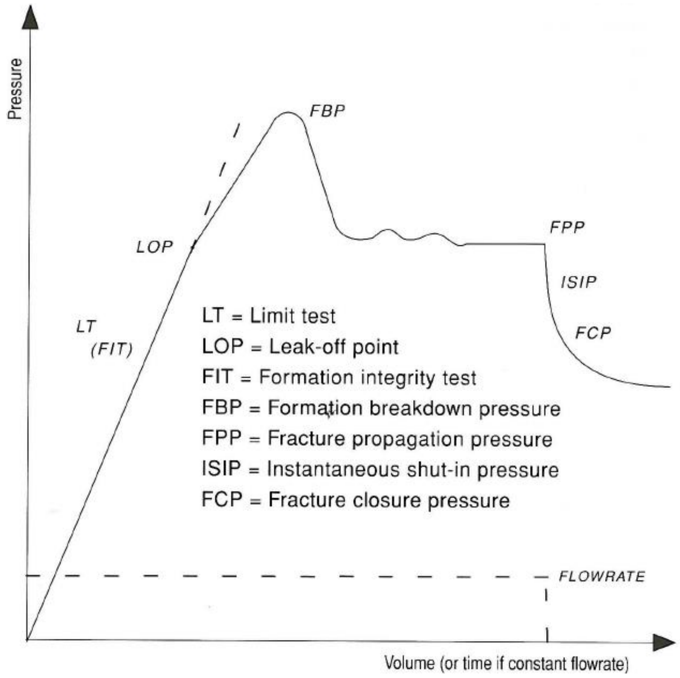

Figure 4.4 *Schematic plot for a mini-frac or extended leak-off test showing pressure as a function of volume or equivalently time (after Zoback, 2007). The Fracture Closure Pressure (FCP) is usually considered to indicate the magnitude of the least in-situ stress.*

There are also empirical equations derived from leak-off tests to determine the magnitude of minimum horizontal stress. For instance, Hillis et al. (1997) based on 61 leak-off tests proposed the following equation for the Bonaparte Basin, the Timor Sea:

$$\sigma_h = 0.36\ (\sigma_v - P) + 1.0 + P \tag{4.3}$$

where σ_h is the minimum horizontal stress, σ_v is the vertical stress and P is pore pressure, all expressed in MPa. Such equations are only valid for the location they were developed for and can be applied to the same area but may mislead if applied beyond the region.

Breckels and van Eekelen (1982) based on fracturing data from the North Sea proposed relations between horizontal stress and depth:

$$\sigma_h = 0.0053\, D^{1.145} + 0.46\left(P - P_{pn}\right) \qquad (D < 3500\ m) \tag{4.4}$$

$$\sigma_h = 0.0246\, D - 31.7 + 0.46\left(P - P_{pn}\right) \quad (D > 3500\ m) \tag{4.5}$$

where D is the depth, P is the pore pressure, P_{pn} is the normal pore pressure (corresponding to a gradient of 10.5 MPa/km) (See Fjær et al., 2008).

Among different types of well tests mentioned above, the minifrac and extended leak-off tests are the most reliable methods that provide maximum information for determination of minimum horizontal stress. In contrary, the leak-off tests are often the least effective measurements that might not provide useful information on in-situ stresses.

4.1.4 Magnitude of the maximum horizontal stress

The magnitude of maximum horizontal stress is the most difficult stress component to determine. However, several methods have been suggested for calculating this parameter from borehole data which are summarized below.

Hydraulic fracture tests
Haimson and Fairhurst (1970) suggested that hydraulic fracture test in open holes can be used for determining the magnitude of the maximum horizontal stress (σ_H):

$$\sigma_H = 3\sigma_h - P_b - P + T_0 \tag{4.6}$$

where P_b is the breakdown pressure, P is pore pressure and T_0 is the tensile strength of rock. If a hydraulic fracture test is repeated, the tensile strength for the second cycle will be zero (T_0 =0), thus we have:

$$\sigma_H = 3\sigma_h - P_b - P \tag{4.7}$$

This equation has been used successfully in many projects to estimate the magnitude of maximum horizontal stress. However, care should be taken when using this concept for deep, cased wellbores, oval-shaped wells and wellbores with irregular cement distribution around casing. The problem in such wellbores is that the value of P_b is very uncertain and so is the magnitude of the maximum horizontal stress from Equation (4.7). However, if a hydraulic fracture test is very well defined and the value of P_b is certain this method can also be used for deep wells.

Drilling induced fractures

Another method proposed for determining the magnitude of maximum horizontal stress is based on the drilling induced fractures for a strike-slip faulting regime (Zoback, 2007):

$$\sigma_H = 3\sigma_h - 2P_b \tag{4.8}$$

This equation is based on the assumption of frictional strength of faults and considers the friction coefficient of 0.6 (μ=0.6). This equation assumes considerable simplifications.

Width of borehole breakouts

Borehole breakouts occur when local stresses around the wellbore exceed the strength of formation. Breakouts occur in a plane perpendicular to the maximum horizontal stress and develop but only in vertical wells. After a while they get stable and deepen. Then, the width of breakouts (W_{BO}) remains almost constant (as seen earlier in Figure 4.2b.

Using the W_{BO}, one can estimate the magnitude of maximum horizontal stress using:

$$\sigma_H = \frac{(C_0 + 2P + \Delta P + \sigma^{\Delta T}) - \sigma_h(1 + 2\cos 2\theta_b)}{1 - 2cos2\theta_b} \tag{4.9}$$

where $2\theta_b \equiv \pi - W_{ob}$ (for further details see Zoback, 2007).

Note that temperature change, $\sigma^{\Delta T}$, (and thermally-induced stress changes) can be quite large in some cases. Thus, thermal stresses may play an important role in determining the magnitude of the maximum horizontal stress obtained from Equation (4.9). Many concepts have been proposed to account for thermal stresses for various applications such as borehole stability, reservoir stimulations, etc. Discussion on thermal stresses is beyond the scope of this chapter. Further details can be found in Perkins and Gonzales (1985), Fjær et al. (2008), Charlez (1997), Tang and Luo (1998) and Ghassemi (2007).

Stress polygon

When exact values of stresses are not available, estimating the likely range of stresses for a certain depth can be helpful. For this purpose, the stress polygon method, which is based on the frictional strength of faults, is utilized. There is an assumption that the stress state in the crust is limited by the frictional strength of faults. The upper bound of the frictional limit of a fault has been given by Jaeger et al. (2007) and Zoback (2007):

$$\frac{\sigma'_1}{\sigma'_3} = \frac{\sigma_1 - P}{\sigma_3 - P} = ((\mu^2 + 1)^{0.5} + \mu)^2 \tag{4.10}$$

Using Anderson's faulting theory, Eq. (4.10) for different types of faulting regimes can be rewritten as:

Normal faulting: $$\frac{\sigma'_1}{\sigma'_3} = \frac{\sigma_v - P}{\sigma_h - P} \leq ((\mu^2 + 1)^{0.5} + \mu)^2 \qquad (4.11)$$

Strike-slip faulting: $$\frac{\sigma'_1}{\sigma'_3} = \frac{\sigma_H - P}{\sigma_h - P} \leq ((\mu^2 + 1)^{0.5} + \mu)^2 \qquad (4.12)$$

Reverse faulting: $$\frac{\sigma'_1}{\sigma'_3} = \frac{\sigma_H - P}{\sigma_v - P} \leq ((\mu^2 + 1)^{0.5} + \mu)^2 \qquad (4.13)$$

where σ_v is vertical stress, σ_H is the maximum horizontal stress, σ_h is the minimum horizontal stress, P is pore pressure and μ is friction coefficient. Equations (4.11) to (4.13) can be plotted in the form of a stress polygon from which places limits on the range of stress magintudes that can be determined (Figure 4.5, for details see e.g. Zoback, 2007).

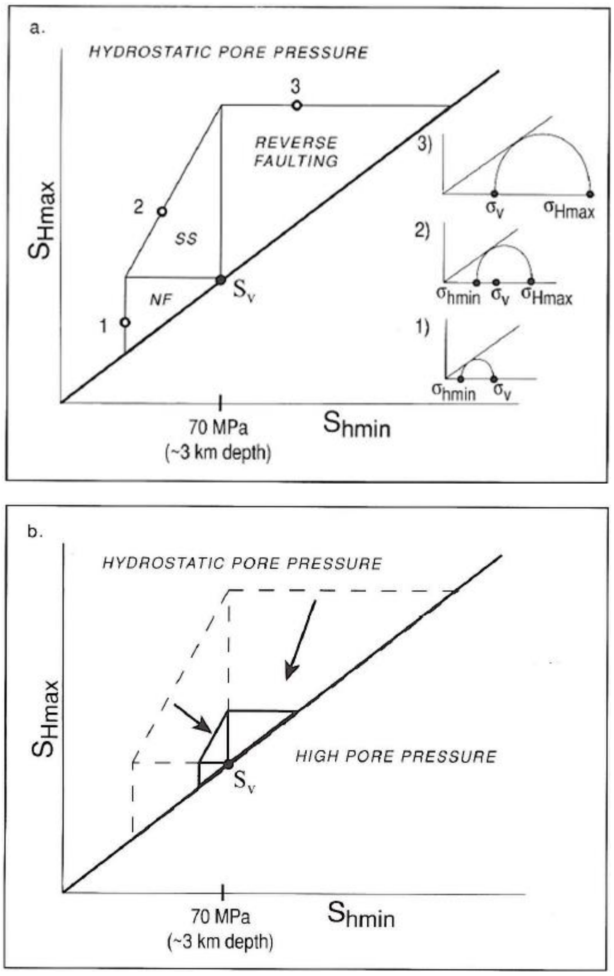

Figure 4.5 *Stress polygon method to define possible range of stress magnitudes at a certain depth (after Zoback, 2007). Range of stresses for a depth of 3 km when a) pore pressure is hydrostatic and b) pore pressure is 80% of the vertical stress.*

4.2 Strength and friction coefficient of faults

Faults may cross both the storage unit and the underburden/overburden and thus provide a pathway to the surrounding formations. Therefore, determining the strength of a fault is crucial prior to planning an injection operation. The strength of faults, τ, may be calculated as a function of depth provided that the correct friction coefficient (μ) value and pore pressure (P) value for the fault plane are known:

$$\tau = \mu(\sigma_n - P) \tag{4.14}$$

Byerlee (1978) studied frictional behavior of various rock types and presented the initial friction and maximum friction for typical rocks (Figure 4.6). Based on a review of laboratory studies of different rock types, he concluded that at normal stresses up to 2000 bar (200 MPa), the shear stress required to cause sliding is given approximately by:

$$\tau = 0.85\ \sigma_n \tag{4.15}$$

And at normal stresses above 2000 bar (200 MPa), the shear stress is approximately given by:

$$\tau = 50 + 0.6\ \sigma_n \tag{4.16}$$

Where both shear and normal stresses are expressed in MPa (Figure 4.7 and Figure 4.8).

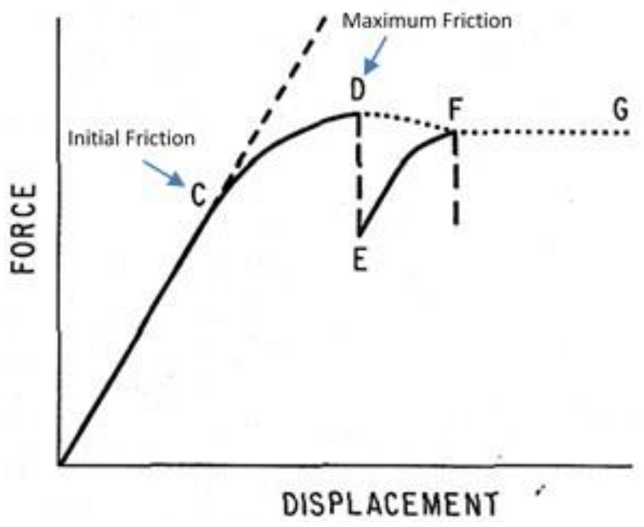

Figure 4.6 Frictional force as a function of displacement (after Byerlee, 1978). Initial friction is indicated by the point where the deformation curve deviates from linearity, point C. Point D marks the maximum friction. For details see Byerlee (1978).

The friction coefficient for all types of rocks is often said to lie in the range of 0.6-0.85 (Figure 4.7) but smaller and larger values are common. Fault gouge may have very low values if hydrated clay is present. Therefore, a coefficient of friction of 0.6 can be considered as the lower bound for fault slip and the onset of leakage (Bretan et al., 2011). If however, the sliding surfaces are separated by large thicknesses of gouge composed of minerals such as montmorillonite or vermiculite, the friction may be very low. Since natural faults often contain gouge composed of various minerals, the friction of natural faults is strongly dependent on the composition of the gouge (Beyerlee, 1978).

Townend and Zoback (2000) and Morrow et al. (2000) presented a similar range of coefficients of friction (see Figure 4.8). This is consistent with what was shown in Figure 4.7 (lower panel). The coefficient of friction is higher at shallow depths (low effective stress) but decreases with increasing the depth.

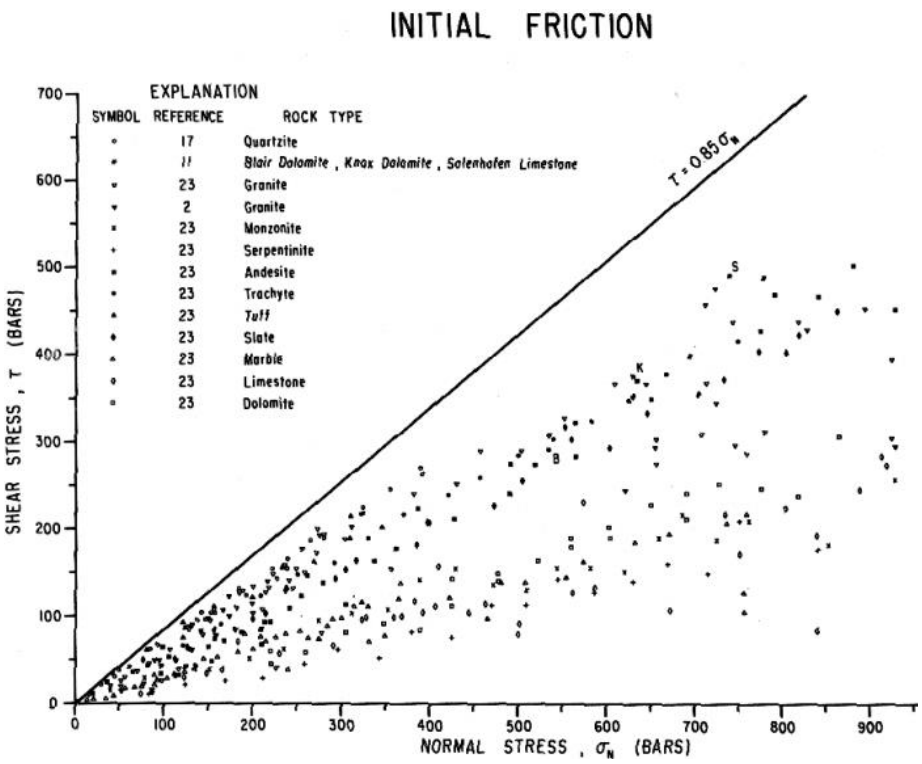

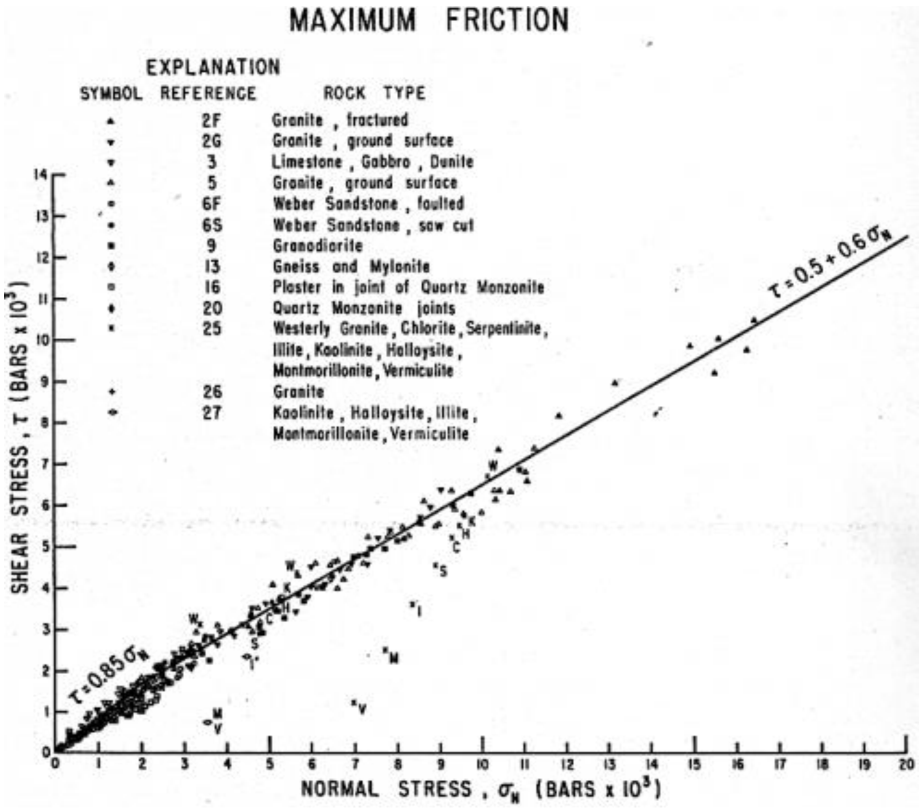

Figure 4.7 *Initial friction and maximum friction for various types of rocks (after Beyerlee, 1978). The data shows the range of the maximum friction coefficient, μ= 0.6 to 0.85. The coefficient is higher at low normal stress (0.85) but decreases to 0.6 with increasing normal stress.*

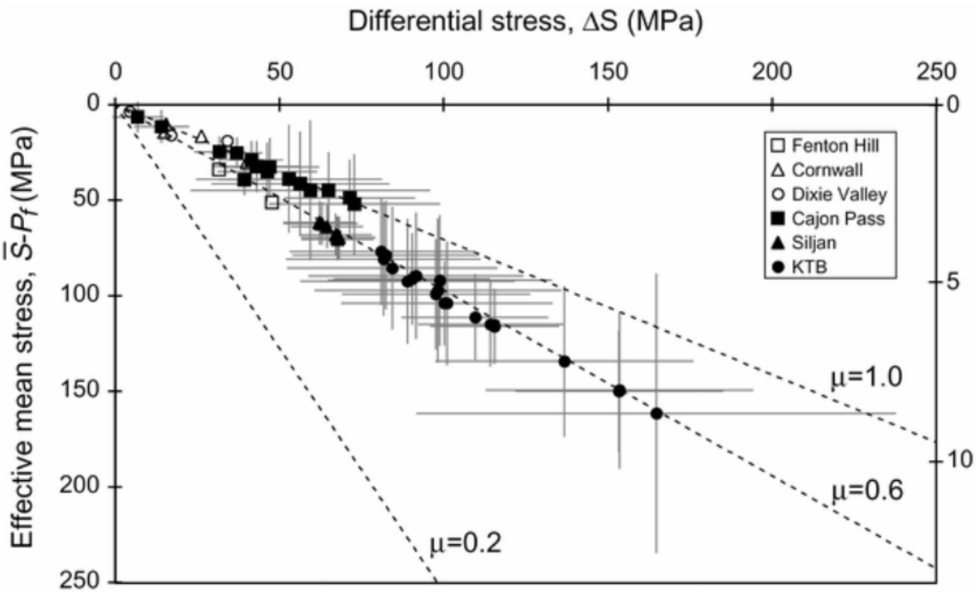

Figure 4.8 *Friction coefficient for different rock types as a function of depth or effective mean stress (after Townend and Zoback, 2000).*

The friction coefficient at stresses lower than 200 MPa is a function of surface roughness. At higher stresses above 200 MPa it is independent of surface properties and thus is independent of rock type. The friction strength of faults is significantly influenced by the mineralogy of fault gouge (Samuelson and Spiers, 2012; Moore et al., 2004; Tembe et al., 2010) and decreases with increasing the bulk clay content.

The coefficient of friction is affected by the type of fluid in the sliding surface as shown by Morrow et al. (2000) and Sone et al. (2012). Morrow et al. (2000) examined the influence of water on the friction coefficient of different gouges (Figure 4.9). The coefficient of friction decreased for all gouges when they were exposed to water, among them Serpentinite which showed the largest reduction. Calcite crystals in dry condition showed the highest friction coefficient (μ=0.85) and Talc and Graphite had the lowest coefficients ($\mu \approx 0.2$). As filling material in a fault plane is usually a mixture of the different minerals present in the host rocks, the friction coefficient of a fault will likely be within the range of the friction coefficient of the constituent minerals. This statement may also be true for cases where mineral alterations occur in the fault plane; the friction coefficient of fault will lie within the friction coefficients of minerals present in the fault plane. This, however, is one of the areas in need of further investigation.

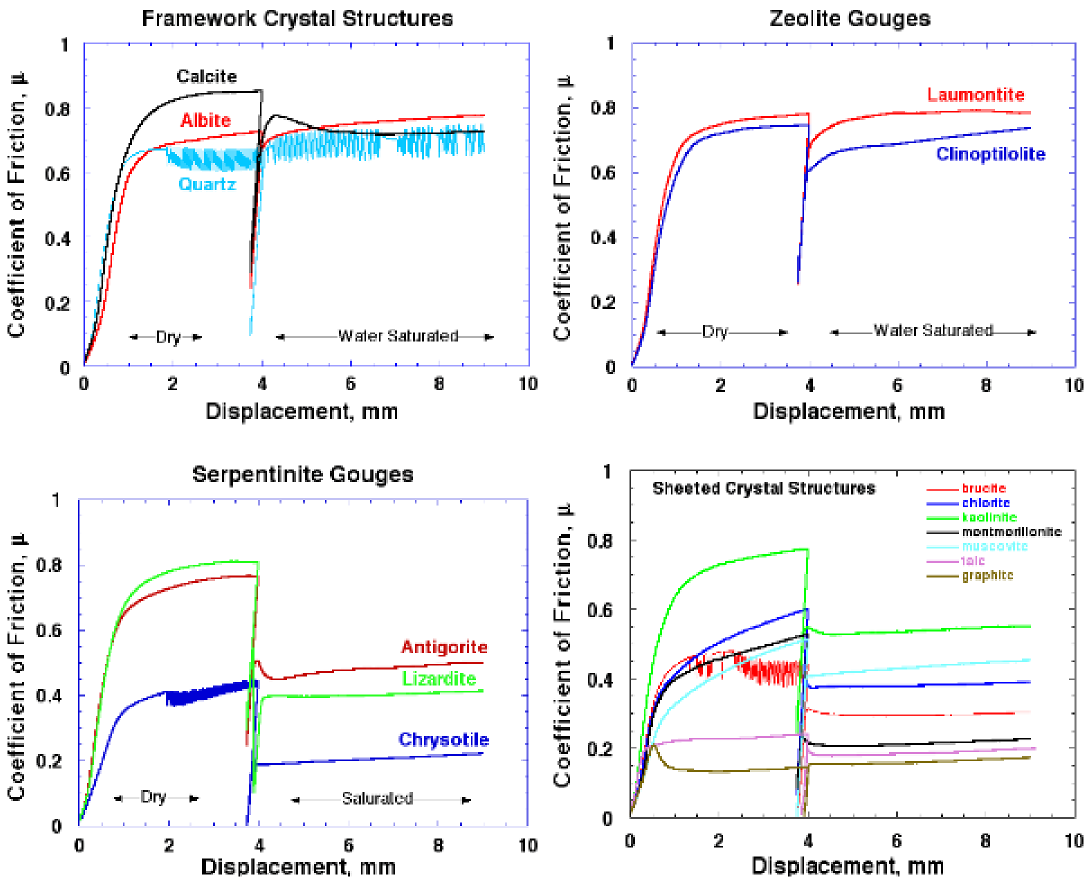

Figure 4.9 *Friction coefficient for different types of minerals/gouges at dry versus saturated conditions (Morrow et al. 2000). The friction coefficient increases with increasing displacement but then flattens. Saturated specimens show a lower friction coefficient than the dry ones. The impact of saturation is largest for Serpentinite but very small for Zeolite gouges.*

Friction coefficient of faults exposed to CO_2

The strength of faults may be affected by various factors; among them is the geochemical reaction between CO_2 and the reservoir/cap rock that may weaken the fault zone rocks. A methodology to explore the impact of the geochemical reaction of CO_2 with rocks on the strength of faults is through mechanical testing of samples exposed to acidic solutions. Such studies have been presented by Liu et al. (2003), Parry et al. (2007) Andreani et al. (2008), Ojala (2011), Samuelson and Spiers (2012), Nouailletas et al. (2013) and Jalilavi et al. (2014). However, the majority of these studies did not use carbonic acid.

In an experimental work, Samuelson and Spiers (2012) studied the effect of CO_2 on the friction coefficient of different rock types. They simulated fault gouge material from three different claystone cap rock samples (Soll-1, Röt-1, Röt-2), one reservoir sandstone sample (Hard-1), and a 50/50 mixture of reservoir rock and cap rock (Hard-1 and Soll-1) from offshore Netherlands. They crushed the rock cores and sieved to provide particles smaller than 50 μm to simulate the very fine grained material common in the slip surface of faults. The fault gouges were then tested in the direct shear box. They found that the friction coefficient for the sandstone gouge was about 0.72 and for the gouges derived from cap rock samples was about 0.58 (Figure 4.10). They concluded that the addition of supercritical CO_2 to either saturated brine or dry gouge layers of the materials examined had no significant effect on the coefficient of friction, indicating that there are no short-term effects of supercritical CO_2 that could enhance fault zone reactivation due to reduced frictional strength. Note that these experiments were carried out relatively fast where the gouge materials were in contact with brine or CO_2 for a few hours only. Therefore, possible long term effects such as chemical reactions may have not been captured by these tests.

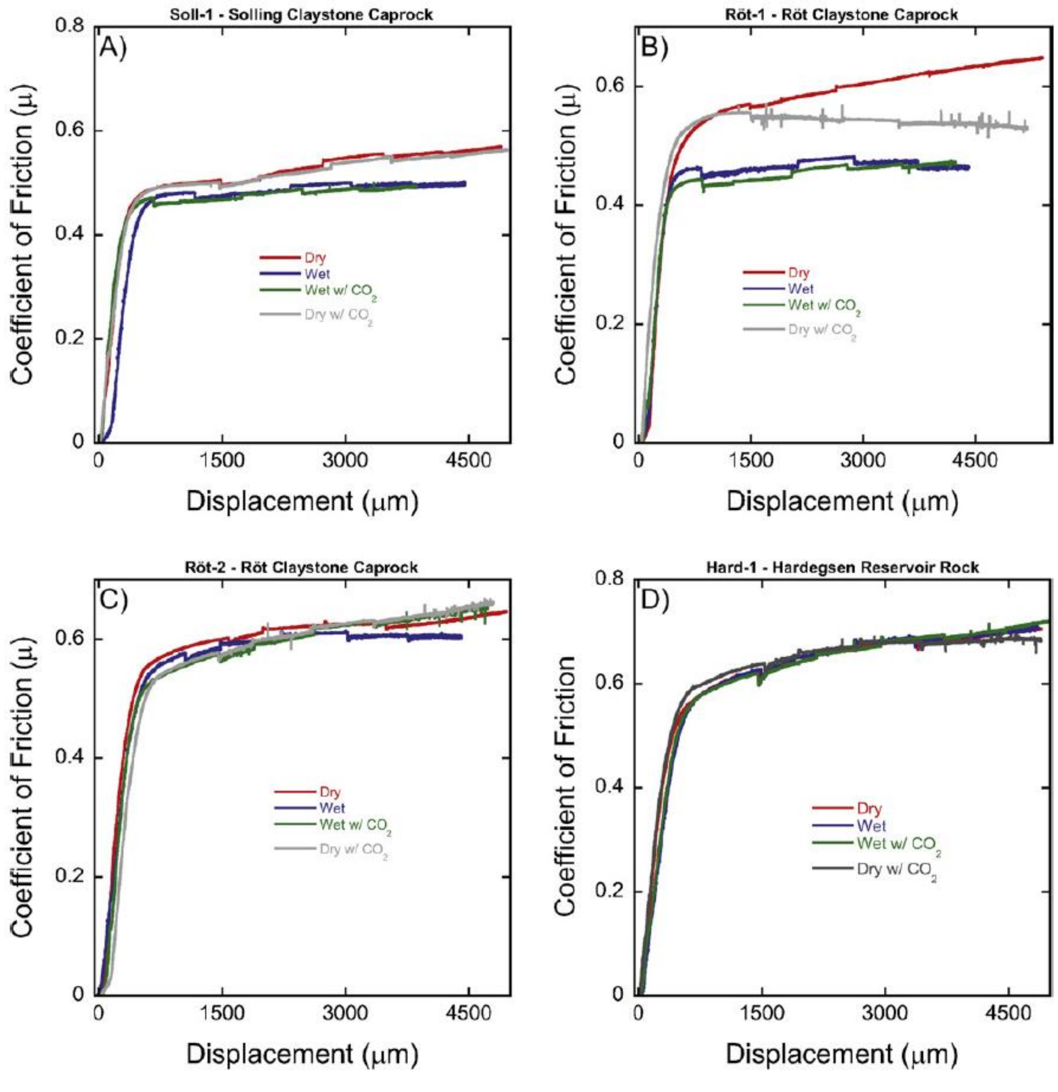

Figure 4.10 Friction coefficient versus displacement for different types of rocks under various pore fluid conditions (after Samuelson and Spiers, 2012). CO_2 does not have a significant impact on the friction coefficient. The presence of water decreases the friction coefficient of the cap rock samples (A, B and C) whilst it does not affect friction of the reservoir sandstone (D).

In another study, Nouailletas et al. (2013) examine the impact of CO_2 on the shear strength of a very low permeable Companian flysch sandstone from the cap rock of Lacq CO_2 storage site, in southern France. Samples were broken to obtain fresh surfaces to expose to fluids. The reference samples were immersed in water. The target specimens, called the damaged samples, were immersed in acidic solution ([HCl]= 0.6 mol.L^{-1}) for 6 hours. Both series of samples were then tested in the direct shear box. Test results showed that the peak shear strength of the damaged samples was lower than that for the reference samples (Figure 4.11). The shape of the shear versus displacement curve was different for the two samples series. The reference samples, with a rough surface, showed a clear peak shear stress followed by a stress drop to the residual stress level. The damaged samples, on the other hand, do not show any clear peak and exhibit a pattern similar to samples with a smooth surface. This observation showed that acid treatment reduced the shear strength of rough surfaces.

Results of the study by Nouailletas et al. (2013) are slightly different from those presented by Samuelson and Spiers (2012). An explanation is that Samuelson and Spiers (2012) used CO_2 for treatment of the samples while Nouailletas et al. (2013) used HCl acid which is much more reactive to rocks than carbonic acid. Further research on samples exposed to CO_2 for a longer time may add knowledge to the state of the art on the impact of geochemical reactions on the mechanical characteristics of rocks and especially friction coefficients.

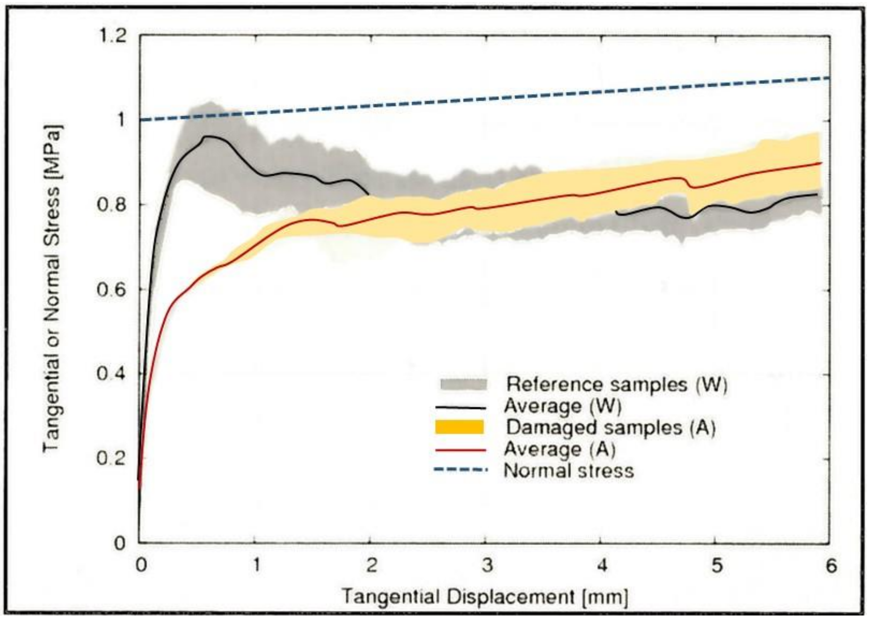

Figure 4.11 Tangential stress versus tangential displacement for the reference and HCl solution exposed (damaged) sandstone samples (modified after Nouailletas et al., 2013). Peak stress for damaged samples is lower than that for the reference sample, although their residual stress is about the same.

Another case of an investigation of the frictional strength of fault material exposed to CO_2 is a laboratory study done by Masoudi et al. (2011) for CO_2 storage in the M4 carbonate reservoir, Malaysia. The M4 Field is located north of Central Luconia Province in the Sarwak Basin, of East Malaysia. The reservoir is approximately 2,000 m below sea level. M4 is a depleted gas reservoir composing of carbonate rocks. The cap rock consists of shale layers composed of horizontally laminated and tightly crystalline clays, predominantly illite, mixed layer illite-smectite, and to a lesser amount chlorite. The limestones comprise highly porous, slightly recrystallized boundstones consisting of coral, algal and other calcareous skeletal particles cemented by sparry calcite. Test samples included two shale cores from the depth of 1762-1768 m and three limestone cores from the depth of 1777-1796 m.

Masoudi et al. (2011) tested untreated specimens versus samples treated with CO_2 saturated brine solution. The treated samples had undergone CO_2 injection treatment to simulate reservoir injection conditions. They adopted two separate approaches to simulate the CO_2 injection for shale and limestone samples. The approach adopted for shale samples was to inject liquid CO_2 using an upstream injection pressure simulating field injection with a downstream (reservoir) pressure until CO_2 breakthrough occurred. At this point, the sample was held with constant pressure for a predetermined treatment period. For the limestone samples, the procedure involved injection of a known quantity of CO_2 saturated sodium chloride solution (carbonic acid brine solution) at a predetermined flow rate, under in-situ hydrostatic confining and reservoir injection pressure conditions. Following the flowing period, the CO_2 saturated brine solution was held in contact with the rock for a set period to allow any dissolution reaction to occur. All treatments and tests were performed at ambient temperature.

For the shale samples, single-stage triaxial compression tests were carried out on untreated and unpreserved samples versus 'sister' samples subjected to CO_2 injection treatment. They tested all the shale samples in "as received" saturation conditions with a standard axial loading strain rate of 1×10^{-5} in/s at room temperature with pore pressure drained to the atmosphere. For carbonate samples, multi-stage triaxial compression tests were performed on untreated samples at three different confining pressures. Similar tests were also performed on 'sister' samples following injection treatment with CO_2 saturated brine. The effect of CO_2 saturation on unconfined compressive strength (UCS), tensile strength, Young's modulus and Poisson's ratio was also investigated (Table 4.1).

They carried out a petrographical evaluation of pre- and post-CO_2 injection of shale and limestone samples to study possible change in mineralogy and texture. They observed no significant difference between pre- and post-CO_2 injection for shale samples. For limestone samples, mineralogy and original rock texture were essentially the same in the pre- and post -injection samples. However, they reported that two post-injection limestone samples exhibited deep etched and corroded calcite grains in small areas of the samples which were not found in the corresponding pre-injection samples.

Table 4.1 Petrophysical and rock mechanical properties of core samples tested before and after treatment with CO_2 saturated brine (data from Masoudi et al., 2011).

Property	**Shale**		**Limestone**	
Core depth (m)	1762-1768		1777-1796	
Test condition	Untreated	CO_2 injected	Untreated	CO_2 injected
Porosity (%)	--	--	33.64%	34.93%
Reduction in brine permeability	--	--	72.4%	76.5%
Compressive strength (MPa)	40.9	41.2	17.8	17.3
Static Young's Modulus (MPa)	1,769	2,061	8,209	7,764
Dynamic Young's Modulus (MPa)	10,603	10,331	16,214	16,105
Static Poisson's ratio	0.15	0.14	0.22	0.23
Dynamic Poisson's ratio	0.17	0.10	0.33	0.29
Indirect tensile strength (MPa)	--	--	0.60	0.67
Internal Friction Angle (°)	23.5	21.2	14.1	12.7
Cohesion (MPa)	7.8	9.01	4.16	3.79
Carbonate classification	--	--	Boundstone	Boundstone
Carbonate grain type	--	--	Red algae, coral, foraminifera	Red algae, coral, foraminifera
Authigenic cements	Calcite, chert, pyrite	Calcite, chert, pyrite	Sparry calcite, minor dolomite	Sparry calcite, minor dolomite

Masoudi et al. (2011) concluded that for treated shale samples, Static Young's modulus and unconfined compressive strength showed an increase while the angle of internal friction and Poisson's ratio showed a decrease. For the post-CO_2 treated limestone samples there is a reduction in Young's modulus, unconfined compressive strength, angle of internal friction and cohesion whilst there is an increase in the Poisson's ratio and permeability (see Also Figure 4.12).

Changes in mechanical properties of reservoir and cap rocks have also been reported by others (e.g. Hangx et al., 2013; Wollenweber et al., 2010; Gaus, 2010).

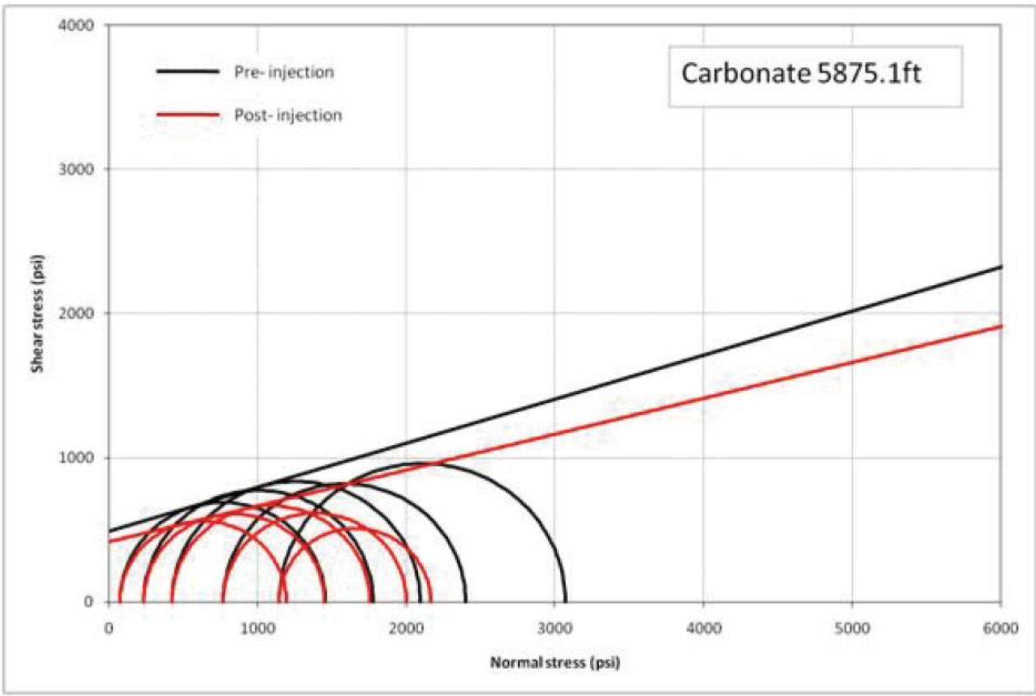

Figure 4.12 Mohr circle and failure envelope for pre- and post –CO_2 treated limestone specimens (after Masoudi et al., 2011).

In a similar study, Pluymakers et al. (2013) investigated the effect of supercritical CO_2 on the frictional behavior of simulated anhydrite fault gouge. They selected intact core samples from the base of the Dutch Zechstein Group and ground the samples to provide a powder with a grain size of less than 50 micron to simulate fault gouge material. They made a sample containing a gouge layer of 1 mm thick. The sample was placed in a direct shear box which in turn was placed in a triaxial cell. Tests were run at different temperatures ranging from 80-150°C and under a constant confining stress of 25 MPa. In addition, the gouge was pressurized with dry supercritical CO_2 and with CO_2-saturated water. The pressure of CO_2 in both cases was 15 MPa. The observation was performed under the following conditions:

$\mu = 0.65$ at 80 °C dry CO_2
$\mu = 0.55$ at 150 °C dry CO_2

Results of the tests with wet CO_2 showed slightly weaker samples but the same trend was observed with increasing the temperature:

$\mu = 0.60$ at 80 °C wet CO_2
$\mu = 0.55$ at 150 °C wet CO_2

This study showed a small effect of wet CO_2 on the friction coefficient of the samples at low temperature. On the other hand, they observed a big inverse impact of temperature on the friction coefficient; the higher the temperature, the lower the friction coefficient.

Pluymakers et al. (2013) also investigated wave velocity changes and observed that all wet samples pressurized with CO_2 exhibited velocity neutral to velocity strengthening over the entire temperature range. This may be applicable to faults in reservoir and cap rock conditions since they are normally wet. They also stated that a slight decrease in the strength of anhydrite fault gouge was observed over a reservoir temperature range of (80-120°C) compared to the room temperature.

Based on this experimental study, Pluymakers et al. (2013) concluded that "it is unlikely that the presence of CO_2 significantly increases seismic potential of anhydrite-filled faults under typical storage site conditions".

5 Conclusions and Knowledge Gaps

5.1 Conclusions

Geological storage of CO_2 requires a reservoir formation contained by very low-permeable layers. Since faults are inherent components of almost all geological formations, their stability during CO_2 storage will be crucial for integrity of the storage site. Fault stability is affected by multiple factors; fault structure, material properties, geochemical reactions between CO_2 and fault gouges, induced stresses due to injection, etc. This report highlights the factors mentioned above and reviews the methodologies generally used to evaluate geomechanical stability of faults during CO_2 sequestration. It also addresses some challenges, among them are the limited amount of data available for fault stability analysis in CO_2 storage sites. The highlights of the study and concluding remarks are summarized as follows.

Structures of old fault zones are rather complex. They are comprised of a central fault core and with a damage zone with composite microstructures. The fault core generally consists of a mixture of material from surrounding formations which have intruded into the fault plane through mechanisms such as smearing. It usually comprises clay and crushed, fine-grained material. Therefore, fault core has very low permeability. The width of the fault core can be from a millimeter up to meter scale. The damage zone, however, is a part of the host rock but with significant strain localization. It usually shows extensive fracture development at micro- and macro-scale. This makes it potentially a very permeable zone. The damage zone can be up to tens of meters wide. Mechanically, the fault core material is very weak, unless it has been cemented after faulting. Thus, it is susceptible to instability upon injection of CO_2 and alteration of the in-situ stresses.

Injection of CO_2 increases pore pressure and reduces the effective stresses. Reduction of effective stress on the fault can lead to reactivation. As pore pressure approaches the critical stress level, the permeability of faults increases. Thus, the risk of fluid flow through faults increases with increasing pore pressure (decreasing effective stresses). However, permeability of faults may be drastically increased at the time of a fault slip. The magnitude of permeability enhancement is a function of the dilatancy of the material during shearing processes. Brittle materials are more dilatant and show large permeability increases during shearing whilst ductile materials show less dilation and may not necessarily result in significant permeability increases.

Different methods have been employed to evaluate fault reactivation potential, as reported in the literature. The widely used failure criterion for fault stability analysis is the Mohr-Coulomb criterion. Both analytical and numerical approaches have been used to study faults. The analytical approach considers the normal and shear stresses on fault planes to evaluate fault stability. This method estimates the maximum sustainable pressure for a fault prior to shearing. The same can be calculated for all possible fault orientations and can be plotted in lower hemisphere stereographs. This will provide a slip potential map, which says how much extra pressure each fault may sustain before it fails. The analytical approach is a simple, yet valuable tool for preliminary or first-order assessment of potential fault reactivation. It, however, relies on many assumptions and simplifications and may face limitations which do not adequately capture complex physical processes occurring in the reservoir following an injection operation. These limitations may be overcome using numerical tools.

Numerical analyses of fault stability can help simulate faults at different scales and within different in-situ conditions. A fault can be presented in a global model as a single discontinuity using both continuum and discontinuum approaches in order to explore the general behavior of faults. If a fault is susceptible to instability and the detailed behaviour of a fault zone is of interest, it may be modelled as a rock mass of continuum material. This may require a local model where detailed properties of the fault zone are assigned to the components of the model. Furthermore, post-failure behaviour of faults are important for predicting fault seal/leakage. Brittle behaviour of rocks in post failure contributes to the enhancement of permeability. If a strain/stress-dependent permeability change is applied in a reservoir/flow model, a realistic range for the dilatancy angle, that varies with plastic strain, should be considered in geomechanical models, especially for a fault zone.

Analytical and numerical analyses require data on the in-situ stresses and strength of faults and of the host rocks. The mechanical strength of a fault is expressed in terms of its cohesion and friction coefficient. For modelling purposes, faults are usually assumed to be cohesionless in a conservative approach. The friction coefficient of faults depends strongly on the fault filling material and the possible pore fluid. Laboratory test data show that the friction coefficient ranges from 0.6 to 0.8 for typical rock samples and fault gouges. The effect of CO_2 on friction coefficients, and the strength and deformation behaviour based on laboratory tests, seems to be small. The effects related to CO_2 seem to be minor compared to other uncertainties that arise due to a lack of data on fault geometry, fault plane properties and general limitations in the analysis method. Fault Stability/instability is related to the two major public concerns about CO_2 storage (i.e. induced microseismicity and gas leakage) and therefore, a more conservative approach on fault strength may be necessary before detailed data and advanced models are available.

5.2 Knowledge Gaps in Understanding Fault Stability Analysis

Fault properties are of paramount importance for geomechaical stability analyses. Characteristics of fault planes, properties of fault core and damage zones along with the in-situ and induced stresses control the behaviour of faults during and post CO_2 injection. Although various methods are utilized to predict the behaviour of faults during such operations there are still several areas in need of development and improvement. Some of these are listed below:

- Faults in reservoirs have been mapped and explored in the field of petroleum exploration and production. In cap rock/overburden sections, however, the

details of faults have been of less interest with limited data from literature. Some questions arise for sealing formations:
- What does fault architecture look like?
- What are the mechanical and hydraulic properties of fault zones in sealing formations and transition zones? These are important elements for CO_2 storage sites, as they will control whether a reactivated fault in the reservoir will propagate into the sealing formations or remain stable.

- In-situ stresses on a fault in the sealing formation may be different from those in the reservoir because of pore pressure differences. While there are plenty of well tests being carried out and reported within reservoirs, much less data for overburden sections have been reported in the literature. Mechanical and hydraulic properties of the overburden can be obtained either from in-situ tests such as Leak-Off tests, Minifrac tests, or Step Rate Tests or from laboratory measurements on core samples. These tests are seldom carried out for sealing formations, and rock cores from the overburden are rarely available. A good description of these elements is required for CO_2 storage site assessment.

- The geomechanical modelling of faults requires detailed data on the geomechanical properties of the fault zone and its geometry. However, access to core samples with fault material is usually limited and the geometry is not well known. This can result in oversimplification in the analysis of fault material and fault properties leading to uncertainties in modelling results. Models that consider only the shear failure envelope as the stability criterion (e.g. Mohr-Coulomb failure), have limitations when applied to possible ductile deformation and slow slip (aseismic events). Thus, proper calibration of fault material properties, using limited data sets, and further development of constitutive models to describe various failure modes of fault reactivation, are essential for reliable geomechanical modelling.

- Fault slip is strongly dependent on the pore pressure in a fault zone. Some approaches assume the fault zone has the same pore pressure as the reservoir. The true initial and gradual development of pore pressure within a zone are usually not known, and pore pressure should be in equilibrium with surrounding formations. The CO_2 gas or fluid capillary entry pressure into the fault zone might be different from the overburden. These details are usually not accounted for due to lack of detailed data, however, sensitivity analysis can indicate an uncertainty range. Thus, more detailed knowledge of the pore pressure distribution for a CO_2 gas or liquid from permeable formations into less-permeable zones (e.g. fault core) can be helpful to improve the precise of modelling and narrow the uncertainty span.

- The strength of faults is governed by the frictional resistance of the material present in the fault zone. Frictional properties of sediments and rocks have been studied extensively for civil engineering projects and hydrocarbon production fields in the past decades. Only a few studies have been done to evaluate the effect of CO_2 on the friction properties of sediments/rocks, although Morrow et al. (2000), Masoudi et al. (2011), Samuelson and Spiers (2012) reported very good experimental results. They all observed (to various degrees) changes in the geomechanical properties of the tested material, although the short time the specimens had been exposed to CO_2 under experimental conditions was a notable limitation. More experiments on samples from reservoir and cap rocks exposed to CO_2 solutions for longer time periods, would provide complementary results and more valuable data.

- The integrity of reservoir and overburden can be affected by minor faults with limited length and small displacements, which may be present in the reservoir and overburden. Such faults may be below the detection threshold of seismic methods and thus require more accurate techniques such as well tests, drilling, etc. to be explored. Exploration and characterization of small faults is very important for the assessment of integrity of CO_2 storage sites.

- Many models, which were mentioned in this report, are able to explain the induced fault slip caused by pore pressure build-up. However, field observations from hydraulic fracturing stimulation of shale gas reservoirs indicate that unexpected fracturing occurs additionally where faults orientated between the directions of the minimum and maximum in-situ stresses exist. These additional fractures are believed to be triggered by propagation of fractures from critically oriented (less stable) to poorly oriented faults (Zoback et al., 2012). More investigations are required on parameters and conditions that trigger fault slip.

- Although many studies have been carried out on correlating the permeability of intact rock to its geomechanical behaviour, they may not be applicable to faults. Faults are characterized by complex internal zonation with various permeabilities and quantifying equivalent/bulk fault permeability can be difficult. The effect of fault reactivation and slip on fault zone permeability, is poorly understood and demand much attention and further investigations.

6 References

ABAQUS/standard: 2001. User's Manual. Hibbitt, Karlsson & Sorensen.

Aki K. and Richards P.G., 1980. Quantitative Seismology, Theory and Methods. Volume I: 557 p., San Francisco, Freeman, ISBN 0716710587.

Allan U.S., 1989. Model for hydrocarbon migration and entrapment within faulted structures. AAPG Bulletin **73**, p. 803-811.

Alves L.M. and de Lacerda L.A., 2012. Applied Fracture Mechanics. Belov A. (edit.), Published by Intech, ISBN 978-953-51-0897-9.

Andreani M. Gouze P., Luquot L. and Jouanna P., 2008. Changes in seal capacity of fractured claystone cap rock induced by dissolved and gaseous CO_2 seepage. Geophysical Research Letters **35**, L14404, 6 p.

Andresen A., Steen Ø. and Hartz E., 1995. Fault population and fault distribution in rotated fault blocks, Traill Ö, East Greenland. *PROFIT Project summary reports*, edited by Olsen et al., p. 43-58.

Antonellini M., Aydin A. and Pollard D., 1994. Microstructure of deformation bands in porous sandstones at Arches National Park, Utah. Journal of Structural Geology **16**, p. 941–959.

Ashby M.F. and Hallam S.D., 1986. The failure of brittle solids containing small cracks under compressive stress states. Acta Metallurgica, Vol. **34**, Issue 3, March 1986, p. 497–510.

Ashby M.F. and Sammis C.G., 1990. The damage mechanics of brittle solids in compression. Pure and Applied Geophysics **133**, p. 489-521.

Aydin A., 2000. Fractures, Faults, and Hydrocarbon Migration and Flow. Marine and Petroleum Geology **17**, p. 797-814.

Baghbanan A. and Jing L., 2008. Stress effects on permeability in a fractured rock mass with correlated fracture length and aperture. Int. J. Rock Mech. Min. Sci. **45**(8), p. 1320-1334.

Balsamo F., Storti F., Salvini F., Silva A.T. and Lima C.C., 2010. Structural and petrophysical evolution of extensional fault zones in low-porosity, poorly lithified sandstones of the Barreiras Formation, NE Brazil. J. Struc. Geol. 32, p. 1806-1828.

Barton N., Bandis, S., and Bakhtar K., 1985. Strength, deformation and conductivity coupling of rock joints. International Journal of Rock Mechanics and Mining Sciences & Geomechanics Abstracts, **22**(3), 121–140.

Bense V. F. and Van Balen R., 2004. The effect of fault relay and clay smearing on groundwater flow patterns in the Lower Rhine Embayment. Basin Research **16** (3), p. 397-411.

Bense V. F., and Person M.A., 2006. Faults as conduit-barrier systems to fluid flow in siliciclastic sedimentary aquifers, Water Resources Research **42**, W05421, doi:10.1029/2005WR004480.

Bissell R.C., Vasco D.W., Atbi M., Hamdani M., Okwelegbe M. and Goldwater M.H., 2011. A full field simulation of the In Salah gas production and CO_2 storage project using a coupled geo-mechanical and thermal fluid Flow simulator. Energy Procedia **4**, p. 3290–3297.

Bjørlykke K. and Høeg K., 1997. Effects of burial diagenesis on stresses, compaction and fluid flow in sedimentary basins. Marine and Petroleum Geol. **14** (3), p. 267-276.

Bjørlykke K., Høeg K., Faleide J. I., and Jahren J., 2005. When do faults in sedimentary basins leak? Stress and deformation in sedimentary basins; examples from the North Sea and Haltenbanken, offshore Norway. AAPG Bulletin, **89**(8), p. 1019–1031.

Bobet A., Fakhimi A., Johnson S., Morris J., Tonon F. and Yeung M., 2009. Numerical Models in Discontinuous Media: Review of Advances for Rock Mechanics Applications. Journal of Geotechnical and Geoenvironmental Engineering, **135**(11), p. 1547–1561.

Bolton A.J., Maltman A.J. and Clennell M.B., 1998. The importance of overpressure timing and permeability evolution in fine-grained sediments undergoing shear. J. Structural Geology **20** (8), p. 1013-1022.

Bostrøm B., and Skomedal E. 2004. Reservoir geomechanics with ABAQUS. 2004 ABAQUS Users' Conference, p. 117–131.

Breckels I.M., and van Eekelen H.A.M., 1982. Relationship between horizontal stress and depth in sedimentary basins. J. Petroleum Technology **34** (9), p. 2191-2199.

Bretan P. and Yielding G., 2005. Using buoyancy pressure profiles to assess uncertainty in fault seal calibration. In: Evaluating Fault and Cap Rock Seals, Boult P. and Kaldi J. (edits.), AAPG Hedberg Series **2**, p. 151-162.

Bretan P., Yielding G., Mathiassen O. M. and Thorsnes T., 2011. Fault-seal analysis for CO_2 storage: an example from the Troll area, Norwegian Continental Shelf. Petroleum Geoscience **17**, p. 181-192.

Brinkgreve R. B. J., 1994. Geomaterial models and numerical analysis of softening. Ph.D. Thesis Technische Univ. Delft (Netherlands). Geotechnical Lab.

Burg J.P., 2013. Structural Geology. Available at:
http://www.files.ethz.ch/structuralgeology/JPB/files/English/2faulting.pdf

Byerlee J. D., 1978. Friction of rocks. Pure Appl. Geophys. **116**, p. 615–626.

Caine J.S., Evans J.P. and Forster C.B., 1996. Fault zone architecture and permeability structure. Geology **24**(11), p. 1025-1028.

Cappa F. and Rutqvist J., 2011. Modeling of coupled deformation and permeability evolution during fault reactivation induced by deep underground injection of CO_2. International Journal of Greenhouse Gas Control, **5**(2), p. 336–346.

Cardellini C., Chiodini G., Frondini F., Giaquinto S., Parello F. and Peruzzi L., 2000. Quantification of Diffuse Carbon Dioxide Earth Degassing from Central Apennine (Italy): The Carbon Mass Balance in Regional Aquifers Approach. Journal of Conference Abstracts Volume **5**(2), Cambridge Publications, P. 285.

Carol I. and Alonso E. E., 1983. A New Joint Element for the Analysis of Fractured Rock. 5th ISRM Congress.

Cerveny K., Davies R., Dudley G., Kaufman P., Knipe R. and Krantz B., 2005. Reducing uncertainty with fault seal analysis. Oilfield Review, winter 2004/2005, p. 38-51.

Chanpura R., 2001. Fault reactivation as a result of reservoir depletion. Georgia Institute of Technology. PhD dissertation.

Charlez P. A., 1997. Rock Mechanics, Petroleum applications. Editions Technip, 2.

Chen J., Yang X., Yao L., Ma S. and Shimamoto T., 2013. Frictional and transport properties of the 2008 Wenchuan Earthquake fault zone: Implications for coseismic slip-weakening mechanisms. Tectonophysics **603**, P. 237-256.

Chester F.M. and Logan J.M., 1986. Implications for mechanical properties of brittle faults from observations of the Punchbowl fault zone, California. Pageoph. **124** (1-2), p. 79-106.

Chester F.M., Evans J.P. and Biegel R.L., 1993. Internal structure and weakening of mechanisms of the San Andreas fault, J. Geophys. Res. **100**, (B6), p. 9761-9788.

Childs C., Watterson J. and Walsh J.J., 1996. A model for the structure and development of fault zones: Journal of the Geological Society London **153**, P. 337-340.

Chin L. Y., Rajagopal R. and Thomas L. K., 2000. Fully Coupled Geomechanics and Fluid-Flow Analysis of Wells with Stress-Dependent Permeability. SPE Journal **5**(1).

Chiodini G., Frondini F., Kerrick D.M., Rogie J., Parello F., Peruzzi L. and Zanzari A.R., 1999. Quantification of deep CO_2 fluxes from Central Italy. Examples of carbon balance for regional aquifers and of soil diffuse degassing. Chem. Geol. **159**, p. 205–222.

Chuhan F.A., Kieldstad A., Biørlykke K. and Høeg K., 2002. Porosity loss in sand by grain crushing-experimental evidence and relevance to reservoir quality. Marine and Petroleum Geol. **19**, p. 39–53.

Clausen J.A. and Gabrielsen R.H., 2002. Parameters that control the development of clay smear at low stress states: an experimental study using ring shear apparatus. J. Struct. Geol. **24**, p. 1569–1586.

Clausen J.A., Gabrielsen R.H., Johnsen E. and Korstgård J.A., 2003. Fault architecture and clay smear distribution. Examples from field studies and drained ring-shear experiments. Norwegian Journal of Geology **83**, p. 131-146.

Cowie P.A. and Scholz C.H., 1992. Growth of faults by accumulation of seismic slip. J. Geophy. Research **97**, No. B7, p. 11085-11095.

Crawford B.R., Faulkner D.R. and Rutter D.H., 2008. Strength, porosity and permeability development during hydrostatic and shear loading of synthetic quartz clay fault gouge. J. Geological research **113**, B03207, doi:10.1029/2006JB004634.

Cuisiat F. and Høeg K., 2002. Mechanical effects of depletion of the Kristin Field Task I.A: Review of fault characterization and properties. NGI Report 20011188-4.

Cuisiat F., Skurtveit E. and Cleave R., 2007. Fault seal prediction in unconsolidated sediments with a novel experimental apparatus. In: Proceedings of the 7th ISRM Congress on Rock Mechanics, Lisboa, Portugal.

Cuisiat F., Skurtveit E. and Cleave R., 2010a. An experimental investigation of the development and permeability of clay smears along faults in uncemented sediments. J. Struct. Geol., **32**, p. 1850-1863.

Cuisiat F., Jostad H. P., Andresen L., Skurtveit E., Skomedal E., Hettema M. and Lyslo K., 2010b. Geomechanical integrity of sealing faults during depressurisation of the Statfjord Field. J. Struct. Geol. **32**, p. 1754–1767.

Cundall P. A. and Hart R. D., 1992. Numerical modelling of discontinua. Engineering Computations **9**(2), p. 101–113.

Day R. A. and Potts D. M., 1994. Zero thickness interface elements—numerical stability and application. Int. J. Numerical and Analytical Methods in Geomechanics, **18**(10), p. 689–708.

Day-Lewis A., 2008. Characterization and Modeling of in Situ Stress Heterogeneity. ProQuest Dissertations and Theses; Ph.D. thesis--Stanford University, Publication Number: AAI3292341; ISBN: 9780549354079.

Dewhurst D.N., Boult P.J., Jones R.M. and Barclay S.A., 2005. Fluid healing and fault sealing in impure sandstones. In: Evaluating Fault and Cap Rock Seals, Boult P. and Kaldi J. (edits.), AAPG Hedberg Series **2**, p. 37-56.

Di Bucci D., Massa B. and Zuppetta A., 2005. Relay ramps in active normal fault zones: A clue to the identification of seismogenic sources (1688 Sannio earthquake, Italy), Bull. Geol. Soci. America **118**(3-4), p. 430-448.

Dyt C.P., Langhi L. and Bailey W.P., 2012. Automating conceptual models to easily assess trap integrity and oil preservation risks associated with fault reactivation. Marine and Petroleum Geology **30**, p. 81-97.

Eaton B.A., 1969. Fracture gradient prediction and its application in oilfield operations. J. Petroleum Technology **246**, p. 1353-1360.

Egholm D.L., Clausen O.R., Sandiford M., Kristensen M.B. and Korstgard J.A., 2008. The mechanics of clay smearing along faults. Geology **36**, p. 787–790.

Ellsworth W.L., 2013. Injection-Induced Earthquakes. Science **341**, 1225942.

Evans W.C., Sorey M.L., Cook A.C., Kennedy B.M., Shuster D.L., Colvard E.M., White L.D. and Huebner M.A., 2002. Tracing and quantifying magmatic carbon discharge in cold groundwaters: lessons learned from Mammoth Mountain, USA. J. Volcan. Geotherm. Res. **114**, p. 291–312.

Fang Z., Khaksar A. and Gibbons K., 2012. Geomechanical risk assessment for sequestration in depleted hydrocarbon sandstone reservoirs. SPE Drilling and Production 2012, p. 367-381.

Faulkner D.R. and Rutter E.H., 2000. Comparisons of water and argon permeability in natural clay-bearing fault gouge under high pressure at 20 degrees C. J Geophys. Research-Solid Earth **105** (B7), p. 16415-16426.

Faulkner D.R., Jackson C.A.L., Lunn R.J., Schlische R.W., Shipton Z.K., Wiberley C.A.J. and Withjack M.O., 2010. A review of recent developments concerning the structure, mechanisms and fluid flow properties of fault zones. J. Struct. Geol. **32**, p. 1557-1575.

Faulkner D. R. and Rutter E. H. 1998. The gas permeability of clay-bearing fault gouge at 20°C. Geological Society, London, Special Publications, **147**(1), 147–156.

Fisher Q.J. and Knipe R.J., 1998. Fault sealing processes in siliciclastic sediments. In: Jones G., Fisher Q. and Knipe R. (Eds.), Faults, Fault Sealing and Fluid Flow in Hydrocarbon Reservoirs. Geological Society of London, special publication **147**, p. 117–134.

Fisher Q.J., Knipe R.J., 2001. The permeability of faults within siliciclastic petroleum reservoirs of the North Sea and Norwegian continental shelf. Marine and Petroleum Geology **18**, p. 1063–1081.

Fjær E., Holt R.M., Horsrud P., Raaen A.M. and Risnes R., 2008. Petroleum Related Rock Mechanics. 2nd edition, Elsevier, Amsterdam, 491 p.

Fossen H., 2010. Structural Geology. Cambridge University Press, Cambridge, UK, 463 p.

Fossen H., Schultz R.A., Shipton Z.K. and Mair K., 2007. Deformation bands in sandstone: a review. J. Geophysical Society **164**, p. 755-769.

Fowler C.M.R., 1990. The solid earth. Cambridge, Cambridge University Press, UK.

Gabrielsen R.H. and Koestler A.G., 1987. Description and structural implication of fractures in late Jurassic sandstones of the Troll Field, northern North Sea. In Norsk Geologisk Tidsskrift **67**, p. 371-381.

Garcia X., Nagel N., Zhang F., Sanchez-Nagel M. and Lee B., 2013. Revisiting Vertical Hydraulic Fracture Propagation through Layered Formations – A Numerical Evaluation. 47th U.S. Rock Mechanics/Geomechanics Symposium, 23-26 June, San Francisco, California, ARMA 2013-23.

Gaus I., 2010. Role and impact of CO2-rock interactions during CO_2 storage in sedimentary rocks. Int. J. Greenhouse Gas Control **4**, p. 73-89.

GeoScience, 2004. Technical note: on the potential shearing during CO_2 injection at Krechba. A short report by GeoScience Limited to In Salah Gas, 10 p.

Ghassemi A., 2007. Stress and pore pressure distribution around a pressurized, cooled crack in low permeability rock. In: Proceedings of the 32nd workshop on geothermal reservoir engineering.

Gibson R.G., 1994. Fault-Zone Seals in Siliciclastic Strata of the Columbus Basin, Offshore Trinidad. AAPG Bulletin **78** (9), p. 1372-1385.

Giger S., Clennel M.B., Ciftci N.B., Harbers C., Clark P., Ricchetti M., 2013. Fault transmissibility in clastic-argillaceous sequences controlled by clay smear evolution. AAPG **97(**5), p. 705-732.

Giger S.B., Tenthorey E., Cox S.F. and Jerald J.D.F., 2007. Permeability evolution in quartz fault gouges under hydrothermal conditions. J. Geophysical Research **112**, B07202, doi:10.1029/2006JB004828.

Gillespie P.A., Walsh J.J. and Watterson J., 1992. Limitations of dimension and displacement data from single fault and the consequences for data analysis and interpretation. J. Struct. Geol. **14**, p. 1157-1172.

Gluyas J. G. and Swarbrick R., 2004. Petroleum Geoscience, Blackwell Publishing, 358 p.

Grasso J.R., 1992. Mechanics of seismic instabilities induced by the recovery of hydrocarbons. Pure and Applied Geophysics **139**, p. 507–534.

Griffith A. A. 1921. The Phenomena of Rupture and Flow in Solids. Philosophical Transactions of the Royal Society of London. Series A, Containing Papers of a Mathematical or Physical Character **221**, p. 582-593.

Gudmundsson A., 2004. Effects of Young's modulus on fault displacement. Comptes Rendus Geoscience **336**(1), p. 85–92.

Gudmundsson A., Simmenes T.H., Larsen B. and Philipp, S.L., 2010. Effects of internal structure and local stresses on fracture propagation, deflection and arrest in fault zones. J. Struct. Geol. **32**, p. 1643-1655.

Gutierrez M., Øino L. E. and Nygård R., 2000. Stress-dependent permeability of a de-mineralised fracture in shale. Marine and Petroleum Geology, **17**(8), 895–907.

Gutierrez M. and Makurat A., 1997. Coupled HTM modelling of cold water injection in fractured hydrocarbon reservoirs. Int. J. Rock Mech. Min. Sci. **34** (3-4), p. 62.e1-62.e15.

Hadizadeh J., Mittempergher S., Gratier J.P., Renard F., Toro G.D., Richard J. and Babaie H.A., 2012. A microstructural study of fault rocks from the SAFOD: Implications for the deformation mechanisms and strength of the creeping segment of the San Andreas Fault. J. Struct. Geol. **42**, p. 246-260.

Hangx S., van der Linden A., Marcelis F. and Bauer A., 2013. The effect of CO_2 on the mechanical properties of the Captain Sandstone: Geological storage of CO_2 at the Goldeneye field (UK). International Journal of Greenhouse Gas Control **19**, p. 609-619.

Haimson B.C. and Fairhurst C., 1970. In-situ stress determination at great depth by means of hydraulic fracturing. In: Somerton W.H. (Ed.), Rock Mechanics-Theory and Practice. Am. Inst. Mining Eng., p. 559-584.

Heggland R., 1998. Gas seepage as an indicator of deeper prospective reservoirs. A study on exploration 3D seismic data. Marine and Petroleum Geol. **15**, p. 1–9.

Hesthammer J. and Fossen H., 2001. Structural core analysis from the Gullfaks area, northern North Sea. Marine and Petroleum Geology **18**, p. 411-439.

Hettema M., Schutjens P.M., Verboom B. and Gussinklo H., 2000. Production-induced compaction of a sandstone reservoir: the strong influence of stress path. SPE Reserv. Eval. Eng. **3**, 342–347.

Hickman S.H. and Zoback M.D., 1983. The interpretation of hydraulic fracturing pressure-time data for in-situ stress determination. Hydraulic fracturing measurements. Washington D.C., National Academy Press.

Hillis R.R., Crosby D.G. and Khurana A.K., 1997. A modified fracture gradient relation and its application to East Texas and the Timor Sea. APPEA Journal **37**, no. 1, p. 536-545.

Holdsworth R.E., van Diggelen E.W.E., Spiers C.J., de Bresser J.H.P, Walker R.J. and Bowen L., 2011. Fault rocks from the SAFOD core samples: Implications for weakening at shallow depths along the San Andreas Fault, California. J. Struct. Geol. **33**, p. 132-144.

Holloway S., 1997. An overview of the underground disposal of carbon dioxide. Energy Convers. Manag. **38**, Supplement, S193–S198.

Horii H. and Nemat-Nasser S., 1985. Compression-Induced Microcrack Growth in Brittle Solids: Axial Splitting and Shear Failure. Journal of Geophysical Research: Solid Earth **90** (B4), p. 3105–25.

Horii H. and Nemat-Nasser S., 1986. Brittle Failure in Compression: Splitting, Faulting and Brittle-Ductile Transition, Philosophical Transactions of the Royal Society of London. Series A, Mathematical and Physical Sciences**319**, No. 1549, p. 337-374.

Hung J-H. and Wu J-C., 2012. In-situ stress and fault reactivation associated with LNG injection the Tiechanshan gas field, fold-thrust belt of Western Taiwan. J. Petroleum Science and Engineering **96-97**, p. 37-48.

Iding M. and Ringrose P., 2010. Evaluating the impact of fractures on the performance of the In Salah CO_2 storage site Int. J. Greenhouse Gas Control **4**, p. 242–248.

IEAGHG 2013. Induced seismicity and its implication for CO_2 storage risk, 2013/09, June 2013.

Ingram G. M. and Urai J. L., 1999. Top-seal leakage through faults and fractures: the role of mudrock properties. Geological Society, London, Special Publications **158**(1), p. 125–135.

Jaeger J.C., Cook N.G.W. and Zimmerman R.W., 2007. Fundamentals of Rock Mechanics, 4th ed. Blackwell, Oxford.

Jalilavi M., Zoveidavianpoor M., Attarhamed F., Junin R. and Mohsin R., 2014. Artificial Weathering as a Function of CO_2 Injection in Pahang Sandstone Malaysia: Investigation of Dissolution Rate in Surficial Condition. Scientific Reports **4**: 3645, DOI: 10.1038/srep03645.

Jeanne P., Rinaldi A.P., Rutqvist J., Cappa F. and Guglielmi Y., 2013. Relation between fault zone architecture, earthquake magnitude and leakage associated with CO2 injection in a multilayered sedimentary system. 47th US Rock Mechanics/Geomechanics Symposium, San Fransisco, CA, USA, ARMA 13-246.

Jewell S., Senoir B., Bellarby J. and Mathias S., 2012. CO_2 Storage Liabilities in the North Sea - An Assessment of Risks and Financial Consequences – Summary Report for DECC May 2012, IN: Department of Energy and Climate Change, available at: https://www.gov.uk/government/publications/co2-storage-liabilities-in-the-north-sea-an-assessment-of-risks-and-financial-consequences-summary-report-for-decc-may-2012.

Jing L., 2003. A review of techniques, advances and outstanding issues in numerical modelling for rock mechanics and rock engineering. Int. J. Rock Mech. Mining Sci. **40**(3), p. 283–353.

Jolley S.J., Dijk H., Lamens J.H., Fisher Q.J., Manzocchi T., Eikmans H. and Huang Y., 2007. Faulting and fault sealing in production simulation models: Brent Province, northern North Sea. Petroleum Geoscience **13**, p. 321–340.

Jung R., 2013. EGS — Goodbye or Back to the Future. Effective and Sustainable Hydraulic Fracturing. A.P. Bunger, J. McLennan and R. Jeffrey (edits.), ISBN 978-953-51-1137-5., Published: May 17, 2013 under CC BY 3.0 license. Available at: http://www.intechopen.com/books/effective-and-sustainable-hydraulic-fracturing/egs-goodbye-or-back-to-the-future-95

Kano Y., Funatsu T., Nakao S., Kusunose K., Ishido T., Lei X.L. and Tosha T., 2013. Fault stability analysis related to CO2 injection at Tomakomai, Hokkaido, Japan. Energy Procedia **37**, p. 4946-4953.

Kim Y.S., Andrews J.R. and Sanderson D.J., 2001. Reactivated strike–slip faults: examples from north Cornwall, UK. Tectonophysics **340**, Issues 3–4, P. 173–194.

Koestler A.G. and Milnes A.G., 1992. The importance of structural reservoir characterization and reservoir mechanics for enhanced oil recovery. Geology of the Arab World, Cairo University.

Koestler A.G., Makurat A., Barton N. and Monsen K., 1992. Numerical simulation of jointed and faulted rock behaviour for petroleum reservoirs. In. Larsen et al. (eds.): Structural and tectonic modelling and its application to petroleum geology, Elsevier, p. 277-288.

Kvaale T., 2002. Et stadium av reservoarsand i ringskjærapparat for å simulere oppførselen i forkastningssoner. Master thesis, University of Oslo.

Langhi L., Zhang Y., Gartrell A., Underschultz J.R. and Dewhurst D.N., 2010. Evaluating hydrocarbon trap integrity during fault reactivation using geomechanical 3D modelling: an example from the Timor Sea, Australia. AAPG **94**, p. 567-591.

LeCain G. D., 1998. Results from air-injection and tracer testing in the Upper Tiva Canyon, Bow Ridge Fault, and Upper Paintbrush contact alcoves of the exploratory studies facility, August 1994 through July 1996, Yucca Mountain Nevada, U.S. Geological Survey, Water-Resources Investigations, 98-4058.

Lehner F.K. and Pilaar W.F., 1997. The emplacement of clay smears in synsedimentary normal faults: inferences from field observations near Frechen, Germany. Norwegian Petroleum Society Special Publications **7**, p. 39-50.

Leijon B., 1993. Mechanical properties of fracture zones. Report, Swedish Nuclear Fuel and Waste Management Company.

Lewicki J. L., Birkholzer J. and Tsang C.F., 2007. Natural and industrial analogues for leakage of CO2 from storage reservoirs: identification of features, events, and processes and lessons learned. Environmental Geology **52**, p. 457-467.

Li Q., Wu Z.S., Bai Y.L., Yin X.C. and Li Z.C., 2006. Thermo-hydromechanical modeling of CO_2 sequestration system around fault environment. Pure Appl. Geophys. **163**, p. 2585–2593.

Lin W., Yamamoto K., Ito H., Masago H. and Kawamura Y., 2008. Estimation of Minimum Principal Stress from an Extended Leak-off Test Onboard the Chikyu Drilling Vessel and Suggestions for Future Test Procedures. Scientific Drilling **6**, p. 43-47.

Lindsay N.G., Murphy F.C., Walsh J.J. and Watterson J., 1993. Outcrop studies of shale smears on fault surfaces, Int. Assoc. Sedimentologists Special Publication **15**, p. 113-123.

Liu L., Stuo Y., Bignall G., Yamasaki N. and Hashida T., 2003. CO_2 injection to granite and sandstone in experimental rock/hot water systems. Fuel and Energy Abstract **44** (5), p. 310.

Lorwongngam N., 2008. The validity of leak-off test for in-situ stress estimation; the effect of the bottom of the borehole. MSc thesis, University of Oklahoma, USA.

Losh S. and Haney M., 2006. Episodic fluid flow in an aseismic over-pressured growth fault, northern Gulf of Mexico. In: Abercrombie R., McGarr A., Di Toro G., Kanamori H. (eds.); Earthquakes: Radiated Energy and the Physics of Faulting. American Geophysical Union Geophysical Monograph Series **170**, p. 199-206.

Lucier A., Zoback M., Gupta N. and Ramakrishnan T.S., 2006. Geoemechanical aspects of CO_2 sequestration in a deep saline reservoir in the Ohio River Valley region. Environmental Geosciences, **13**(2), p. 85-103.

Ludwig W.J., Nafe J.E. and Drake C.L., 1970. Seismic refraction. In: A.E. Maxwell (edit.), The Sea: ideas and observation on progress in the study of the seas, new concepts for sea floor evolution: New York, Wiley Interscience **4**, p. 53-84.

Luther A., Axen G. and Selverstone J., 2013. Particle-size distributions of low-angle normal fault breccias: Implications for slip mechanisms on weak faults. J. Structural Geology **55**, p. 50-61.

Lyakhovsky V., Ben-Zion Y. and Agnon A., 2001. Earthquake cycle, faults and seismicity patterns in rheologically layered lithosphere. J. Geophy. Res. **106**, p. 4103-4120.

Main L.G., Kwon O., Ngwenya B.T. and Elphick S.C., 2000. Fault sealing during deformation-band growth in porous sandstone. Geology 28 (2), p. 1131-1134.

Mandl G., 2000. Faulting in brittle rock: an introduction to mechanics of tectonic faulting, Springer-Verlag Berlin, 434 p.

Marone C., Raleigh C.B. and Scholz C.H., 1990. Frictional behavior and constitutive modeling of simulated fault gouge. J. Geophysical research: Solid Earth **95** (B5), p. 7007-7025.

Masoudi R., Abd Jalil A.M., Press D., Lee K.H., Tan C.P., Leo A., Darman N. and Othman M., 2011. An integrated reservoir simulation-geomechanical study on feasibility of CO_2 storage in M4 carbonate reservoir, Malaysia. Int. Petroleum Technology Conf., Bangkok, Thailand 7-9 February 2012.

Mathias S., 2012. Fault Study, Annex 3 in "CO_2 Storage Liabilities in the North Sea –An Assessment of Risks and Financial Consequences, Summary report for DECC, UK" by Jewell S. and Senior B. Available at: https://www.gov.uk/government/publications/co2-storage-liabilities-in-the-north-sea-an-assessment-of-risks-and-financial-consequences-summary-report-for-decc-may-2012.

Medieros W.E., do Nascimento A.F., Alves da Silva F.C. and Demetrio J.G.A., 2010. Evidence of hydraulic connectivity across deformation bands from field pumping tests: two examples from Tucano Basin, NE Brazil. J. Structural Geol. **28** (7), p. 1214-1227.

Mildren S.D., Hillis R.R. and Kaldi J., 2002. Calibrating predictions of fault seal reactivation in the Timor Sea. APPEA Journal 2002, p. 187-202.

Miller S.A., Collettini C., Chiaraluce L., Cocco M., Barchi M. and Kaus B.J.P., 2004. Aftershocks driven by a high-pressure CO_2 source at depth. Nature **427** (6976), p. 724-727.

Millington R. J. and Quirk J. P., 1961. Permeability of porous solids. Transactions of the Faraday Society **57**(0), 1200–1207.

Mitchell T.M. and Faulkner D.R., 2009. The nature and origin of off-fault damage surrounding strike-slip fault zones with a wide range of displacements: A field study from the Atacama fault system, northern Chile. J. Structural Geology **31**, p. 802-816.

Moeck I., Kwitatek G. and Zimmermann G., 2009. Slip tendency analysis, fault reactivation potential and induced seismicity in a deep geothermal reservoir. J. Structural Geol. **31**, p. 1174-1182.

Moore D.E. and Lockner D.A., 1995. The role of microcracking in shear-fracture propagation in granite. J. Structural Geology **17**, No. 1, p. 95-111.

Moore D.E., Lockner D.A., Tanaka H. and Iwata K., 2004. The coefficient of friction of chrysotile gouge at seismogenic depths. International Geology Review **46**, p. 385–398.

Morris A., Ferrill D.A. and Henderson D.B., 1996. Slip-tendency analysis and fault reactivation. Geology **24**, p. 275–278.

Morris J. P., Hao Y., Foxall W. and McNab W., 2011. A study of injection-induced mechanical deformation at the In Salah CO_2 storage project. International Journal of Greenhouse Gas Control **5**(2), p. 270–280.

Morrow C.A., Moore D.E. and Lokner D.A., 2000. The effect of mineral bond strength and adsorbed water on fault gouge frictional strength. Geophysical Research Letters **27** (6), p. 815-818.

Morrow C.A., Lockner D.A., Moore D.E. and Hickman S., 2013. Deep permeability of the San Andreas Fault from San Andreas Fault Observatory at Depth (SAFOD) core samples, J. Struct. Geol., Available at: doi: 10.1016/j.jsg.2013.09.009.

Nakamura K., 1977. Volcanoes as possible indicators of tectonic stress orientation-principle and proposal. Journal of Volcanology and Geothermal Research **2**, p. 1-16.

Noir J. E., Bekri J.S., Adler P.M., Tapponnier P. and King G.C.P., 1997. Fluid flow triggered migration of events in the 1989 Dobi earthquake sequence of Central Afar, Geophys. Res. Lett. **24**, p. 2328– 2335.

Nouailletas O., Perlot C., Borderie C.L., Rousseau B and Ballivy G., 2013. Shear behavior evolution of a fault due to chemical degradation of roughness: application to the geological storage of CO_2. In: G.P. Cabot and J.M. Preira (edis.) Geomechanics in CO_2 storage facilities, Wiley, 234 p.

O'Brian G.W., Lisk M., Duddy I., Eadington P.J., Cadman S. and Fellows M., 1996. Late Tertiary fluid migration in the Timor Sea: A key control on thermal and diagenetic histories? APEA Journal 1996, p. 399-426.

O'Brian G.W., Lisk M., Duddy I., Hamilton J., Woods P. and Cowley R., 1999. Plate convergence, foreland development and fault reactivation; primary controls on brine migration, thermal histories and trap breach in the Timor Sea, Australia. Marine and Petroleum Geology 16 (6), p. 533-560.

Ojala I.O., 2011. The effect of CO_2 on the mechanical properties of reservoir and cap rock. Energy Procedia **4**, p. 5392- 5397.

Olsen M.P., Scholz C.H. and Leger A., 1998. Healing and sealing of a simulated fault gouge under hydrothermal conditions: implications for fault healing. J. Geophysical Research **103**, B4, p. 7421-7430.

Orlic B., 2009. Some geomechanical aspects of geological CO_2 sequestration. KSCE J. Civ. Eng. **13**, p. 225–232.

Orlic B., Heege J. and Wassing B., 2011. Assessing the integrity of fault- and top seals at CO_2 storage sites. Energy Procedia, 4, 4798–4805.

Orlic B., Wassing B.B.T. and Geel C.R., 2013. Field scale geomechanical modeling for prediction of fault stability during underground gas storage operations in a depleted gas field in the Netherlands. 47th U.S. Rock Mechanics/Geomechanics Symposium, 23-26 June, San Francisco, California, ARMA 2013-300.Parry W. T., Forster C. B., Evans J. P., Bowen B. B. and Chan M. A., 2007. Geochemistry of CO_2 Sequestration in the Jurassic Navajo Sandstone, Colorado Plateau, Utah. Environ Geosci. **14**, p. 91–109.

Paul P. and Zoback M.D., 2008. Wellbore stability study for the SAFOD borehole through the San Andreas Fault, SPE 102781, SPE Drilling and Completion, Dec. 2008, p. 394-408.

Peacock D.C.P. and Parfitt E.A., 2002. Active relay ramps and normal fault propagation on Kilauea, Hawaii. J. Struct. Geol. **24**, p. 729-742.

Pearce J., Czernichowski-Lauriol I., Lombardi S., Brune S., Nador A., Baker J., Pauwels H., Hatziyannis G., Beaubien S. and Faber E., 2004. A review of natural CO_2 accumulations in Europe as analogues for geological sequestration. Geological Society, London, Special Publications 2004, 233:29-41. doi:10.1144/GSL.SP.2004.233.01.04.

Perkins T. K. and Gonzales J. A., 1985. The effect of thermo-elastic stresses on injection well fracturing, SPE no. 11332.

Peska P. and Zoback M.D., 1998. Drilling-induced tensile fractures: formation and constraints on the full stress tensor. In "Mechanics of Jointed and Faulted Rock" H.P. Rossmanith (edit.), A.A. Balkema, Brookfield, Vermont, p. 331-337.

Pluymakers A., Samuelson J. and Spiers C., 2013. The effects of supercritical carbon dioxide on the frictional behavior of simulated anhydrite fault gouge. Geophysical Research Abstracts **15**, EGU2013-11208.

Potts D.M. and Zdravkovic L., 1999. Finite element analysis in geotechnical engineering: theory, London, Thomas Telford Publ.

Preisig M. and Prévost J.H., 2011. Coupled multi-phase thermo-poromechanical effects. Case study: CO_2 injection at In Salah, Algeria. Int. J. Greenhouse Gas Control **5**, p. 1055-1064.

Price N.J. and Cosgrove J.W., 2005. Analysis of geological structures. Cambridge University Press, Cambridge, UK, 502 p.

Priest S. D., 1993. Discontinuity Analysis for Rock Engineering. Springer.

Raaen A.M., Horsrud P., Kjørholt H. and Økland D., 2006. Improved routine estimation of the minimum horizontal stress component from extended leak-off tests. Int. J. Rock Mech. & Min. Sci. **43**, p. 37–48.

Rice J. R., and Rudnicki J. W., 1979. Earthquake Precursory Effects due to Pore Fluid Stabilization of a Weakening Fault Zone. Journal of Geophysical Research: Solid Earth **84** (B5), p. 2177–2193.

Rinaldi A. P., Rutqvist J. and Cappa F., 2014. Geomechanical effects on CO_2 leakage through fault zones during large-scale underground injection. International Journal of Greenhouse Gas Control **20**, p. 117–131.

Rudnicki J.W., 1999. Alteration of regional stress by reservoirs and other inhomogeneities: stabilizing or destabilizing? In: Proceedings of the 9th International Congress on Rock Mechanics **3**, p. 1629–1637.

Rudnicki J.W., 2001. Coupled Deformation-Diffusion Effects in the Mechanics of Faulting and Failure of Geomaterials. Applied Mechanics Reviews **54** (6), p. 483

Rutqvist J., 2012. The Geomechanics of CO2 Storage in Deep Sedimentary Formations. Geotech. Geol. Eng. **30**, p. 525–551.Rutqvist J., Rinaldi A.P., Cappa F. and Moridis G.J., 2013. Modeling of fault reactivation and induced seismicity during hydraulic fracturing of shale-gas reservoirs. Journal of Petroleum Science and Engineering **107**, p. 31-44.

Rutqvist J., Birkholzer J., Cappa F. and Tsang C.F., 2007. Estimating maximum sustainable injection pressure during geological sequestration of CO2 using coupled fluid flow and geomechanical fault-slip analysis. Energy Convers. Manag. **48**, p. 1798–1807.

Rutqvist J. and Tsang C.F., 2002. A study of cap rock hydromechanical changes associated with CO_2 injection into a brine aquifer. Environ. Geol. **42**, p. 296–305.

Rutter E.H., Maddock R.H., Hall S.H. and White S.H., 1986. Comparative microstructures of naturally and experimentally produced clay-bearing fault gouge. Pure and Applied Geophysics **124**, p. 3-30.

Sammis C., King J. and Biegel R., 1987. The kinematics of gouge deformation. Pageoph. **125** (5), p. 777-812.

Samuelson J. and Spiers C.J., 2012. Fault friction and slip stability not affected by Co2 storage: Evidence from short-term laboratory experiments on North Sea reservoir sandstones and caprocks. Int. J. Greenhouse Gas Control **11S**, P. S78-S90.

Schlische R.W., Young S.S., Ackermann R.V. and Gupta A., 1996. Geometry and scaling relations of a population of very small rift-related normal faults. Geology **24**, p. 683-686.

Schmatz J., Vrolijk P.J. and Urai J.L., 2010. Clay smear in normal fault zones – The effect of multilayers and clay cementation in water-saturated model experiments. J. Struct. Geol. **32** (11), p. 1834-1849.

Scholz C.H., Dawers N.H., Yu J.Z., Anders M.H. and Cowie P.A., 1993. Fault growth and fault scaling laws: Preliminary results. Journal of geophysical Research **98**, Issue B12, p. 21951–21961.

Schultz R.A. and Fossen H., 2002. Displacement-length scaling in three dimensions: the importance of aspect ratio and application to deformation bands. J. Struct. Geol. **24**, p. 1389–1411.

Segall P. and Fitzgerald S.D., 1998. A note on induced stress changes in hydrocarbon and geothermal reservoirs. Tectonophysics **289**, p. 117–128.

Selley R. C., 1997. Elements of Petroleum Geology. Morgan Kauffmann Publishers, 2nd edit., 449 p.

Sibson R.H., 2000. Fluid involvement in normal faulting. J. Geodynamics **29**, p. 469–499.

Sibson R.H., 2003a. Brittle-failure controls on maximum sustainable overpressure in different tectonic regimes. AAPG Bulletin **87(**6), p. 901-908.

Sibson R. H., 2003b. Thickness of the Seismic Slip Zone. Bulletin of the Seismological Society of America **93**(3), p. 1169–1178.

Shipton Z.K., Evans J.P., Robeson K., Forster C.B. and Snelgrove S., 2002. Structural heterogeneity and permeability in faulted eolian sandstone: implications for subsurface modelling of faults. AAPG Bulletin **86**, p. 863–883.

Soltanzadeh H. and Hawkes C.D., 2008. Semi-analytical models for stress change and fault reactivation induced by reservoir production and injection. J. Petroleum Science and Engineering **60**(2), p. 71-85.

Sone H., Shimamoto T. and Moore D.E., 2012. Frictional properties of saponite-rich gouge from a serpentinite-bearing fault zone along the Gokasho-Arashima Tectonic Line, central Japan. J. Struct. Geol. **38**, p. 172-182.

Sperrevik S., Gillespie P.A., Fisher Q., Halvorsen T. and Knipe R.J., 2002. Empirical estimation of fault rock properties. In: Koestler A.G., and Hunsdale R. (Eds.), Hydrocarbon Seal Quantification. NPF Special Publications **11**, p. 109-125.

Streit J. M. and Watson M. N., 2004. Estimating rates of potential CO_2 loss from geological storage sites for risk and uncertainty analysis. Proceedings of the 7th International Conference on Greenhouse Gas Control Technologies GHGT-7. Vancouver, Canada, p. 1309-1314.

Streit J.E. and Hillis R.R., 2004. Estimating fault stability and sustainable fluid pressures for underground storage of CO_2 in porous rock. Energy **29**, p. 1445–1456.

Sulem J. and Vardoulakis I.G., 2004. Bifurcation Analysis in Geomechanics. CRC Press.

Sylvester A.G., 1988. Strike-slip faults. Geol. Soc. Amer. **100**, p. 1666-1703.

Tadokoro K., Ando M. and Nishigami K., 2000. Induced earthquake accompanying the water injection experiment at the Nojima fault zone, Japan: seismicity and its migration. J. Geophys. Research –Solid Earth **105** (B3), p. 6089-6104.

Takahashi M., Mizoguchi K., Kitamura K. and Masuada K., 2007. Effects of clay content on the frictional strength and fluid transport property of faults. J. Geophysical Research **112**, B08206, doi:10.1029/2006JB004678.

Talwani P., Chen L., and Gahalaut K., 2007. Seismogenic permeability, ks. Journal Geophys. Res. **112**, B07309, doi:10.1029/2006JB004665.

Talwani P., Cobb J.S. and Schaeffer M.F., 1999. In-situ measurements of hydraulic properties of a shear zone in northwestern South Carolina. J. Geophys. Research- Sold Earth **104** (B7), p. 14993-15003.

Tang L. and Luo P., 1998. The effect of the thermal stress on wellbore stability, SPE no. 39505.

Tejchman J. and Bauer E., 1996. Numerical Simulation of Shear Band Formation with a Polar Hypoplastic Constitutive Model. Computers and Geotechnics **19**(3), p. 221–44.

Tembe S., Lockner D.A. and Wong T.F., 2010. Effect of clay content and mineralogy on frictional sliding behavior of simulated gouges: Binary and ternary mixtures of quartz, illite, and montmorillonite. Journal of Geophysical Research **115**, p. 1–22.

Tenthorey E., Cox S.F. and Todd H.F., 2003. Evolution of strength recovery and permeability during fluidrock reaction in experimental fault zones. Earth and Planetary Science Letters **206**, no. 1-2, p. 161-172.

Tenthorey E., Vidal-Gilbert S., Guillaume B., Puspitasari R., Pallikathekathil Z.J., Maney B. and Dewhurst D., 2013. Modeling the Geomechanics of gas storage: a case study from the Iona gas field, Australia. Int. J. Greenhouse Gas Control **13**, p. 138-148.

Teufel L.W., Rhett D.W. and Farrell H.E., 1991. Effect of reservoir depletion and pore pressure drawdown on in-situ stress and deformation in the Ekofisk field, North Sea. In The 32nd US Symposium on Rock Mechanics (USRMS).

Thakur V., 2011. Numerically Observed Shear Bands in Soft Sensitive Clays. Geomechanics and Geoengineering **6**(2), p. 131–46.

Torabi A., Braathen A., Cuisiat F. and Fossen H., 2007. Shear zones in porous sand: Insights from ring-shear experiments and naturally deformed sandstones. Tectonophysics **437**, p. 37-50.

Townend J. and Zoback M.D., 2000. How faulting keeps the crust strong, Geology **28**(5), p. 399– 402.

Van der Zee W., 2002. Dynamics of fault gouge development in layered sand-clay sequences. ISBN 38322 05853, Shaker Verlag, Aachen, 155 p.

van der Zee W. and Urai J.L., 2001. Fault zone evolution in layered sand-mudstone sequences. Hydrocarbon Seal Quantification Conference, Stavanger (Norway), Extended abstracts, ISBN 82-92032-02-9, p. 171-180.

van der Zee W. and Urai J. L., 2005. Processes of normal fault evolution in a siliciclastic sequence: a case study from Miri, Sarawak, Malaysia. J. Struct. Geol. **27**, p. 2281-2300.

Verdon J.P., 2010. Microseismic Monitoring and Geomechanical Modelling of CO_2 Storage in Subsurface Reservoirs. PhD dissertation, Department of Earth Science, University of Bristol, UK, 194 p.

Vermilye J.M. and Scholz C.H., 1998. The process zone: a microstructural view of fault growth. J. Geophysical Research **103**, B6, p. 12223-12237.

Vidal-Gilbert S., Tenthorey E., Dewhurst D., Ennis-King J., Van Ruth P. and Hillis R., 2010. Geomechanical analysis of the Naylor Field, Otway Basin, Australia: Implications for CO_2 injection and storage. Int. J. Greenhouse Gas Control **4**, p. 827–839.

Vidal-Gilbert S., Nauroy J.F. and Brosse E., 2009. 3D geomechanical modelling for CO_2 geologic storage in the Dogger carbonates of the Paris Basin. International Journal of Greenhouse Gas Control **3**(3), p. 288–299.

Walsh J.J., Nicol A. and Childs C., 2002. An alternative model for the growth of faults. J. Struct. Geol. **24**, p. 1669-1675.

Watts N.L., 1987. Theoretical aspects of cap-rock and fault seals for single and two-phase hydrocarbon columns. Marine and Petroleum Geology **4**(4), p. 274-307.

White A.J., Traugott M.O. and Swarbrick R.E., 2002. The use of leak-off tests as means of predicting minimum in-situ stress. Petroleum Geoscience **8**, p. 189-193.

Wibberley C. A. ., and Shimamoto T., 2003. Internal structure and permeability of major strike-slip fault zones: the Median Tectonic Line in Mie Prefecture, Southwest Japan. Journal of Structural Geology **25**(1), p. 59–78.

Wilson J.E., Chester J.S. and Chester F.M., 2003. Microfracture analysis of fault growth and wear processes, Punchbowl fault, San Andreas System, California. J. Struct. Geol. **25**(11), p. 1855-1873.

Wang P. and Xu L.R., 2006. Dynamic interfacial debonding initiation induced by an incident crack. Int. J. Solids Struct. **43**, p. 6535-6550.

Wiprut D. and Zoback M., 2002. Fault reactivation, leakage potential, and hydrocarbon column heights in the northern North Sea. In: Koestler, A.G., Hunsdale R. (Eds.), Hydrocarbon Seal Quantification. NPF Special Publication **11**, p. 203-219.

Wollenweber J., Alles S., Busch A., Krooss B.M., Stanjek H. and Littke R., 2010. Experimental investigation of the CO2 sealing efficiency of caprocks. Int. J. of Greenhouse Gas Control **4**(2), P. 231-241.

Xu L.R., Huang Y.Y. and Rosakis A.J., 2003. Dynamic crack deflection and penetration at interfaces in homogeneous materials: experimental studies and model predictions. J. Mech. Phys. Solids **51**, p. 461-486.

Yamaji A., 2007. An Introduction to Tectonophysics: Theoretical Aspects of Structural Geology. ISBN No. 4-88704-135-7, Terrapub, Tokyo, Japan.

Yasuhara H., Marone C. and Elsworth D., 2005. Fault zone resetrengthening and frictional healing:the role of pressure solution. J. Geophysical Research **110**, B06310, doi:10.1029/2004JB003327.

Zhang S. and Tullis T.E., 1998. The effect of fault slip on permeability and permeability anisotropy in quartz gouge. Tectonophysics **295** (1-2), p. 41–52.

Zhang S.Q., Tullis T.E. and Scruggs V.J., 1999. Permeability anisotropy and pressure dependency of permeability in experimentally sheared gouge materials. J. Struct. Geol. **21** (7), p. 795-806.

Zhang Y., Oldenburg C. M. and Finsterle S., 2010. Percolation-theory and fuzzy rule-based probability estimation of fault leakage at geologic carbon sequestration sites. Environ. Earth Sci. **59**, p. 1447–1459.

Zoback M.D. and Hickman S.H., 2005. Preliminary observations of stress and fluid pressure in and near the San Andreas Fault at depth in the SAFOD boreholes. Transactions of the American Geophysical Union **86**(52), Fall Meeting Supplement, Abstract T21A-0438.

Zoback M.D., 2007. Reservoir Geomechanics. Cambridge University Press, Cambridge, UK, 449 p.

Zoback M.D., Hickman S.H. and Ellsworth B., 2007. The role of fault zone drilling. Earth Systems and Environmental Sciences **4**, p. 649-674.

Zoback M.D., Hickman S.H. and Ellsworth B., 2010. Scientific drilling into the San Andreas fault zone. Transactions of the American Geophysical Union **91**(22), p. 197-199.Zoback M.D., Kohli A., Das I. and McClure M., 2012. The importance of slow slip on faults during hydraulic fracturing stimulation of shale gas reservoirs. In: SPE Americas Unconventional Resources Conference.

Zoback M.D. and Pollard D.D., 1978. Hydraulic fracture propagation and the interpretation of pressure-time records for in-situ stress determination. Proc. 19th US Symposium on Rock Mechanics, University of Nevada-Reno, p. 14-22.

Zoback M.D. and Zinke J.C., 2002. Production-induced normal faulting in the Valhall and Ekofisk oil fields. Pure and Applied Geophysics **159**, p. 403–420.

Kontroll- og referanseside/
Review and reference page

NGI

Dokumentinformasjon/*Document information*			
Dokumenttittel/*Document title* Criteria of Fault Geomechanical Stability During a Pressure Build-up. Final report		**Dokument nr./*Document No.*** 20130613-02-R	
Dokumenttype/*Type of document* Report	**Distribusjon/*Distribution*** Limited	**Dato/*Date*** 26 September 2014 **Rev.nr.&dato/*Rev.No&date.*** 0	
Oppdragsgiver/*Client* IEAGHG			
Emneord/*Keywords*			

Stedfesting/*Geographical information*	
Land, fylke/*Country, County*	**Havområde/*Offshore area***
Kommune/*Municipality*	**Feltnavn/*Field name***
Sted/*Location*	**Sted/*Location***
Kartblad/*Map*	**Felt, blokknr./*Field, Block No.***
UTM-koordinater/*UTM-coordinates*	

Dokumentkontroll/*Document control*

Kvalitetssikring i henhold til/*Quality assurance according to* NS-EN ISO9001

Rev./ *Rev.*	**Revisjonsgrunnlag/*Reason for revision***	**Egen-kontroll/ *Self review* av/*by:***		**Sidemanns-kontroll/ *Colleague review* av/*by:***		**Uavhengig kontroll/ *Independent review* av/*by:***		**Tverrfaglig kontroll/ *Inter-disciplinary review* av/*by:***	
0	Original document	BB		NHM					

Dokument godkjent for utsendelse/ *Document approved for release*	**Dato/*Date*** 26 September 2014	**Sign. Prosjektleder/*Project Manager*** Bahman Bohloli

NGI (Norges Geotekniske Institutt) er et internasjonalt ledende senter for forskning og rådgivning innen geofagene. Vi utvikler optimale løsninger for samfunnet, og tilbyr ekspertise om jord, berg og snø og deres påvirkning på miljøet, konstruksjoner og anlegg.

Vi arbeider i følgende markeder: olje,gass og energi, bygg, anlegg og samferdsel, naturskade og miljøteknologi. NGI er en privat stiftelse med kontor og laboratorier i Oslo, avdelingskontor i Trondheim og datterselskap i Houston, Texas, USA.

NGI ble utnevnt til "Senter for fremragende forskning" (SFF) i 2002.

www.ngi.no

NGI (Norwegian Geotechnical Institute) is a leading international centre for research and consulting in the geosciences. NGI develops optimum solutions for society, and offers expertise on the behaviour of soil, rock and snow and their interaction with the natural and built environment.

NGI works within the oil, gas and energy, building and construction, transportation, natural hazards and environment sectors. NGI is a private foundation with office and laboratory in Oslo, branch office in Trondheim and daughter company in Houston, Texas, USA.

NGI was awarded Centre of Excellence status in 2002.

www.ngi.no

Hovedkontor/Main office:
PO Box 3930 Ullevål Stadion
NO-0806 Oslo
Norway

Besøksadresse/Street address:
Sognsveien 72, NO-0855 Oslo

Avd Trondheim/Trondheim office:
PO Box 1230 Sluppen
NO-7462 Trondheim
Norway

Besøksadresse/Street address:
Pirsenteret, Havnegata 9, NO-7010 Trondheim

T: (+47) 22 02 30 00
F: (+47) 22 23 04 48

ngi@ngi.no
www.ngi.no

Kontonr 5096 05 01281/IBAN NO26 5096 0501 281
Org. nr/Company No.: 958 254 318 MVA

BSI EN ISO 9001
Sertifisert av/Certified by BSI, Reg. No. FS 32989